

# **POLITECNICO DI TORINO**

**Corso di Laurea Magistrale  
in Ingegneria Energetica e Nucleare**

**Tesi di Laurea Magistrale**

**Development of a lumped multi-physics  
model for Tritium Extraction Systems based  
on the Permeator Against Vacuum Technique  
for the next fusion machine**



**Supervisor**  
Prof. Laura Savoldi

**Candidate**  
Aldo Collaku

**marzo, 2022**



*Alla mia Famiglia.*

## Abstract

In the framework of next fusion machines, the tritium cycle is of particular interest since its central role in fusion reaction as a fuel element. The high permeability of Tritium, as well as its decay time, requires an “in situ” production. The Tritium Extraction and Removal System is the system aimed to manage the tritium cycle inside the reactor and the Permeator Against Vacuum (PAV) is one of the technologies proposed for the TERS of the Water-Cooled Lithium Lead Breeding Blanket. The aim of this work is to develop a lumped model for the tritium extraction based on the PAV. This work is carried on in collaboration with the research centre of ENEA-Brasimone (Camugnano, BO) where a PAV mock-up has been installed and is under test in the TRIEX-II facility. The lumped multi-physics 1D model is developed in Modelica grouping unit elements called “Radiatubes”, based on separate models of the different physical aspects characterizing the tubes in the PAV. The driving phenomena of the PAV technology is the tritium permeation and diffusion, due to the pressure difference between the tritium in the PbLi flowing into the bank of tubes and the vacuum inside the PAV. The permeation model is described considering a diffusion limited permeation regime and its governing equations, moreover, a sensitivity analysis on the solubility constant is done to deal with some uncertainties found in literature. A detailed 3D thermal-hydraulic model using the commercial software STAR-CCM+ allowed the computation of the hydraulic characteristic of the U-tubes, used as input to the Radiatubes. Beside the advection, the lumped model accounts also for the radiative effects present in the detailed 3D thermal model, in the form of view factors between the Radiatubes and the envelope. Eventually, a suitable coupling of the different Radiatubes to inlet and outlet manifolds leads to the assembly of the whole PAV lumped model. A first benchmark of the lumped model is performed reproducing the global behaviour of the 3D thermal-hydraulic model, and cross-checking the permeation results against the ones obtained using a consolidated MATLAB model.

# Contents

<b>1</b>	<b>Introduction</b>	<b>9</b>
1.1	Fusion . . . . .	9
1.2	T cycle . . . . .	11
1.3	Aim of the work . . . . .	12
<b>2</b>	<b>Permeation model for PAV</b>	<b>13</b>
2.1	The permeation model . . . . .	14
2.2	Benchmark . . . . .	19
2.3	Sizing of PAV unit for DEMO reactor . . . . .	22
<b>3</b>	<b>CFD model for PAV mock-up</b>	<b>28</b>
3.1	Geometry . . . . .	28
3.2	Continua . . . . .	31
3.3	The mesh . . . . .	32
3.4	Hydraulic analysis . . . . .	36
3.5	Thermal analysis . . . . .	39
<b>4</b>	<b>Lumped model for PAV mock-up</b>	<b>44</b>
4.1	Permeation characterization . . . . .	44
4.2	Hydraulic characterization . . . . .	48
4.3	Thermal characterization . . . . .	49
4.4	Assembling of RadiaTubes . . . . .	53
<b>5</b>	<b>Conclusions</b>	<b>57</b>

# List of Figures

1.1	Sketch of D-T nuclear fusion reaction, [2]	9
1.2	Cross section of different nuclear fusion reaction [3].	10
2.1	Schematic of Permeator Against Vacuum taken from [15].	13
2.2	Different Permeation regimes. $J$ is the permeated flux across the solid membrane. $P$ is the partial pressure of the gas and $C$ the concentration of the specie [12].	16
2.3	Sketch of tritium transport-permeation phenomena, from [11].	17
2.4	Left) Overall PAV design showing the length (L), width (a) and total height (H). Right) Detailed view of PbLi flowing channels (not real dimensions), from [16].	19
2.5	Efficiency computed using the DLR model as function of a) height of channels in [16] and b) diameter of tubes in this model.	20
2.6	Required length to reach efficiency of 90% at different values of internal diameter. (a) Results of Bonifetto et al. [17] and (b) the results of the model of this work.	21
2.7	Flow chart of the design process of PAV unit.	23
2.8	Results obtained with the DLR at a PbLi inlet temperature of 330 °C. Velocity, in blue, and pressure drop, in red, as function of the number of tubes with tube diameter of 9.2 mm (a) and 13 mm (b), respectively. Horizontal dashed lines represent design constraints. The # PP shaded in yellow refers to only one of IB or OB, while that in green refers to a range common to both.	25
2.9	Ranges of tubes at different number of PAVU per OB and IB loop with 9.2 mm design (a) and with 13 mm design (b). Red color refers to normal condition (no PAVU unavailability), blue color refers to one unavailability for each loop. In green the common range of # PP at different temperatures.	26

2.10	Efficiency along the tubes computed with Aiello's solubility constant for H, at 9.2 <i>mm</i> (a) and at 13 <i>mm</i> (b). Solid and dashed line refers to maximum and minimum allowable number of tubes identified in the previous part of the analysis. . . .	27
3.1	Sketches of the PAV mock-up . . . . .	30
3.2	PAV mock-up grid development . . . . .	33
3.3	Section view of inlet (on the right) and outlet (on the left) manifolds. Highlight of jet effects at the inlet and at the outlet of the tubes. . . . .	34
3.4	Section view of inlet (on the right) and outlet (on the left) manifolds. Highlight of temperature field at the inlet and at the outlet of the tubes. . . . .	34
3.5	Details on the mesh. Detail on tubes in (a) with fluid domain in grey and solid domain in orange. Detail on tubes extrusion in (b) with fluid tube domain in grey and fluid manifold domain in green. Detail on bulk refinement in (c). . . . .	35
3.6	Mass flow repartition and maximum speed among the PAV mock-up pipes. . . . .	38
3.7	Flow field computed in the manifolds, for a mass flow rate of 0.75 <i>kg/s</i> . . . . .	39
3.8	Pressure drop of the PAV mock-up as function of PbLimass flow rate, results from CFD analysis . . . . .	40
3.9	Friction factor as function of Reynolds number. Power law fitting of the CFD results with Excel. . . . .	40
3.10	Steady-state normalized temperature difference . . . . .	42
3.11	Fluid domain temperature field at 0.75 <i>kg/s</i> . . . . .	42
4.1	Set up for the validation of the permeation lumped model. . . .	45
4.2	The comparison of the two results obtained with different OpenModelica (a) and Matlab (b) from the permeation model of this work. . . . .	46
4.3	Different set-up for TP and RadiaTube objects. Input parameters for the set-up of the Tritium Permeation object in (a) and for the RadiaTube in (b). . . . .	47
4.4	Relative error, defined in (4.1), of pressure drop of the tubes. Tubes of the second passage are selected to get rid of jet effects due to the PAV inlet flow rate. . . . .	48

4.5	Sketch of of tubes-envelope section in (a) and detail on a generic tube in (b). In yellow and in orange the thermal connectors implemented in OpenModelica to account of view factors. . . . .	49
4.6	RadiaTube characterized by 8 view factor and tritium permeation calculus . . . . .	50
4.7	Planck's law that shows the spectrum of thermal radiation at different temperatures. . . . .	51
4.8	View factor associated with radiation exchange between elemental surfaces of area $dA_i$ and $dA_j$ . Image from [22]. . . . .	52
4.9	Section of two cylinders infinitely long with generic radii $r$ and pitch $s$ . . . . .	52
4.10	Field function (4.5) for each tube of the first passage. . . . .	53
4.11	Section view of the 8 tubes (1/4 of the whole bank of tubes) lumped in one single, equivalent, tube. . . . .	54
4.12	Condensation of PAV mock-up tubes. Each passage is modelled with two RadiaTube . . . . .	55
4.13	Suggested lumped model for PAV mock-up . . . . .	56



# List of Tables

2.1	Permeation number at different temperatures. . . . .	16
2.2	List of symbols of the permeation model. . . . .	18
2.3	Design constraints for PAV unit. . . . .	22
2.4	Design operating conditions taken from [30]. . . . .	22
2.5	Solubility constant of hydrogen isotopes in PbLi according different authors. . . . .	24
3.1	PAV mock-up main dimensions. . . . .	29
3.2	PAV mock-up operating conditions. . . . .	31
3.3	PAV mock-up material properties. . . . .	31
3.4	PbLi properties from [29]. . . . .	32
3.5	Boundary conditions of PAV mock-up simulation . . . . .	41
4.1	Input parameter for the validation of lumped permeation model	47
4.2	Comparison of mean temperature, pressure drop and Tritium extraction efficiency of each U-tubes passage obtained with CFD and lumped RadiaTube model at 0.75 kg/s. . . . .	56

# Chapter 1

## Introduction

### 1.1 Fusion

Nuclear fusion energy will be the turning point of the future energy scenario. In the medium term, energy production will have to rely on renewable energies and nuclear fission, the only technologies capable of guaranteeing clean energy production and a reduction in dependence on fossil fuels. Nuclear fusion is based on the reaction of hydrogen isotopes: Deuterium and Tritium, this reaction is the easiest and most efficient to carry out, as can be appreciate in Fig.1.2.

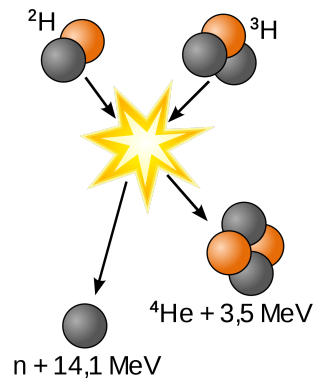
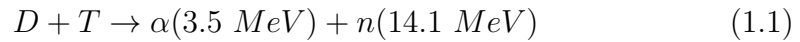
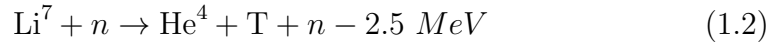


Figure 1.1: Sketch of D-T nuclear fusion reaction, [2].  $^2\text{H}$  and  $^3\text{H}$  are the isotopes of hydrogen, Deuterium and Tritium respectively. The two isotopes undergo nuclear reaction according (1.1) giving rise to a neutron and an  $\alpha$  particle ( $^4\text{He}$ ).

To obtain this reaction, temperatures of 100 million degrees and a magnetic confinement of the plasma are required. *Plasma* is a state of matter in which the atoms are completely ionized and therefore subject to an electromagnetic field.

The availability of nuclear fusion fuel is almost unlimited. Deuterium is found in small percentages in the water molecule ( $30 \text{ g/m}^3$ )[4] from which it can be easily extracted. Tritium, on the other hand, is bred by reacting with Lithium according to (1.2) and (1.3)



Natural Li is made of 92.5 % by  $\text{Li}^7$  and 7.5 % by  $\text{Li}^6$  and abounds in the earth's crust ( $20 \div 30 \text{ mg/kg}$ )[4] of earth crust, in addition it is not localized just in few areas, like oil.

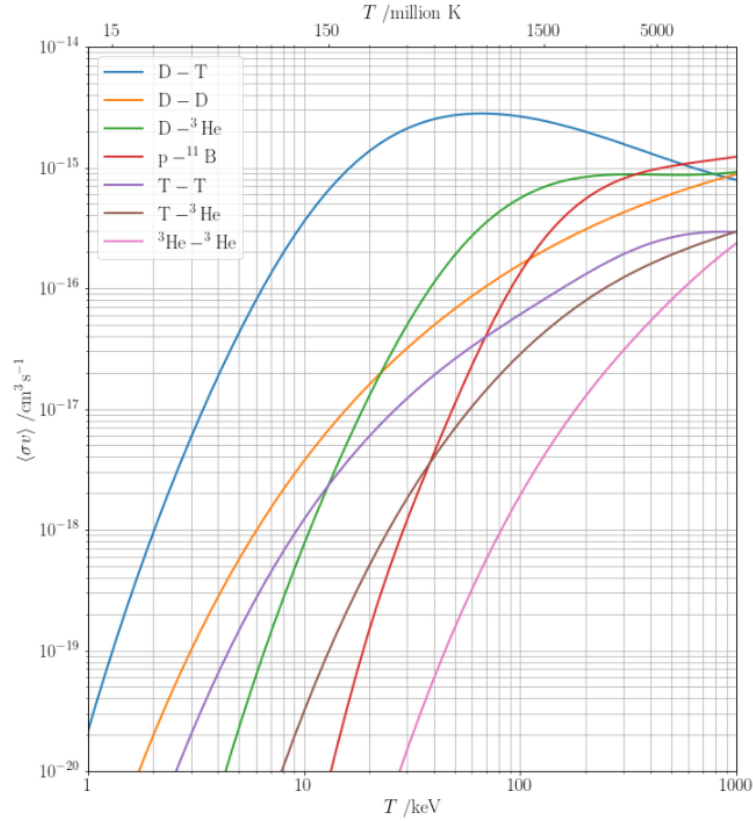


Figure 1.2: Cross section of different nuclear fusion reaction [3].

## 1.2 T cycle

In nuclear fusion reaction, Tritium is the only radioactive element: it is a  $\beta^-$  emitter characterized by an half-life of 12.32 years [1]. Its low half life together with its extremely high permeability make Tritium very difficult, and hazardous, to store and transport when needed. For these reasons Tritium is breed in loco in the *Breeding Blanket* (BB) of the reactor to ensure the right fuel supply to the fusion reaction. Tritium produced in the blanket is then transport through the Tritium Extraction System where it is separated from the operating fluid, PbLi in case of the foreseen DEMO reactor. Tritium supply into the plasma must be equal to Tritium burnout, for that reason the *Tritium Breeding Ratio* (TBR), defined as (1.4) [5]

$$TBR = \frac{T \text{ produced in blanket}}{T \text{ burnt in plasma}} \quad (1.4)$$

should be equal to one, meaning equilibrium in production and destruction of Tritium. Nevertheless, in order to account of TES efficiencies, in particular extraction efficiency and Tritium leakage through the system, TBR must be higher then one. To achieve this result a proper design of the BB and TES is necessary otherwise the fusion reaction will stop due to lack of fuel. A good TES design is needed also for safety reasons, indeed, higher efficiency will minimize Tritium permeation and release to the environment.

The three main technologies under investigation for the TES are: *Vacuum Sieve Tray* (VST), the *Gas Liquid Contactor* (GLC) and the *Permeator Against Vacuum* (PAV).

The VST simply consists in letting droplets fall from an upper tank to a lower tank under vacuum through nozzles. The efficiency of the extraction is governed by the falling time and so the velocity of the droplets [6].

The GLC uses mechanisms of diffusion interchange between gas and liquid phases to extract tritium from the breeder: to do this, PbLi and the process gas are mixed together and their contact surface is maximized, in order to obtain a higher value of particle flux from one boundary layer to the other [7].

Both the VST and the GLC are characterized by a low extraction efficiency, for this reason the PAV is considered as an alternative choice. Nevertheless the *technology readiness level* TRL of the PAV technology is lower compared to the VST and the GLC ones.

The *Permeator Against Vacuum* relies on partial pressure gradient of Tritium, it is studied as one of the proposed technologies for the TES of the *Water-Cooled Lithium Lead (WCLL) Breeding Blanket*.

### 1.3 Aim of the work

The design of a real-size PAV, like for DEMO reactor, should rely on thermal hydraulic models along with permeation models. Concerning the permeation of Tritium, it can be easily scaled up to real-size designs, like it has been done in this work, by adopting analytical models. About the thermal hydraulic aspect, computing the whole domain would be extremely costly and time consuming, a different approach is necessary.

This work addresses the problem of develop a lumped model of the PAV mock-up technology, with *Modelica language*, to be used for the design of real-size PAVs.

The work-flow can be divided in three parts:

- Tritium permeation analysis through niobium membrane and PAV design for future DEMO reactor and a single PAV design for future DEMO reactor capable to withstand *outboard* and *inboard* constraints.
- Detailed thermo-hydraulic 3D model of the PAV mock up, that will be tested at ENEA-Brasimone, by means of CFD software STAR-CCM+. The model accounts for thermal radiation which is the only heat transfer mechanism between the tubes and the envelope.
- Characterization and validation of the lumped model against the permeation model and CFD results of the previous sections. The lumped model is based on the development of a single tube, named *RadiaTube*, able to account thermal radiation between different tubes and the envelope of the PAV. Multiple *RadiaTubes* are then assembled to model the PAV mock-up.

The lumped model should be capable of calculating the permeation of Tritium and the radiative heat exchange reproducing at the same time the hydraulic characteristic of the PAV.

## Chapter 2

# Permeation model for PAV

In this section the permeation model is presented along with the benchmark against two different publications. Once the model is confirmed to be reliable it used to size the PAV for the future WCLL DEMO reactor. The results of the former design, especially Tritium extraction efficiency, are used as starting point for the permeation lumped model characterization.

Tritium permeation in the PAV technology is driven by the different tritium partial across the solid high-permeability membrane. Outside the tubes, and inside the envelope, vacuum is maintained to guarantee maximum partial pressure gradient, see Fig. 2.1.

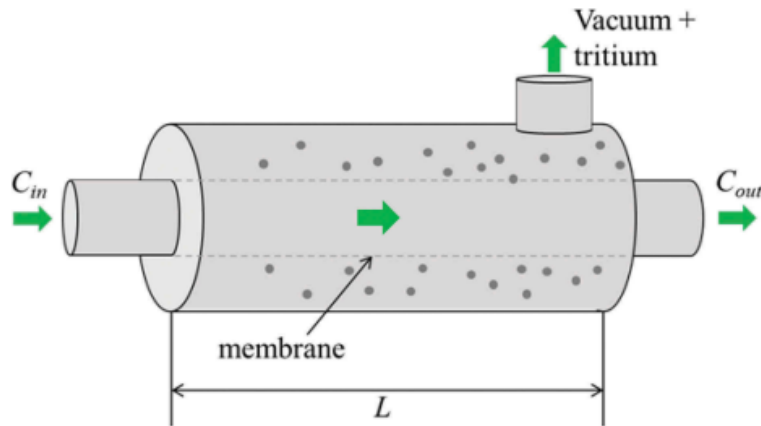


Figure 2.1: Schematic of Permeator Against Vacuum taken from [15].

## 2.1 The permeation model

Permeation of Tritium occurs in radial direction and it can be described with three transport process:

- Radial transport in liquid.
- Surface transport phenomena on the solid membrane.
- Bulk transport phenomena on the solid membrane.

*Radial transport in the fluid* is dictated by

$$J_T = K_T \cdot (C_{bulk} - C_{wall,liquid}) \quad (2.1)$$

where  $K_T$  is the mass transport coefficient and  $C$  is the Tritium concentration at the bulk and at the wall (liquid side).

The mass transfer coefficient  $K_T$  have the same units of a velocity, in fact it indicates how fast Tritium travels from the bulk to the wall. This coefficient is evaluated with the empirical correlation of the *Sherwood number*  $Sh$  provided by Harriott et al. in [8], reported here for simplicity

$$Sh = 0.0096 \cdot Re^{0.913} \cdot Sc^{0.346} \quad (2.2)$$

$Sh$  is the ratio of convective mass transfer rate over diffusion mass transfer rate (analogy with the  $Nu$  number with heat transport). Thus,  $Sh$  is given by

$$Sh = \frac{d_i \cdot K_T}{D_{PbLi}} \quad (2.3)$$

where  $d_i$  is the internal diameter,  $K_T$  the mass transport coefficient and  $D_{PbLi}$  the diffusivity constant of the liquid metal. Recalling that,  $Sc$  is the *Schmidt number*

$$Sc = \frac{\mu_{PbLi}}{\rho_{PbLi} \cdot D_{PbLi}} \quad (2.4)$$

with  $\mu_{PbLi}$ ,  $\rho_{PbLi}$  and  $D_{PbLi}$  the liquid metal viscosity, density and diffusivity respectively. BY inverse formula the  $K_T$  can be calculated as

$$K_T = \frac{D_{PbLi}}{d_i} \cdot 0.0096 \cdot \left( \frac{\rho_{PbLi} \cdot v \cdot d_i}{\mu_{PbLi}} \right)^{0.913} \cdot \left( \frac{\mu_{PbLi}}{\rho_{PbLi} \cdot D_{PbLi}} \right)^{0.346} \quad (2.5)$$

The driving phenomena to transport of (2.1), is the difference in Tritium concentration at the bulk  $C_{bulk}$  and at the wall  $C_{wall,liquid}$ . These concentrations are related to the partial pressure by *Sieverts' law*

$$C_T = K_S \sqrt{P_T} \quad (2.6)$$

where  $K_S$  is the solubility constant. The subscript liquid refers to the concentration on the liquid side of the *liquid-solid interface*, which is assumed in equilibrium with the solid-side of the interface according to

$$\frac{C_{T,liquid}}{C_{T,wall}} = \frac{K_{S,solid}}{K_{S,liquid}} \quad (2.7)$$

In the *bulk of the solid membrane* the transport mechanism is diffusion, governed by the *Fick's law equation* (2.8)

$$J = -D_{solid} \frac{\partial C}{\partial r} \quad (2.8)$$

Two permeation regimes can be identified based on the limiting transport mechanism across the solid membrane. The choice is made among a *Surface Limited Regime* (SLR) or *Diffusion Limited Regime* (DLR). In the first regime the surface phenomena are slower and then limits the permeation through the membrane, diffusion is much faster and can be neglected. On the other hand, in DLR, Tritium diffusion in the bulk of the membrane is much slower, thus, surface phenomena can be omitted being way faster compared to diffusion.

The permeation number  $W$ , defined in (2.9), allows to correctly select between those regimes.

$$W = \frac{K_r \cdot K_S}{D} \cdot t \cdot \sqrt{p_{T,b}} \quad (2.9)$$

where the constants refer to the Nb solid membrane, selected because an high-permeability material,  $t$  is the thickness of it and  $p$ , is the Tritium partial pressure in the bulk of the fluid.

The dimensionless number  $W$  can be seen as the ratio of surface phenomena over diffusive ones. When the system is characterized by an high diffusivity, the limiting permeation phenomena are found on the surfaces, in fact,  $W$  tends to be lower. On the other hand, when diffusivity is low, or the membrane thickness is large, diffusion becomes the limiting phenomena and  $W$  tends to higher values. More details on the regime found in [11] and [15], a sketch of the permeation regime is reported in Fig.2.2.

It results that, when  $W > 1$ , the system is better described by the diffusion-limited regime, while for  $W < 1$  the surface limited regime better



describes the permeation of Tritium across the membrane. The evaluated number of  $W$  follows in Table 2.1 for different operating temperatures.

Tritium distribution in radial direction and the mass balance performed on an infinitesimal liquid volume are reported in Fig.2.3.

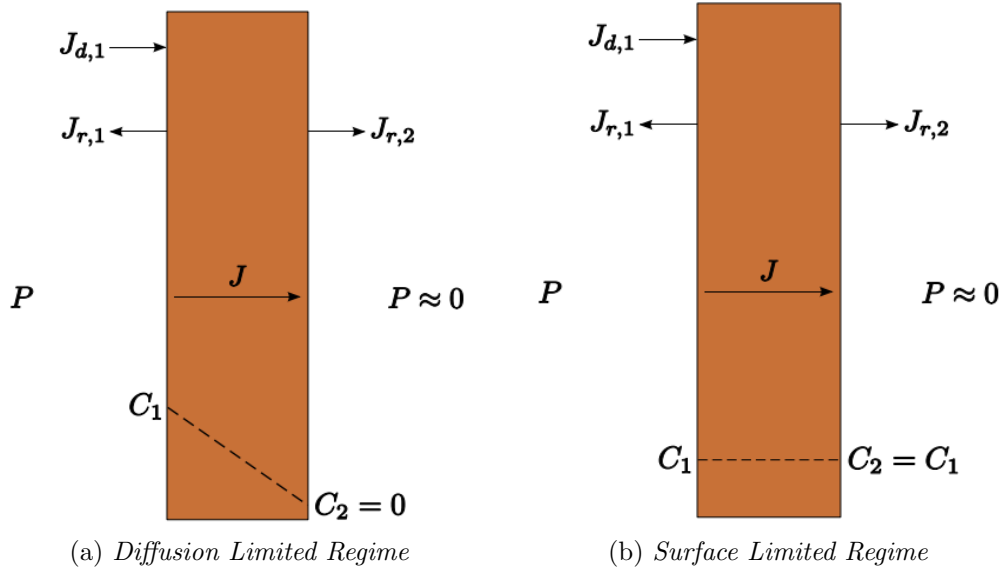
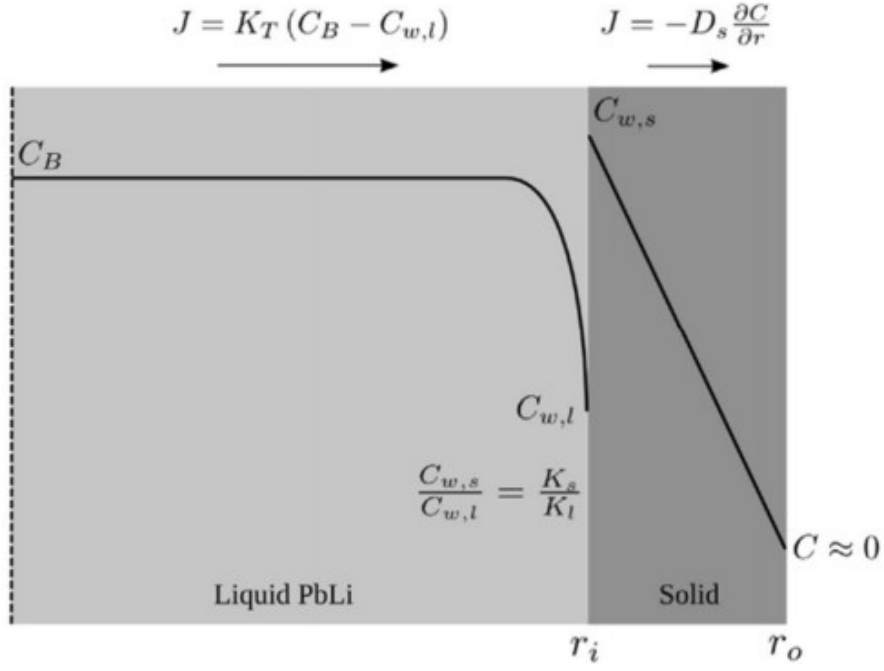


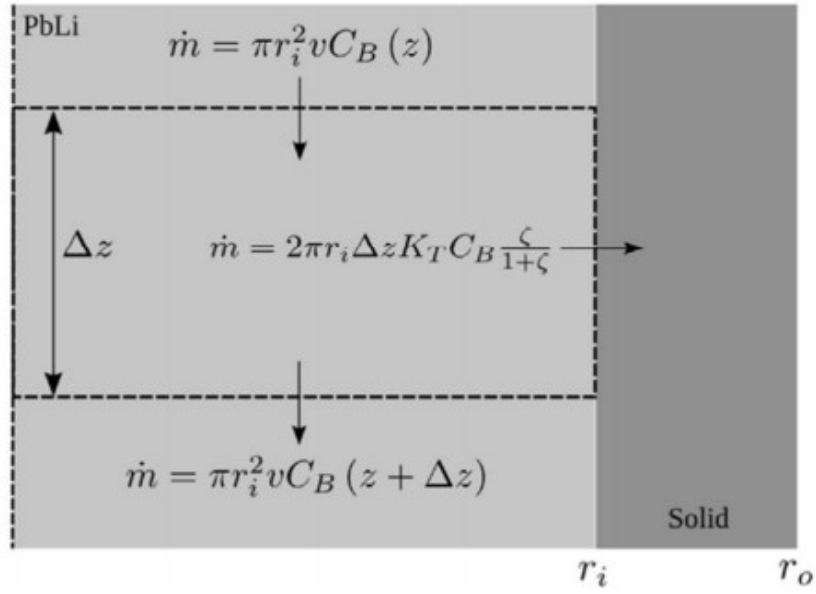
Figure 2.2: Different Permeation regimes.  $J$  is the permeated flux across the solid membrane.  $P$  is the partial pressure of the gas and  $C$  the concentration of the specie [12].

Table 2.1: Permeation number at different temperatures.

Temperature	W
330 °C	2.26
400 °C	1.18
500 °C	0.51



(a) Tritium radial distribution



(b) Tritium mass balance on infinitesimal liquid volume

Figure 2.3: Sketch of tritium transport-permeation phenomena, from [11].

Table 2.2: List of symbols of the permeation model.

Symbol	Parameter
$C$	Concentration
$J_T$	Tritium permeated flux
$v$	Velocity
$d$	Diameter
$K_T$	Tritium mass constant coefficient
$D$	Diffusivity constant
$K_{rec}$	Recombination constant
$K_S$	Solubility ( <i>Sieverts</i> ) constant

The Tritium concentration, and consequently the permeated flux, along the pipe can be retrieved from the following set of equation:

- Mass balance in fluid volume

$$\frac{\partial C_{bulk}(z)}{\partial z} = -\frac{4}{v \cdot d} \cdot J_T(z) \quad (2.10)$$

- Tritium transport in radial direction in the fluid

$$J_T = K_T \cdot (C_{bulk} - C_{wall,liquid}) \quad (2.11)$$

- Diffusion of tritium in the bulk of the membrane (DLR)

$$J_{diffusion} = \frac{2}{d \cdot \ln\left(\frac{d_o}{d}\right)} \cdot D_{solid} \cdot C_{wall,solid} \quad (2.12)$$

- Recombination/dissociation of tritium on the liquid-solid interface (SLR), more details found in [13] and [14]

$$J_{surface} = K_{rec,solid} \cdot C_{wall,solid}^2 \quad (2.13)$$

- Thermodynamic equilibrium at the liquid-solid interface

$$C_{wall,solid} = C_{wall,liquid} \cdot \frac{K_{S,solid}}{K_{S,liquid}} \quad (2.14)$$

The meanings of the adopted symbols are listed in Table 2.2.

In this work only results adopting DLR have been considered due the lack of literature on the SLR for systems with liquid-solid interface. Thus, the permeated flux in case of DLR is given in (2.15)

$$J_{T,DLR} = K_R \cdot C_{bulk} \left( 1 + \frac{1}{1 + \frac{D_{solid} \cdot K_{S,solid}}{K_T \cdot K_{S;liquid}} \cdot \frac{2}{d \cdot \ln\left(\frac{d_o}{d}\right)}} \right) \quad (2.15)$$

And the Tritium concentration along axial direction is given by applying a *Forward Euler Approximation method* on (2.10), resulting in (2.16)

$$C_{T,b}(z_{n+1}) = C_{T,b}(z_n) - \frac{2 \cdot \Delta z}{r_i \cdot v} \cdot J_T(r_i, z_n) \quad (2.16)$$

## 2.2 Benchmark

In order to validate the permeation model in the diffusion limited regime the results presented in the work of Garcinuño et al. [16] were considered. In the geometrical set-up in [16], PbLi flows in squared channels characterized by a height  $h$ , and Tritium permeates across them, see Fig.2.4.

In the model developed here, PbLi flows in circular pipes, thus, tritium permeates in the radial direction. Eventually a comparison with results was performed evaluating the efficiency as function of  $h$  [16] and  $d$  (this work). The results are reported in Fig.2.5, showing a good agreement in shape but a slightly overestimation in the results of this work probably due the different geometries.

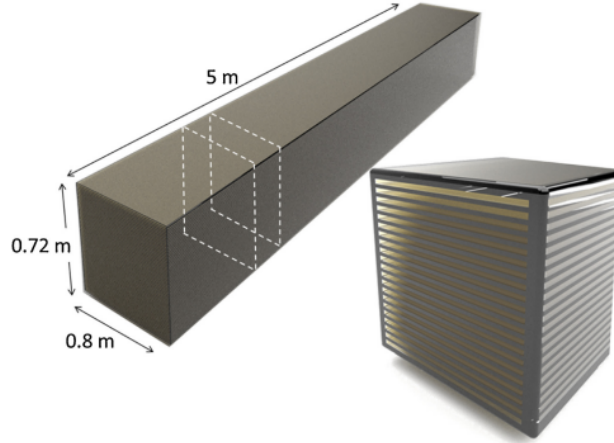
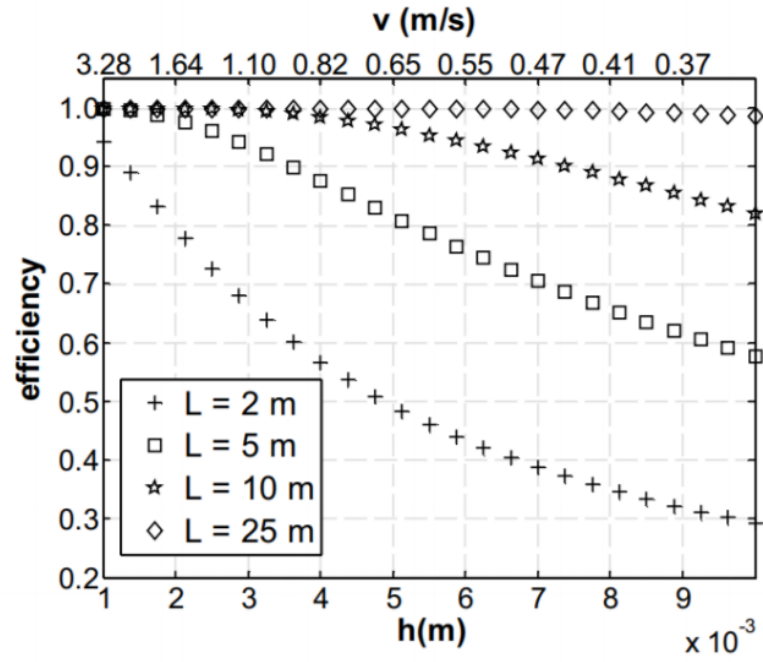
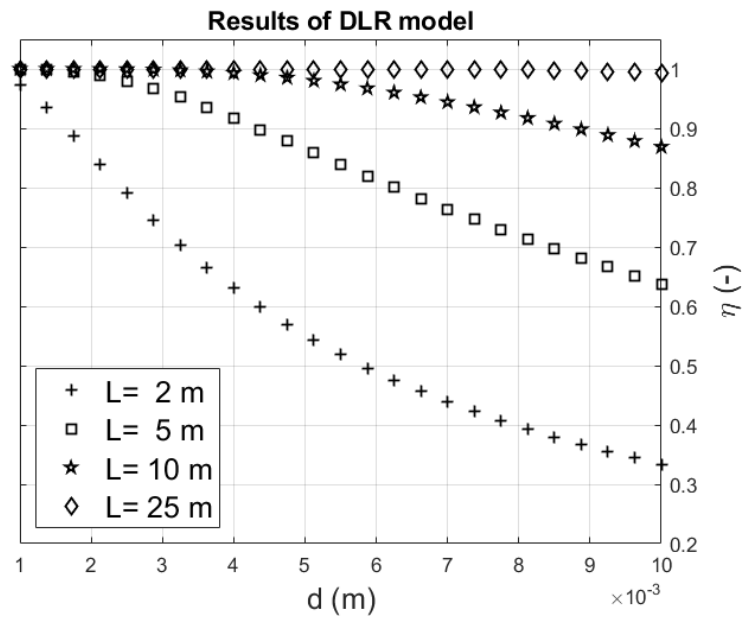


Figure 2.4: Left) Overall PAV design showing the length (L), width (a) and total height (H). Right) Detailed view of PbLi flowing channels (not real dimensions), from [16].



(a)



(b)

Figure 2.5: Efficiency computed using the DLR model as function of a) height of channels in [16] and b) diameter of tubes in this model.

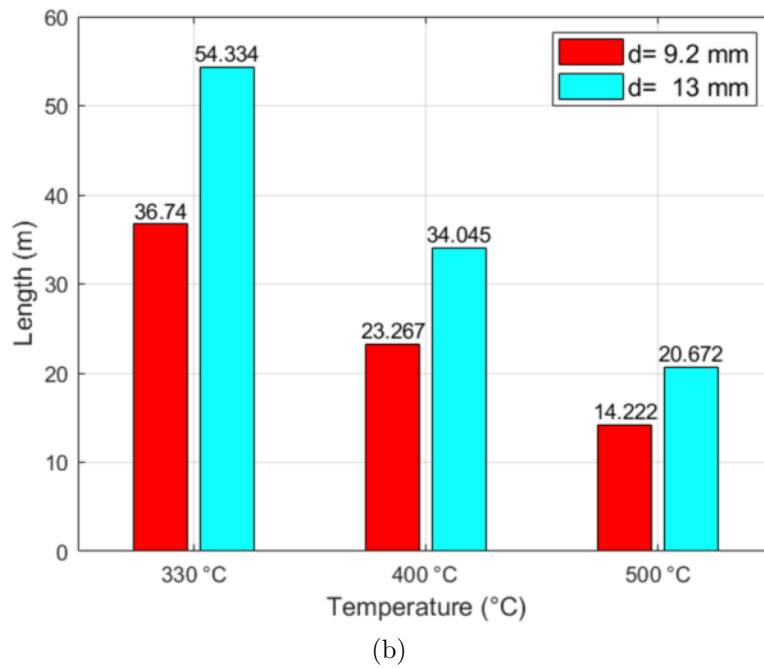
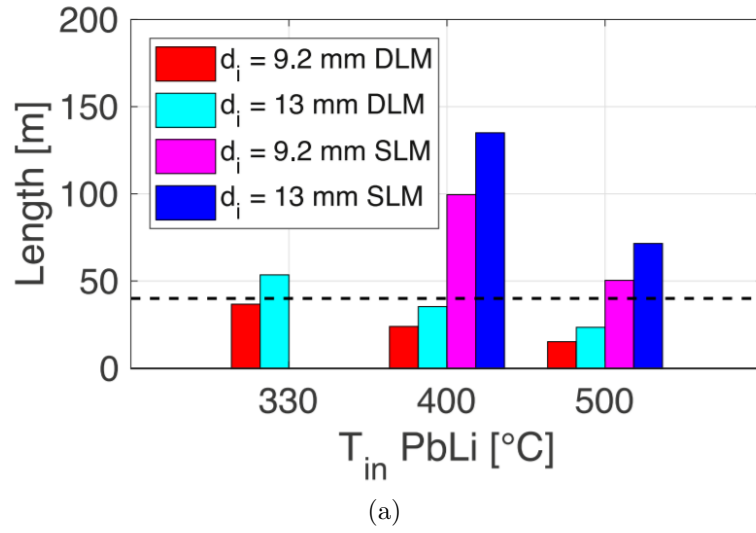


Figure 2.6: Required length to reach efficiency of 90% at different values of internal diameter. (a) Results of Bonifetto et al. [17] and (b) the results of the model of this work.

A second benchmark has been performed against the results presented by Bonifetto et al. [17] which work with a cylindrical geometry. The same mass flow rate and number of pipes has been adopted. The results are reported in Fig.2.6, considering that the dashed line in Fig.2.6a is located at 40 *m* a rough comparison can be made stating that the results are quite similar.

## 2.3 Sizing of PAV unit for DEMO reactor

Once the model is properly benchmarked against other works, a set of result is retrieved. In particular, the design of a modular PAV unit (PAVU), to be used in to be used in parallel configurations, which could serve both the *Inboard* (IB) and the *Outboard* (OB) BB loops. The number of lines in parallel for such modular PAVU for the OB and IB loops have been computed, exploring two possible alternatives for the pipe diameter within the PAVU. Different inlet temperature value for the PbLi have been parametrically explored, to check the robustness of the design.

Table 2.3: Design constraints for PAV unit.

Parameter	Value	Units
Maximum overall height of PAV	10	[ <i>m</i> ]
Maximum allowable Pressure drops	2	[ <i>bar</i> ]
Efficiency	80%	
Reynolds number in the pipes	$10^4 < Re < 10^5$	[–]

Table 2.4: Design operating conditions taken from [30].

Parameter	Value	Units
Total $\dot{m}_{PbLi}$ Outboard	1127	[ <i>kg/s</i> ]
Total $\dot{m}_{PbLi}$ Inboard	499	[ <i>kg/s</i> ]
PbLi Temperature	330 – 400 – 500	[°C]
Tritium partial pressure ( inlet of PAV)	200	[ <i>Pa</i> ]
Membrane thickness	$4 \times 10^4$	[ <i>m</i> ]
Internal diameter	$9.2 - 13 \times 10^{-3}$	[ <i>m</i> ]

The flowchart in Fig.2.7 represents the work flow of the design process.

In Fig.2.8 the results concerning operating temperature at 330 °C, accounting for all constraints in Table 2.3 are presented. The same plot have

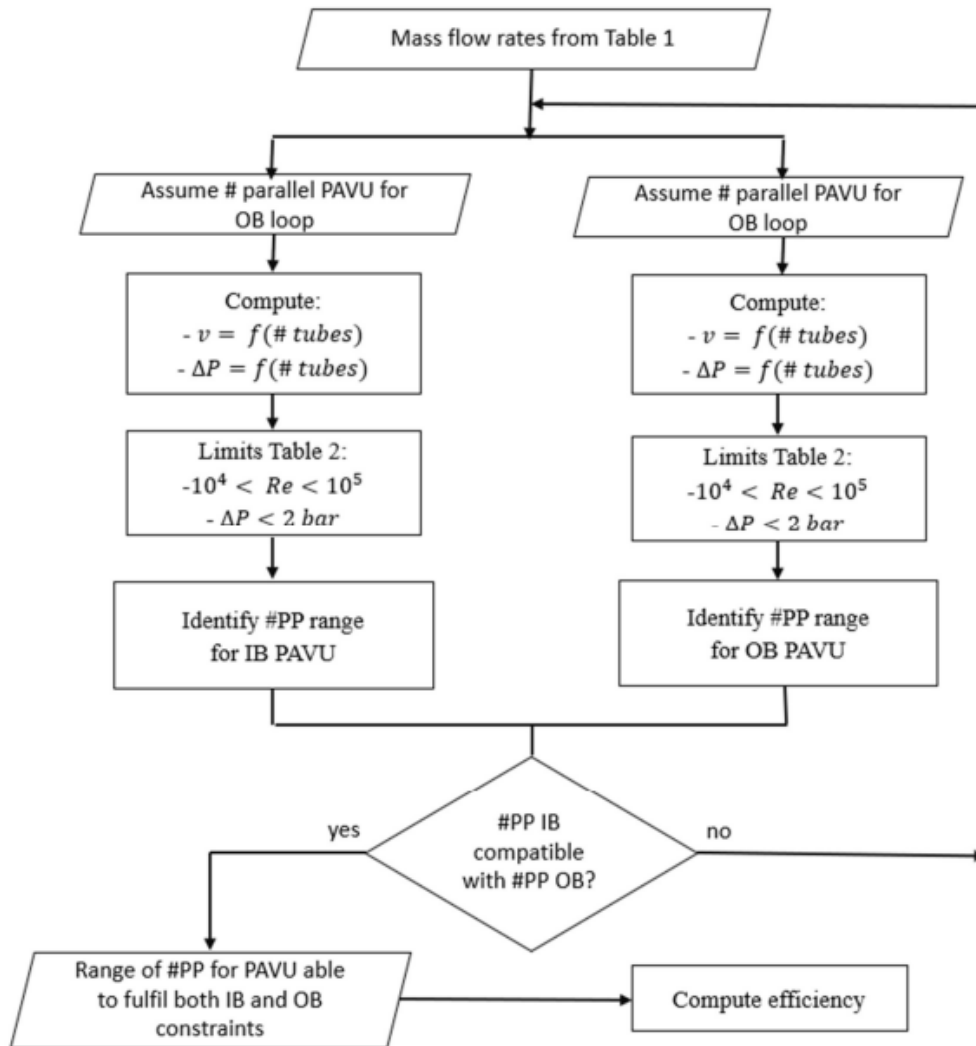


Figure 2.7: Flow chart of the design process of PAV unit. To be noted that Table 1 and Table 2, mentioned in the flow chart, refers to Table 2.4 and Table 2.3 respectively.



been carried out at different operating temperatures (400 and 500 °C). The yellow area in the plot identifies the number of *parallel pipes* (PP) that satisfies either OB or IB constraints only, while, the green regions identifies a common range of PP. In Fig.2.9.

The extraction efficiency  $\eta$  as function of tubes length is calculated as:

$$\eta = 1 - \frac{C_{out}}{C_{in}} \quad (2.17)$$

where  $C_{in}$  and  $C_{out}$ , refer to the inlet and outlet tritium concentration in the tubes. Among the proposed solubility constants for H/D/T, see Fig. 2.5, the ones suggested by Aiello provide the most pessimistic results. In Fig.2.10 the extraction efficiency computed with Aiello is plotted as function of tube length, at different operating temperature. The target efficiency is reached even in the worst case scenario (lower temperature with Aiello's constant) only in the design adopting tubes with internal diameter equal to 9.2 mm while for the 13 mm design it is reached at higher temperatures. Complete analysis found in [31].

Table 2.5: Solubility constant of hydrogen isotopes in PbLi according different authors.

Isotope	Formula	Units	Ref
H	$2.44 \times 10^{-8} \exp(-1350/R/T)$	$[atomic\ fr \cdot Pa^{-0.5}]$	Reiter [9]
T	$2.32 \times 10^{-8} \exp(-1350/R/T)$	$[atomic\ fr \cdot Pa^{-0.5}]$	Reiter [9]
H	$0.237 \exp(-12844/R/T)$	$[mol \cdot Pa^{-0.5} \cdot m^{-3}]$	Aiello [10]

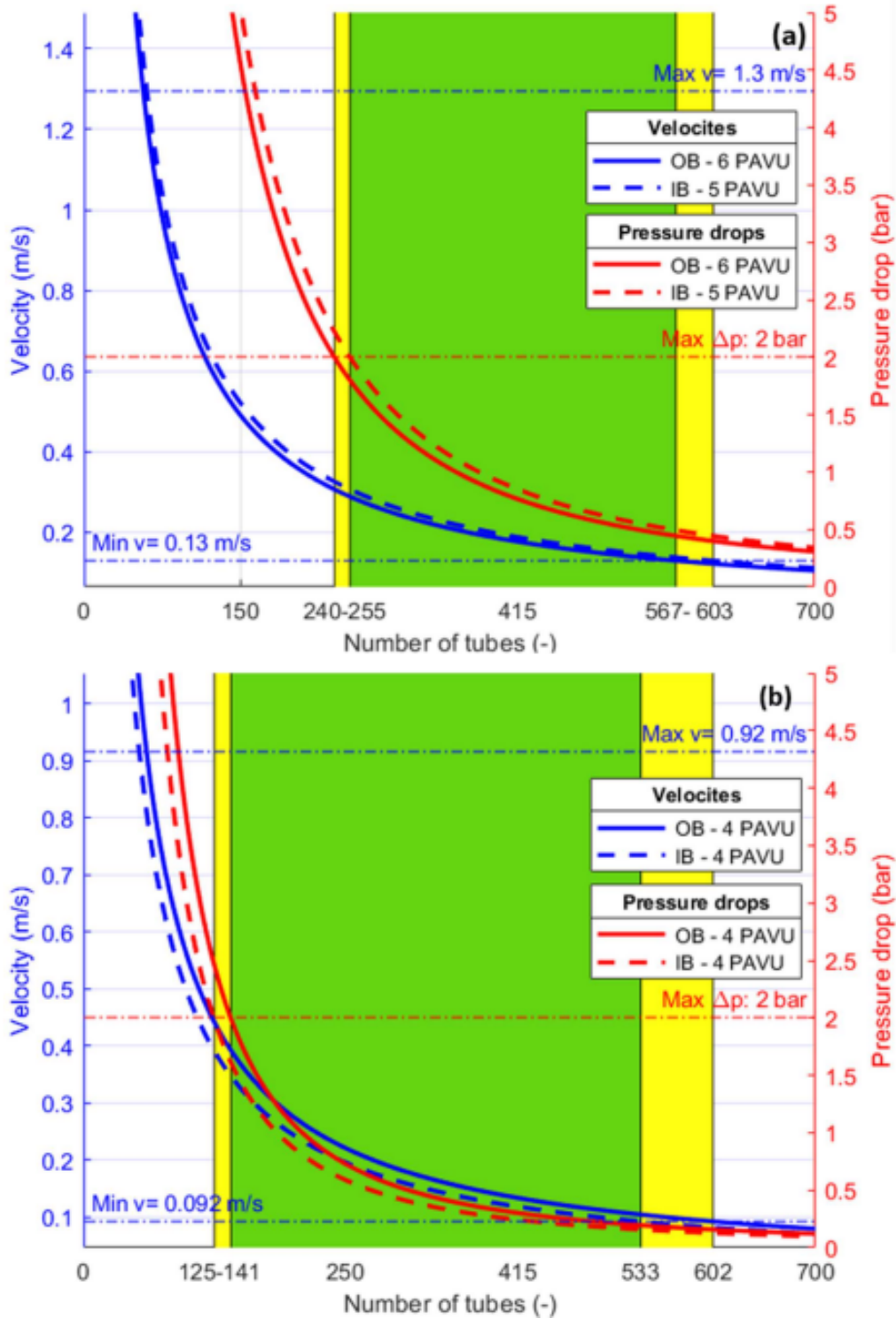
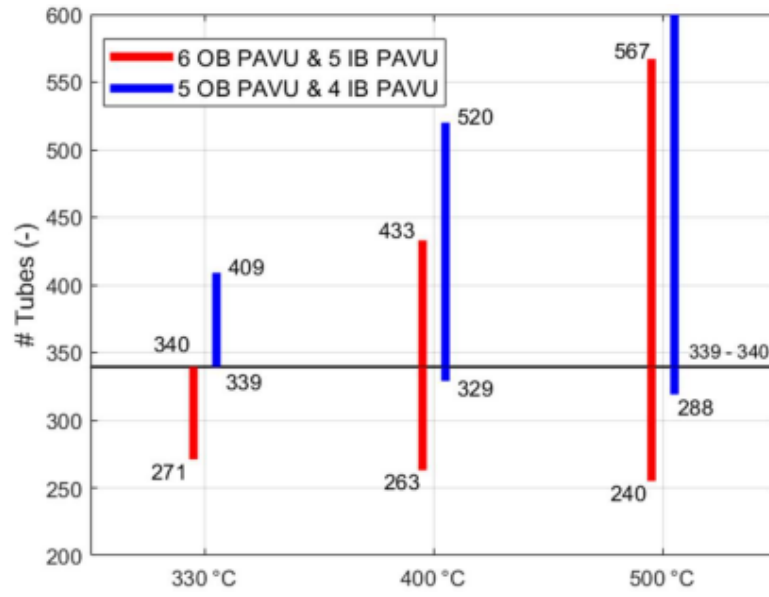
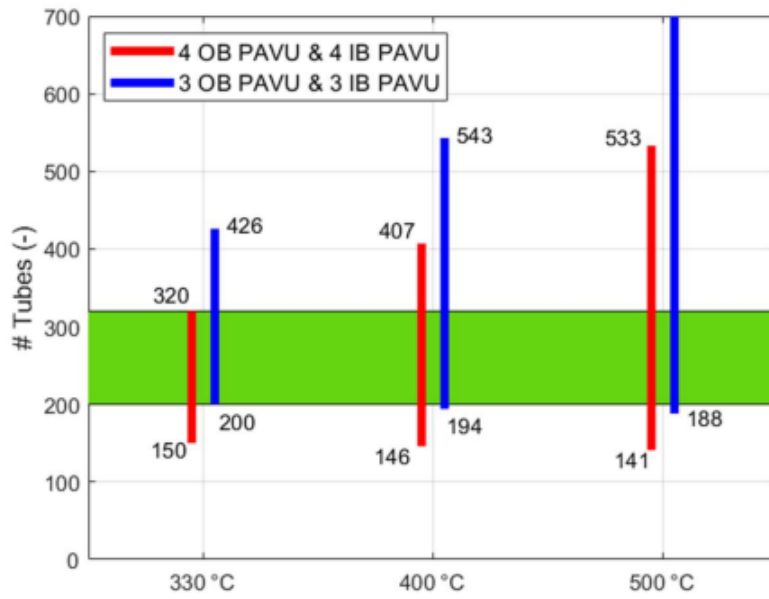


Figure 2.8: Results obtained with the DLR at a PbLi inlet temperature of 330 °C. Velocity, in blue, and pressure drop, in red, as function of the number of tubes with tube diameter of 9.2 mm (a) and 13 mm (b), respectively. Horizontal dashed lines represent design constraints. The # PP shaded in yellow refers to only one of IB or OB, while that in green refers to a range common to both.

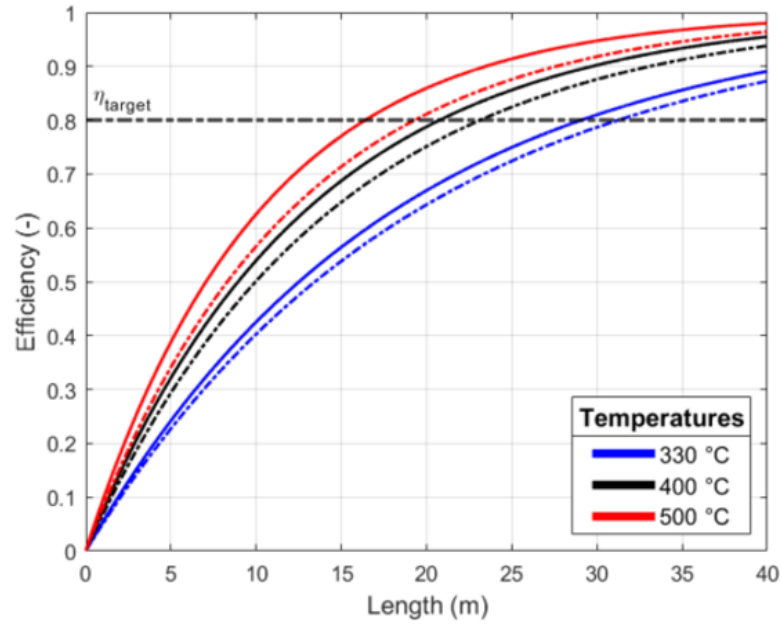


(a)

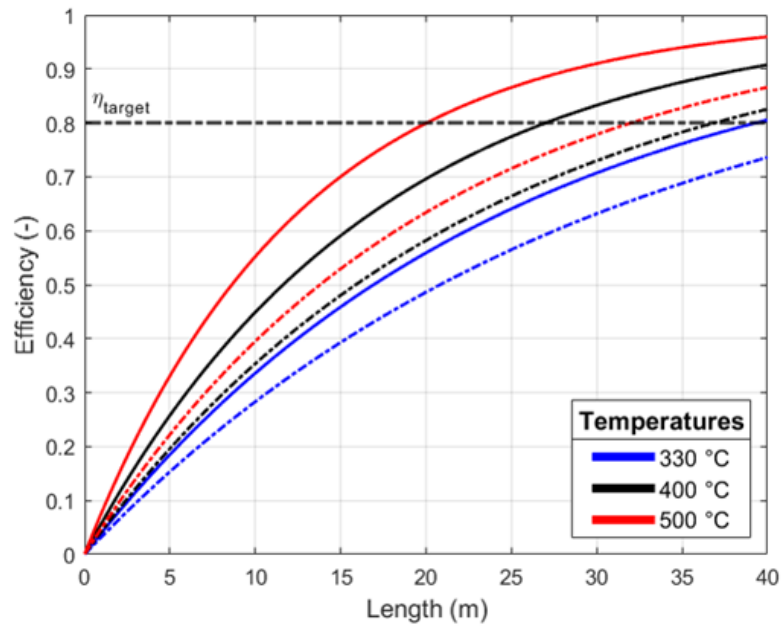


(b)

Figure 2.9: Ranges of tubes at different number of PAVU per OB and IB loop with 9.2 mm design (a) and with 13 mm design (b). Red color refers to normal condition (no PAVU unavailability), blue color refers to one unavailability for each loop. In green the common range of # PP at different temperatures.



(a)



(b)

Figure 2.10: Efficiency along the tubes computed with Aiello's solubility constant for H, at 9.2 mm (a) and at 13 mm (b). Solid and dashed line refers to maximum and minimum allowable number of tubes identified in the previous part of the analysis.

# Chapter 3

## CFD model for PAV mock-up

This section presents the calculations regarding the hydraulic and thermal analyses performed on the 3D PAV mock-up. The simulations have been carried out using the commercial software STAR-CCM+ [20], solving the problem of 3D conjugate heat transfer in the entire mock-up with a *segregated* solver. More details can be found in [23].

### 3.1 Geometry

Geometrically, the PAV mock-up is structured as a tube-and-shell heat exchanger, as shown in Fig.3.1. It is composed by a cylindrical vessel with 16 niobium U-tubes, the membranes for hydrogen permeation, welded on a F22 plate. This material has been chosen for his corrosion resistance in LiPb environments. A medium vacuum is pumped in the vessel while the LiPb flows in the niobium pipes. The LiPb is distributed into the niobium pipes by a collector which constitutes the lower part of the PAV. The collector is divided in three parts; each part is connected with one pipe in P22, which connects the mock-up with the LiPb loop of the facility. The three pipes are:

- the inlet pipe;
- the discharged pipe;
- the outlet pipe.

The inlet pipe is connected with the part of the collector that allows the LiPb distribution in the first 8 niobium tubes. This part is indicated in red in Fig.3.1b. The discharge pipe is connected with the part of the collector (called mixing collector) where the LiPb coming out from the first 8 niobium tubes mixes. From this section of the collector, indicated in yellow

Table 3.1: PAV mock-up main dimensions.

Dimensions	[mm]
Height of the vessel	1106.00
External diameter of the vessel	323.85
Thickness of the vessel	6.35
	1805.25 (S)
Length of the pipes	1899.5 (M)
	1993.74 (L)
External diameter of the Nb pipes	10.00
Internal diameter of the Nb pipes	9.20
Pitch of the Nb pipes	30.00
Height of the LiPb collector	156.00
Thickness of the plate	38.00
External diameter of the P22 pipes (inlet/outlet LiPb)	33.40
Thickness of P22 pipes (inlet/outlet LiPb)	3.38
External diameter of the draining pipe	21.34
Thickness of the draining pipe	2.77

in Fig.3.1b, the LiPb is distributed in the remaining 8 niobium tubes. The discharge pipe is needed to allow the gravity draining of the mixing collector. The outlet pipe is connected with the section of the collector, indicated in red in Fig.3.1b, where the LiPb coming out from the last 8 niobium tubes mixes before leaving the mock-up. Therefore, LiPb will double pass through the vessel, as shown in Fig.3.1c and 3.1d.

The main dimensions of the mock-up, adopted for the CAD geometry are reported in Table 3.1 and the operating conditions are reported in Table 3.2.

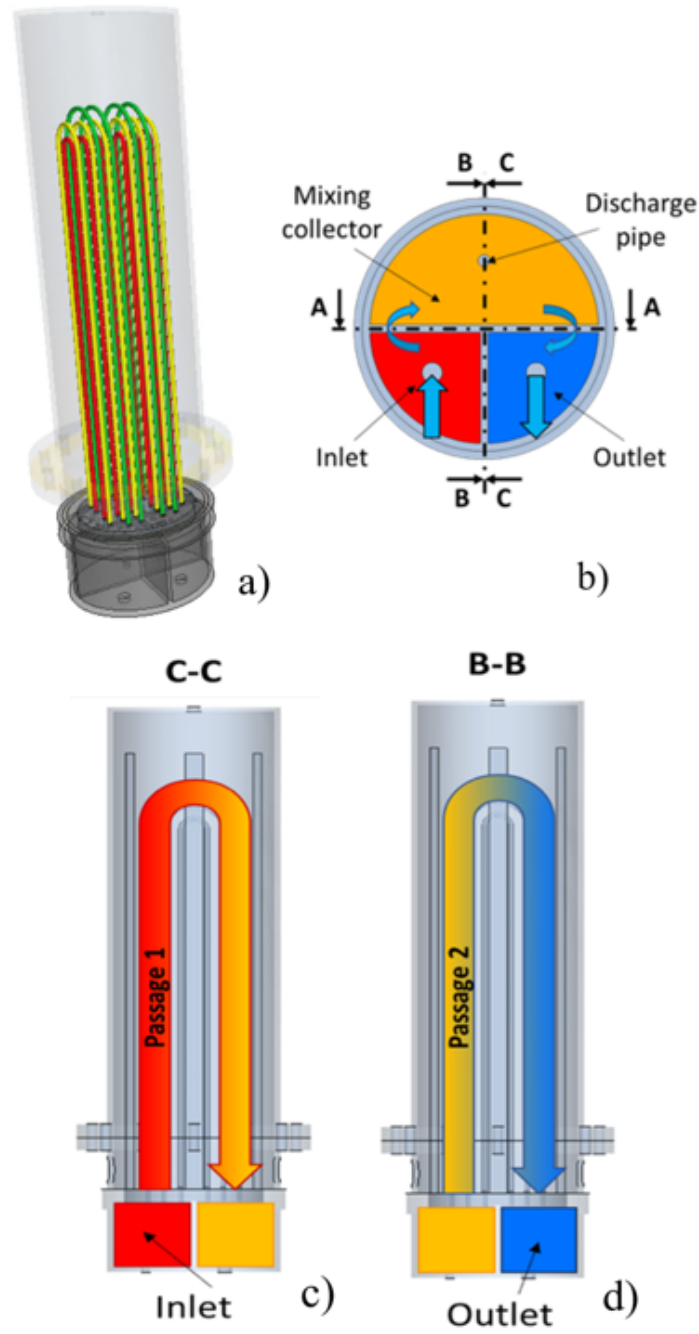


Figure 3.1: Sketches of the PAV mock-up: (a) simplified sketch of the cylindrical vessel with the 16 niobium U-tubes: Long pipes (L) in green, medium-length pipes (M) in yellow and short pipes (S) in red; (b) horizontal section of the PAV collector showing its 3 parts and the connecting pipes; (c) vertical section of the PAV showing the first passage of LiPb through the vessel; (d) vertical section of the PAV showing the second passage of LiPb through the vessel.

Table 3.2: PAV mock-up operating conditions.

Parameter	Value	Unit
Operative internal pressure of the vessel	$10^{-1} \div 10^5$	[Pa]
Max internal pressure of the vessel	$1.1 \cdot 10^5$	[Pa]
Max internal pressure of the Nb pipes	$4 \cdot 10^5$	[Pa]
Max internal pressure of the LiPb collector	$5 \cdot 10^5$	[Pa]
Max temperature of the collector	530	[°C]
Max temperature of the Nb pipes	500	[°C]
Max temperature of the vessel	100	[°C]
Operative LiPb temperature	$350 \div 500$	[°C]
Max speed of LiPb in the Nb pipes (at 4.6 kg/s)	0.97	[m/s]
Total flow rate of LiPb in the Nb pipes	$0.2 \div 4.5$	[kg/s]
Vessel filling gas (during long stops)	Helium	[–]

Table 3.3: PAV mock-up material properties.

Material	Property	Value	Units	Ref
Nb	Density	8570.00	[kg/m <sup>3</sup> ]	[28]
	Specific Heat	290.00	[J/kg/K]	
	Thermal conductivity	57.00	[W/m/k]	
SS304	Density	7800.00	[kg/m <sup>3</sup> ]	[25]
	Specific Heat	560	[J/kg/K]	[26]
	Thermal conductivity	21.5	[W/m/k]	[27]

## 3.2 Continua

The PAV mock-up is made of stainless steel SS 304, while the membrane of the tubes are made of niobium and the fluid is, of course, PbLi. The properties of the materials are summarized in Table 3.3.

To ease the set-up of the simulation, constant values have been used where possible, referring to the values around operating temperature. The default value for *turbulent Prandtl number* of PbLi, proposed by STAR-CCM+, was 0.9. Being PbLi an heavy material, the turbulent Prandtl number has been changed to 4.12 according to (3.1) from [19]

$$Pr_t = \begin{cases} 4.12 & Pe \leq 1000 \\ \frac{0.01 \cdot Pe}{[0.018 \cdot Pe^{0.8} - (7-A)]^{1.25}} & 1000 \leq Pe \leq 6000 \end{cases} \quad (3.1)$$



Table 3.4: PbLi properties from [29].

Property	Expression
$\rho \left[\frac{kg}{m^3}\right]$	$10520.35 - 1.19 \cdot T [K]$
$c_p \left[\frac{J}{g \cdot K}\right]$	$0.195 - 9.116 \times 10^{-6} \cdot T [K]$
$\alpha \left[\frac{cm^2}{s}\right]$	$3.46 \times 10^{-4} \cdot T [K] - 0.105$
$k \left[\frac{W}{cm \cdot K}\right]$	$0.145 + 1.963 \times 10^{-4} \cdot T [^\circ C]$
$\mu [Pa \cdot s]$	$6.11 \times 10^{-3} - 2.26 \times 10^{-5} \cdot T + 3.77 \times 10^{-8} \cdot T^2 - 2.29 \times 10^{-11} \cdot T^3$

where

$$A = \begin{cases} 4.5 & Pe \leq 1000 \\ 5.4 - 9 \times 10^{-4} \cdot Pe & 1000 \leq Pe \leq 2000 \\ 3.6Pe \geq 2000 \end{cases} \quad (3.2)$$

and  $Pe = Re \cdot Pr$ .

The hydraulic and thermal results have not been affected by that change, this may be due to the low turbulence of the fluid regime.

### 3.3 The mesh

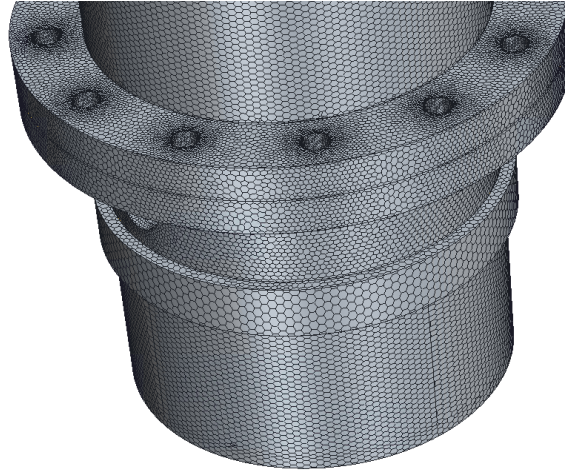
In this section the mesh developed to describe the mock-up geometry is presented. The types of mesh adopted are:

- Surface mesher;
- Polyhedral mesher;
- Thin mesher;
- Prism layer mesher;

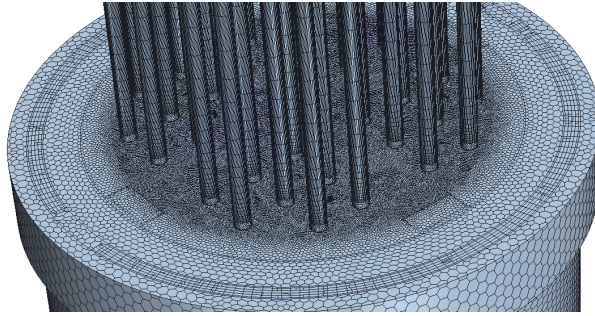
and the total number of cells resulted to be 4.5 MCells.

#### Fluid domain mesh

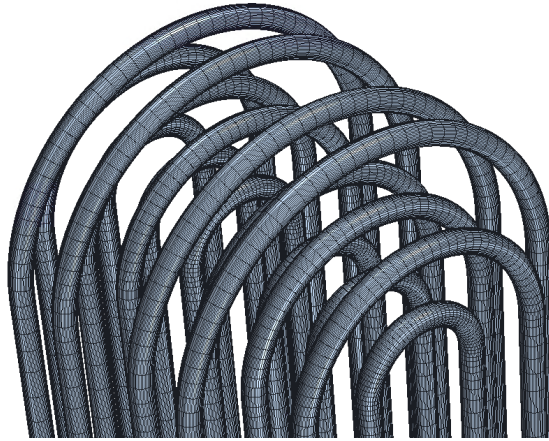
The mesh base size adopted for the fluid domain is 10 *mm* but a significant refinement (to 1 *mm*) is needed for the bulk fluid, near the inlets and outlets of Nb tubes, to properly account for the entrance and jet effects, visible in Fig.3.3. This refinement is shown in Fig. 3.5c.



(a)



(b)



(c)

Figure 3.2: Grid developed for the 3D CFD simulations of the PAV mock-up. (a) External view of the PAV, detail on the bottom part. (b) Detail on the connection tubes-manifold where the refinement can be appreciate. (c) Detail on the bends of the Tubes.

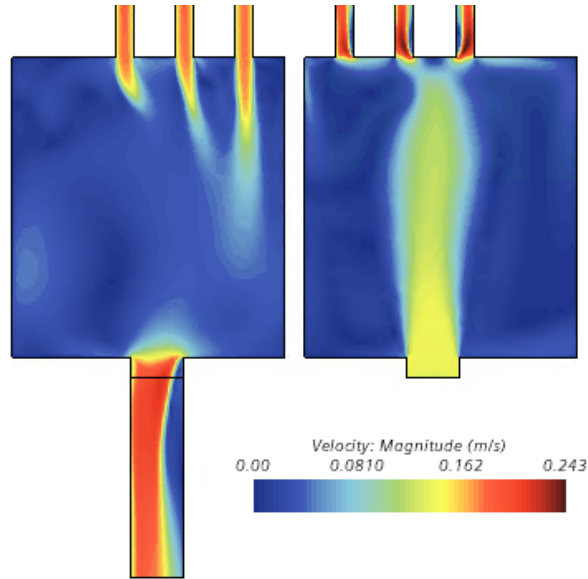


Figure 3.3: Section view of inlet (on the right) and outlet (on the left) manifolds. Highlight of jet effects at the inlet and at the outlet of the tubes.

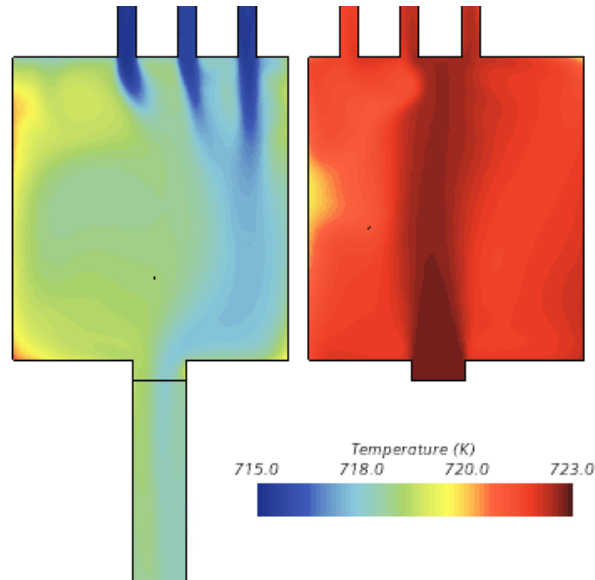


Figure 3.4: Section view of inlet (on the right) and outlet (on the left) manifolds. Highlight of temperature field at the inlet and at the outlet of the tubes.

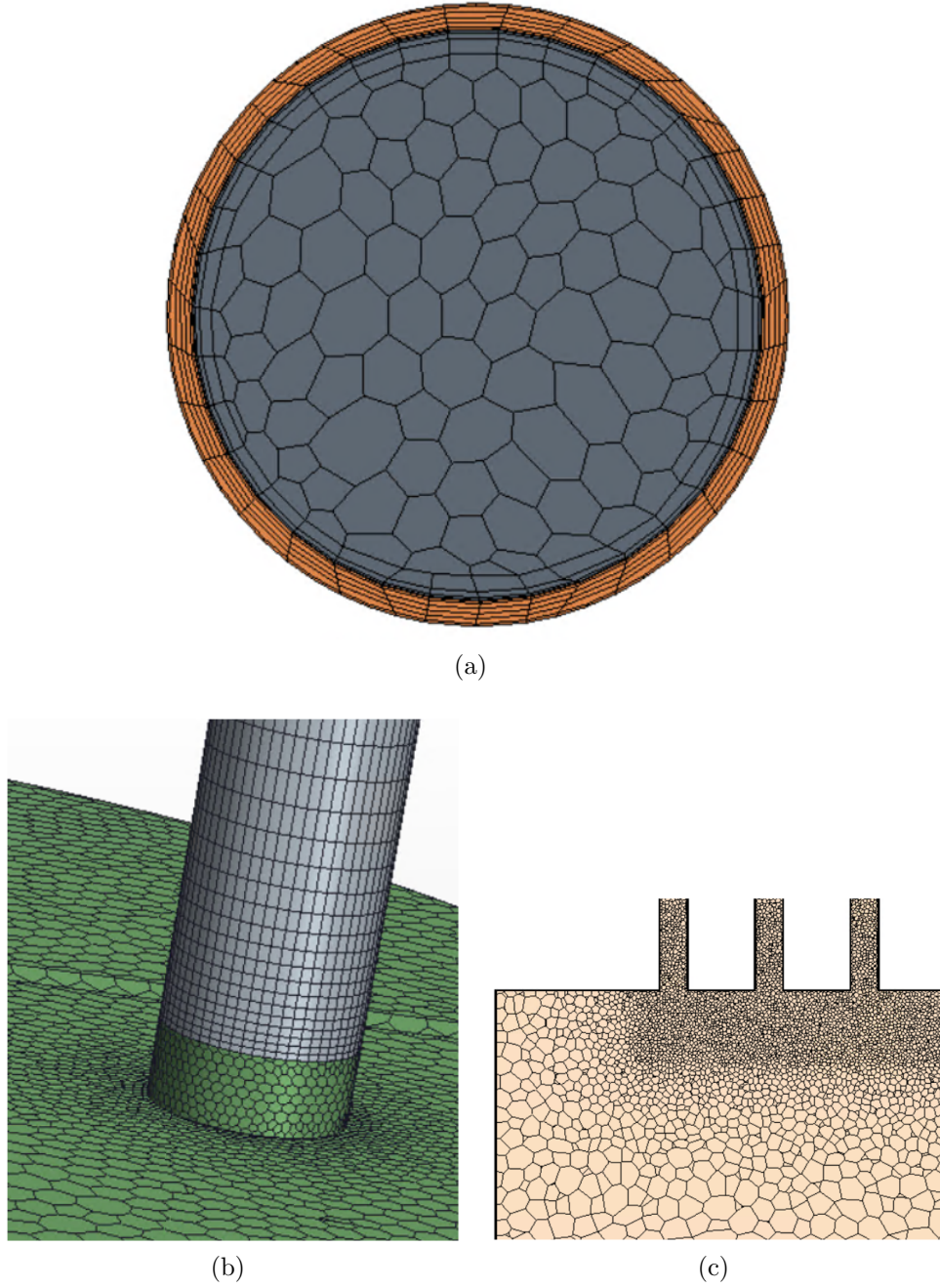


Figure 3.5: Details on the mesh. Detail on tubes in (a) with fluid domain in grey and solid domain in orange. Detail on tubes extrusion in (b) with fluid tube domain in grey and fluid manifold domain in green. Detail on bulk refinement in (c).

Treating a turbulent flow regime in the tubes, prismatic layers at the wall were adopted. The number of layers was set to four, allowing a good solution of the Navier-Stokes equations in the boundary layer, it can be appreciated in Fig.3.5a.

In the Nb tubes, an extruded mesh with element of 45 mm is used. The mesh guarantees continuity in cell size at the interfaces as reported in Fig.3.5b where the size of the extrusion starts with the size of the manifold cell size up to 45 mm.

### Solid domain mesh

For the solid computational domain, the mesh is made by a mix of polyhedral cells in thick regions, and prismatic cells, in thin regions, with a base size that locally matches the fluid one.

The *Surface mesher* and the *Polyhedral mesher* was adopted in the automated mesh for the solid region with a base size of 10mm

The *Thin mesher* creates a prismatic type mesh for the areas that are recognized as thin and the bulk areas are meshed with the core volume mesher that is selected. It creates a conformal mesh between any concurrent parts that are included in the same Automated mesh operation. This mesher is adopted for the PAV envelope and for the Nb membrane, the number of thin layers was set to 6 as shown in the orange region in Fig.3.5a.

## 3.4 Hydraulic analysis

The LiPb flow distribution among the different pipes have been computed to check the homogeneity of the flow distribution: a severe flow unbalance, causing a deviation from the average speed, would affect the extraction efficiency.

The LiPb flow in the tubes is in turbulent conditions for the entire range of operational mass flow rate. A two-equation Reynolds-averaged Navier-Stokes (RANS)  $k - \omega$  SST model is adopted in the simulations, with an all-y + wall treatment.

### k-Omega SST model

The k-Omega turbulence model is a two-equation model that solves transport equations for the turbulent kinetic energy  $k$  and the specific dissipation rate  $\omega$  in order to determine the turbulent eddy viscosity.

The advantage of k-Omega model over k-Epsilon model is its high performance under adverse pressure gradients in the boundary layer without requir-

ing further modification. While, the big disadvantage is that the boundary layer computations is strongly affected to the values of  $\omega$  in the free-stream, thus extreme sensitivity to inlet boundary conditions for internal flows.

This problem was addressed by Menter [21], who transformed the Standard  $\epsilon$  transport equation in the k-Epsilon model into an  $\omega$  transport equation by variable substitution. This transformation adds a non-conservative cross-diffusion term containing the dot product  $\nabla k \cdot \nabla \omega$ . Menter suggested using a blending function that would include the cross-diffusion term far from walls, but not near the wall. This approach effectively blends a k-Epsilon model in the far-field with a k-Omega model near the wall. Menter also introduced a modification to the linear constitutive equation and named the model containing this modification the SST (shear-stress transport) k-Omega model.

### Results of the hydraulic analysis

The flow repartition among different tubes is reported in Fig. 3.6a. It is close to the average value within  $< 5\%$  for different values of the mass flow rates giving an acceptable homogeneity of the speed. Values of maximum speed around  $0.5 \text{ m/s}$  could be achieved with mass flow rates of  $2\text{--}2.5 \text{ kg/s}$ . Note that the maximum difference in velocities among the tubes remains below  $0.1 \text{ m/s}$  at the higher total flow rate,  $4.5 \text{ m/s}$ , which corresponds to the worst flow distribution.

As expected, the flow repartition shows a slightly lower flow rate in the longest channels, while the shortest channels have, on average, the largest flow rate. This is especially true for the second pipe passage, while the first passage is affected by some jet effects from the inlet pipe that affects, in particular, the central pipes, as shown in Fig. 3.7.

The pressure drop of the whole PAV mock-up is plotted in Fig. 3.8. While, concerning the characterization of each tube, the friction factors of each tube, at different total mass flow rates, have been gathered in Fig. 3.9 and by means of *power law fitting*, the friction factor as function of Reynolds number can be expressed by:

$$FF = 0.2413 \cdot Re^{-0.235} \quad (3.3)$$

where  $FF$  is the friction factor of the tubes. To obtain the friction factor the following method was adopted:

- Take pressure drop of each U-tube from the CFD simulation at different total mass flow rates in the range  $0.2 \div 4.5 \text{ [kg/s]}$ .
- Compute linear pressure drop by dividing from the length of each tube, for tube length refer to 3.1.



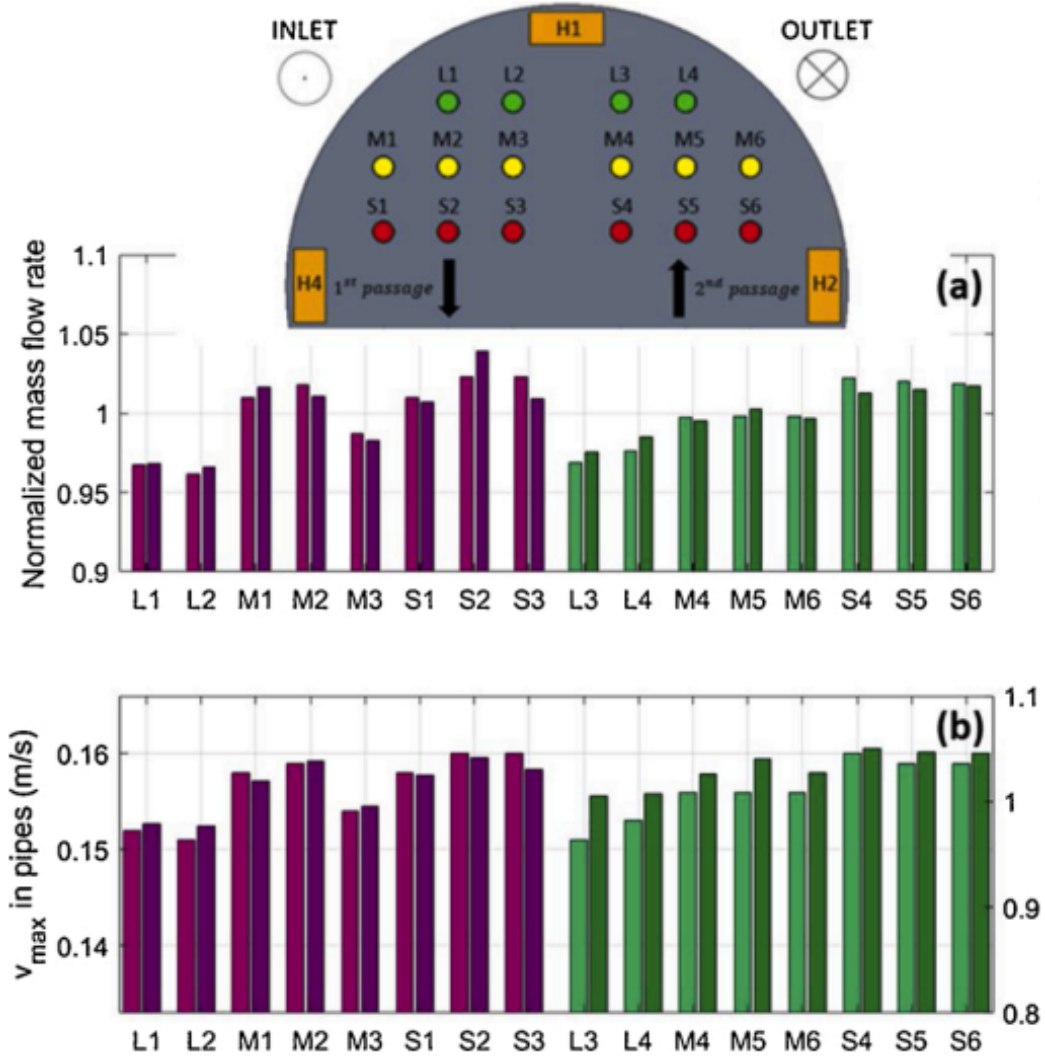


Figure 3.6: (a) Mass flow rate repartition among the mock-up pipes, normalized to the average value and (b) maximum speed in the pipes (first passage: pipes L1-L2, M1-M3, S1-S3, see inset, and second passage: pipes L3-L4, M4-M6, S4-S6), for the total mass flow rate of 0.75 kg/s (light bars) and 4.5 kg/s (dark bars). In (b), the dark bars refer to the right axis.

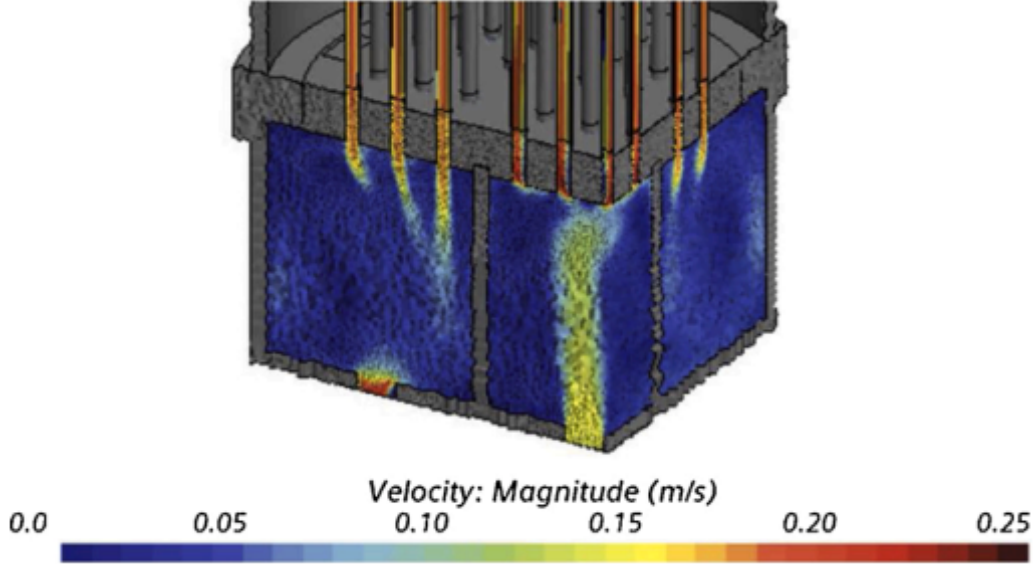


Figure 3.7: Flow field computed in the manifolds, for a mass flow rate of  $0.75 \text{ kg/s}$ .

- By inverse formula (3.4) compute the friction factor.

$$FF = \frac{2}{16} \cdot \pi^2 d^5 \cdot \rho \frac{\Delta P}{l} \cdot \frac{1}{\dot{m}^2} \quad (3.4)$$

- Express friction factors as function of Re number by substituting the mass flow rate

$$m = \frac{4 \cdot \dot{m}}{\pi \cdot \mu \cdot d} \quad (3.5)$$

- Fitting of the results, Fig.3.9.

The adopted symbols refer to: mass flow rate  $\dot{m}$ , pressure drop  $\Delta P$ , viscosity  $\mu$ , internal diameter  $d$  and density  $\rho$ .

### 3.5 Thermal analysis

The steady-state thermal-fluid analysis of the entire mock-up has been performed in the most conservative case (higher LiPb temperature) imposing a uniform temperature of  $450 \text{ }^\circ\text{C}$  ( $723 \text{ K}$ ) on the outer surface of the manifolds, while allowing convective and radiative heat transfer from the vessel to the environment, assumed at  $15 \text{ }^\circ\text{C}$  ( $288 \text{ K}$ ), with a heat transfer coefficient of



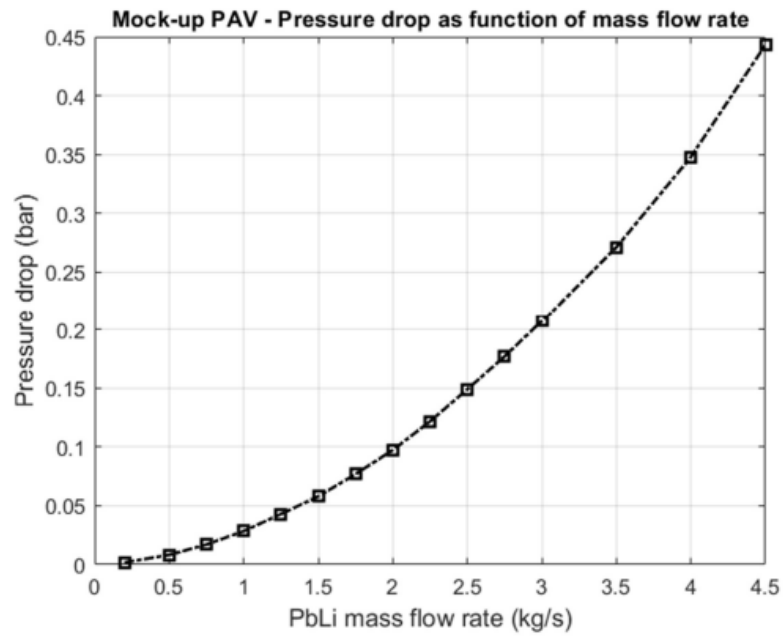


Figure 3.8: Pressure drop of the PAV mock-up as function of PbLi mass flow rate, results from CFD analysis

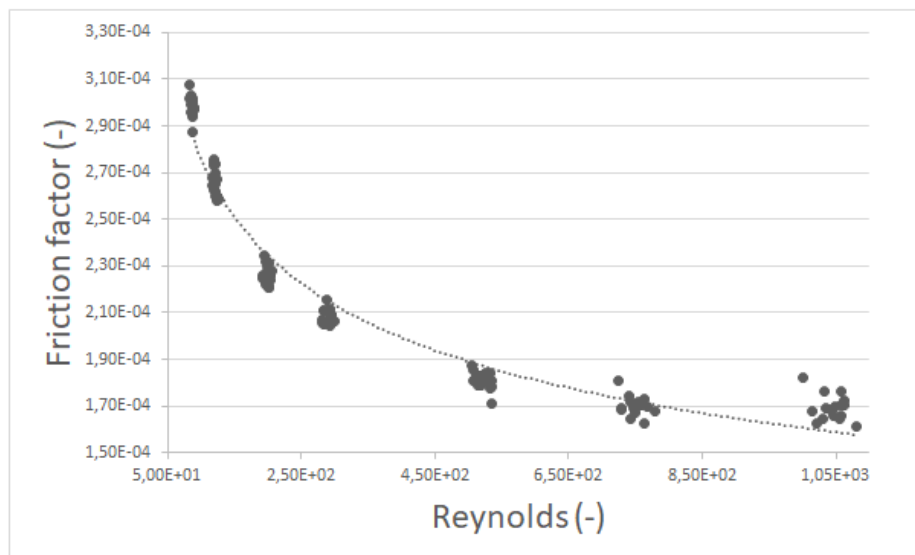


Figure 3.9: Friction factor as function of Reynolds number. Power law fitting of the CFD results with Excel.

Table 3.5: Boundary conditions of PAV mock-up simulation

Boundary	Value	Units
<b>Temperatures</b>		
External manifold surface	723	[K]
Inlet	723	[K]
Ambient	288	[K]
<b>Mass flow rate</b>		
Inlet	0.2 ÷ 4.5	[kg/s]
<b>Emissivities</b>		
Nb	0.15	[–]
SS304	0.40	[–]
<b>Heat transfer coefficient</b>		
External surface of Envelope	10	[W/m <sup>2</sup> /K]
Internal surface of Envelope	0	[W/m <sup>2</sup> /K]
Nb surface	0	[W/m <sup>2</sup> /K]

10 W/m<sup>2</sup>/K [22] and an emissivity of the surface of 0.4 for the vessel wall and of 0.15 for the niobium pipes. The LiPb is entering the manifold conservatively at a constant temperature of 450 °C. The boundary conditions are summarized in Table 3.5

In the simulations, the internal radiation transfer from the pipes to the vessel is modelled using a *surface-to-surface* approach, which automatically evaluates the view factors for all the radiative surfaces. The resulting temperature map in the mock-up is shown in normalized form (3.6) in Fig.3.10.

$$\frac{T_{inlet} - T}{T_{inlet} - T_{ambient}} \quad (3.6)$$

While the manifolds are globally at a temperature close to the fluid nominal inlet temperature (as expected, see Fig.3.10a), the pipes loose power by radiation to the vessel, which is at the temperature very close to the ambient one. Without an additional heating inside the vessel, at low mass flow rates, the pipes are expected to be at a temperature quite lower than the nominal one, and non-uniform along their length due to the thermal bridge of the plate, see Fig. 3.10b. This temperature reduction affects extraction efficiency of the PAV that is why a heating system is proposed in the work of Papa et al. [23].

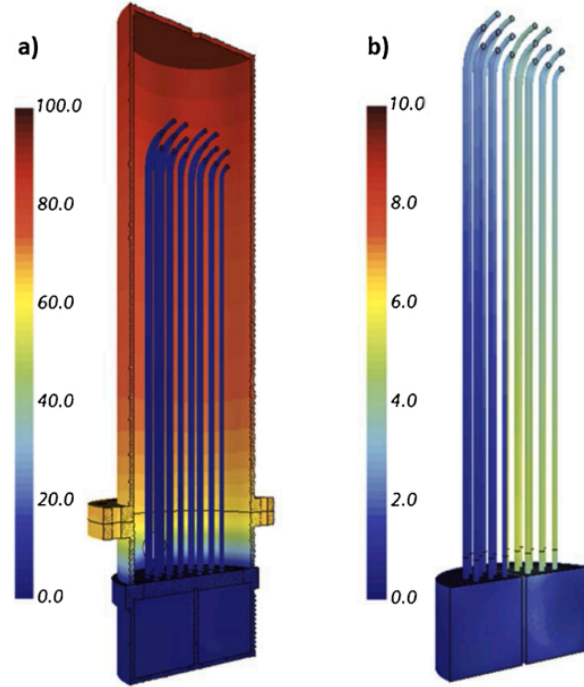


Figure 3.10: Steady-state normalized temperature difference computed as  $(T_{inlet} - T)/(T_{inlet} - T_{ambient})$  in the mock-up (a), with a zoom on the fluid domain (b), for the minimum mass flow rate ( $0.2 \text{ kg/s}$ ).

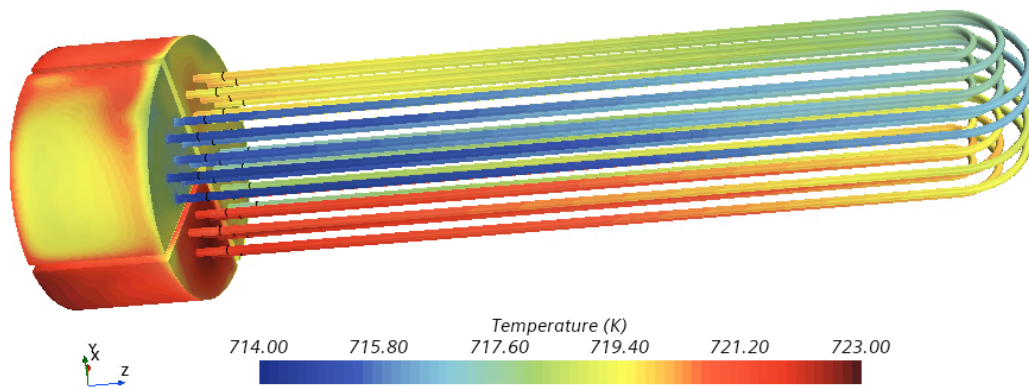


Figure 3.11: Fluid domain temperature field at  $0.75 \text{ kg/s}$ .

### Surface-2-Surface Heat transfer radiation

Being thermal radiation the only heat transfer mechanism inside the PAV, it must be taken into account. The Surface-2-Surface (S2S) model is a deterministic model that computes radiative heat transfer between surfaces using view factors. The model evaluates the view factor for each surface cell of the domain and compute thermal radiation with the rest of the domain. The view factors calculation is computationally expensive, but it needs to be done only once at the beginning of the simulation since the geometry does not change, this calculus is done by the *View Factor Calculator* model automatically. The accuracy of the S2S model depends on the number of rays used in the view factor computations, that means that it depends on the number of surface cell used in the grid development.

Each material is characterized by:

- *Emissivity*. The ratio of the power that a body emits to the power it would emit as a black body at the same temperature.
- *Reflectivity*. The ratio of reflected radiant energy over incident radiant energy at a given surface.
- *Transmissivity*. The ratio of transmitted radiant energy over incident radiant energy at a given surface.

In the radiative model it is possible to simulate wavelength-dependent radiation properties, this is possible with *Multiband Thermal Radiation* model. For sake of simplicity, in this work the radiation properties are assumed constant in wavelength, the *Gray Thermal Radiation* model is adopted. In particular, the radiation model is used only for solid domain (SS304 and Nb), their emissivity have been reported in Table 3.5. Clearly the transmissivity is equal to zero since the material are opaque and the reflectivity is calculated by the solver.

## Chapter 4

# Lumped model for PAV mock-up

This section aims to create a lumped model for the RadiaTube, a single tube corresponding to half of one U-shaped tube of the PAV mock-up. The RadiaTube will account for: Tritium permeation, radiative heat transfer and pressure losses. Once the Radiatube is defined, the lumped model PAV mock-up is assembled by properly connect different RadiaTubes.

The lumped model is built in OpenModelica, based on Modelica language. This modelling language main characteristics are:

- *A-causal* meaning that the model is based on equation and not on algorithm (like Matlab and C/C++). The model is built in such a way that there are no inputs and outputs defined a priori.
- *Object Oriented language* OOL, meaning that the modelling rely on modularity and code re-use: a single model can be made of multiple (re-used) sub-models. OLL follows 3 principles: Encapsulation, Aggregation, Inheritance.
- Both algebraic equation and ODEs may be written [18].

### 4.1 Permeation characterization

Following the order of this work, the first characterization is related to Tritium permeation through the Nb membrane. All the equation reported in Section 2 have been implemented in the Modelica code. From these model have been created an object, called TP (*Tritium Permeation*) in Fig. 4.6, capable to calculate Tritium permeation considering the RadiaTube parameters.

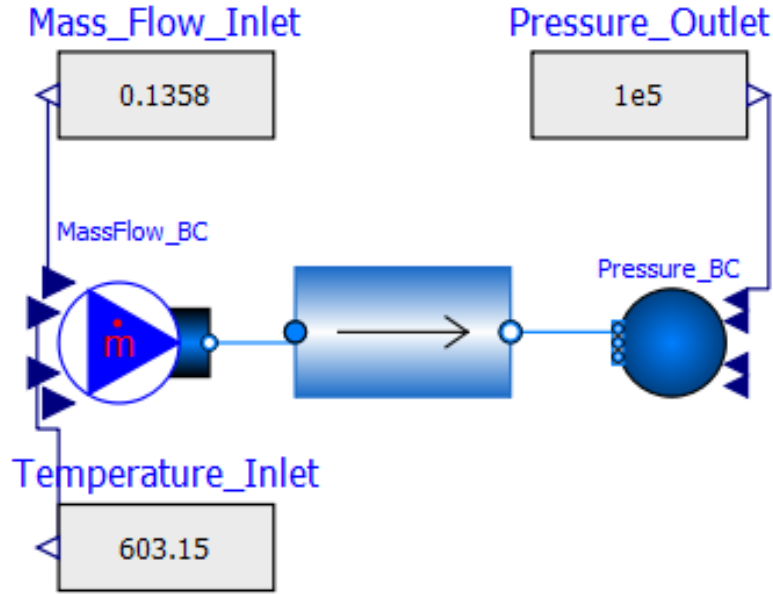


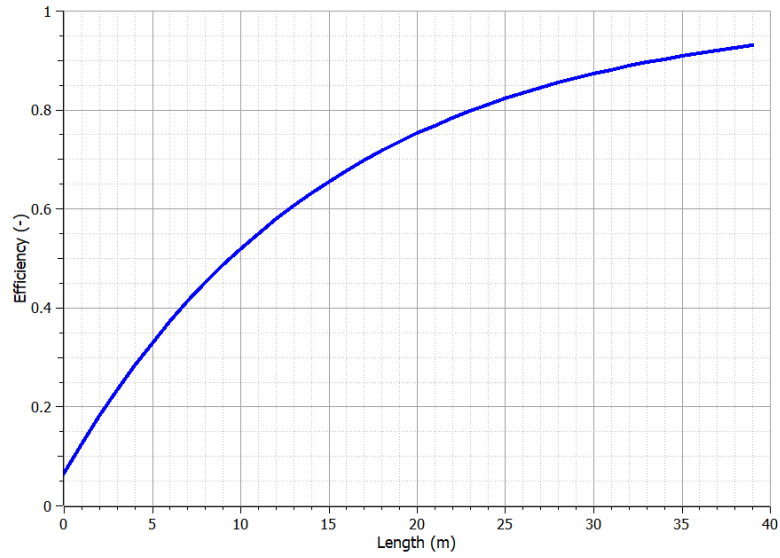
Figure 4.1: Set up for the validation of the permeation lumped model.

The inputs for the TP object are:

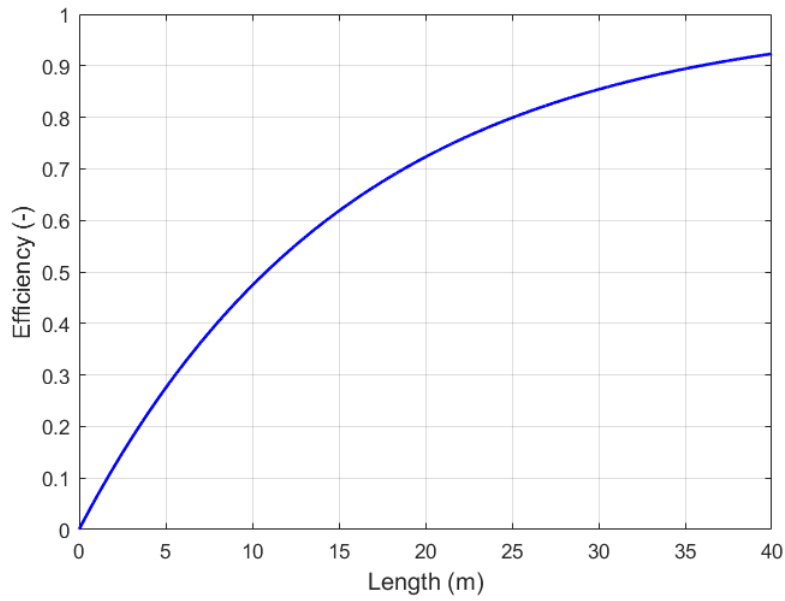
- Length of the pipe;
- Inner diameter of the pipe;
- Thickness of the Nb membrane;
- Mean Temperature of the PbLi flow;
- Tritium partial pressure at the inlet.

Tritium Permeation object is built according *encapsulation* concept to provide permeation results: when drag and dropped in the RadiaTube object no further modelling is needed. The TP object hides all the equations that will give the results according the operating conditions of the RadiaTube. The aforementioned inputs are taken from the RadiaTube, where TP is located, except Tritium partial pressure at the inlet that is consider always at  $100Pa$ . An example of the input dialogue window is provided by Fig. 4.3.

Concerning the result of TP model, they are the same of those obtained with Matlab script as can be appreciate in Fig.4.2. The input parameters for the validation are listed in Table 4.1 and in Fig.4.1 is shown the simulated model in OpenModelica.



(a)

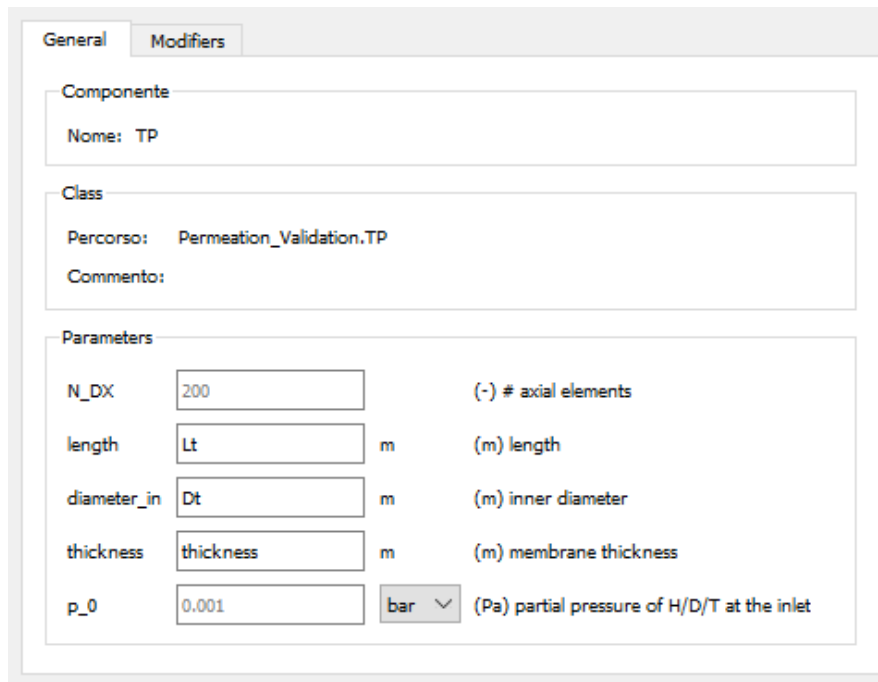


(b)

Figure 4.2: The comparison of the two results obtained with different OnpenModelica (a) and Matlab (b) from the permeation model of this work.

Table 4.1: Input parameter for the validation of lumped permeation model

Parameter	Value
Solubility constant	Aiello
Mass flow rate	0.1358 [kg/s]
Mean velocity	0.21 [m/s]
Density	9800 [kg/m <sup>3</sup> ]
Temperature	603.15 [K]



General Modifiers

Componente

Nome: TP

Class

Percorso: Permeation\_Validation.TP

Commento:

Parameters

N\_DX 200 (-) # axial elements

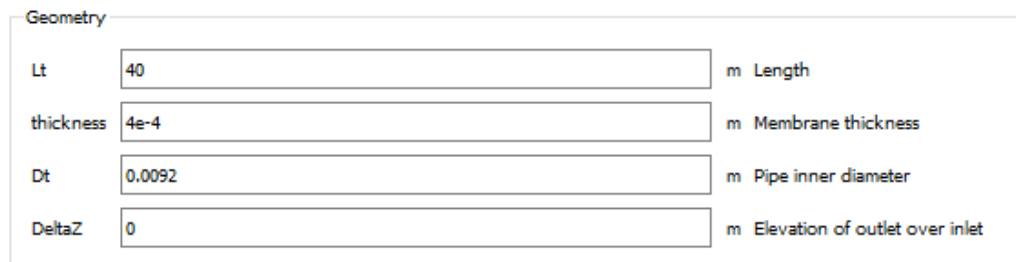
length Lt m (m) length

diameter\_in Dt m (m) inner diameter

thickness thickness m (m) membrane thickness

p\_0 0.001 bar (Pa) partial pressure of H/D/T at the inlet

(a)



Geometry

Lt 40 m Length

thickness 4e-4 m Membrane thickness

Dt 0.0092 m Pipe inner diameter

DeltaZ 0 m Elevation of outlet over inlet

(b)

Figure 4.3: Different set-up for TP and RadiaTube objects. Input parameters for the set-up of the Tritium Permeation object in (a) and for the RadiaTube in (b).



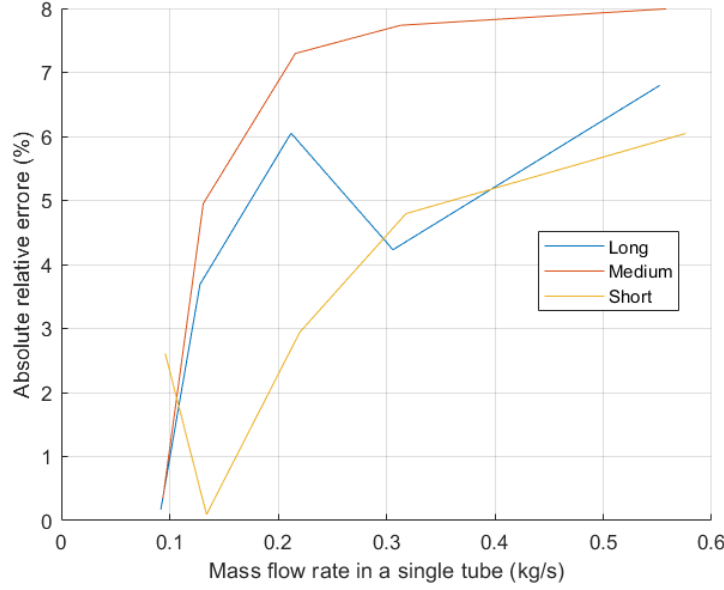


Figure 4.4: Relative error, defined in (4.1), of pressure drop of the tubes. Tubes of the second passage are selected to get rid of jet effects due to the PAV inlet flow rate.

## 4.2 Hydraulic characterization

From the CFD results it was possible to retrieve the friction factor of the tubes as function of  $Re$  number from (3.3). By implementing this equation in the RadiaTube script it is possible to correctly compute the pressure drop. The results of this validation are carried out at constant temperature equal to  $723.15\text{ K}$  (inlet temperature of CFD simulations). The relative error, defined according (4.1), between pressure drop result with lumped model and CFD simulation is reported in Fig. 4.4

$$error = \left| \frac{\Delta P_{Modelica} - \Delta P_{STAR-CCM+}}{\Delta P_{STAR-CCM+}} \right| \quad (4.1)$$

it can be seen that the results are good at low mass flow rate, as soon as mass flow rate increases the error increases as well, this behaviour is coherent with the fitting in Fig.3.9 where the fitting curve properly approximate the friction factor at low  $Re$  numbers.

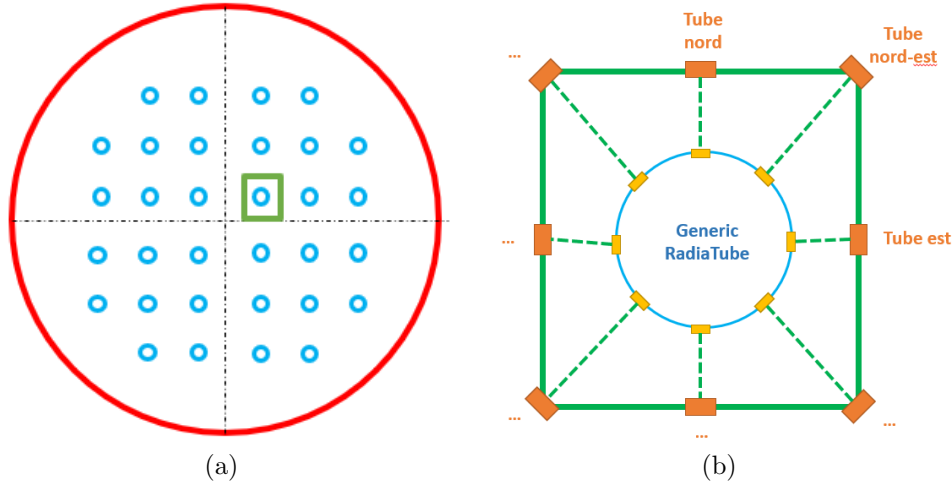


Figure 4.5: Sketch of of tubes-envelope section in (a) and detail on a generic tube in (b). In yellow and in orange the thermal connectors implemented in OpenModelica to account of view factors.

### 4.3 Thermal characterization

For the thermal characterization of the tubes view factors are needed. The RadiaTube transfers heat only by thermal radiation and especially with the neighbouring tubes, where the view factor is higher, and, for the external tubes, with the envelope. The yellow connectors in Fig.4.5b are the red *HeatPorts*, called *VF\_X*, in Fig.4.6. These connectors are needed to allow thermal radiation between tubes. Indeed, they provides the temperature values of the different tubes to be implemented in the energy balance equation of each Radiatube.

#### Thermal Radiation

Every body at temperature higher then 0 K emits radiation, a *black body* is a perfect emitter of thermal radiation meaning that it emits thermal radiation according to the *Planck's law*, plotted in Fig.4.7. In reality the bodies are not black bodies, indeed they are called *gray bodies*, meaning that they would emit less thermal radiation compared to a black body at the same temperature, this is the concept of emissivity  $\epsilon$  in (4.2)

$$\epsilon = \frac{\text{Radiation emitted by a gray body at temperature T}}{\text{Radiation emitted by a black body at temperature T}} \quad (4.2)$$

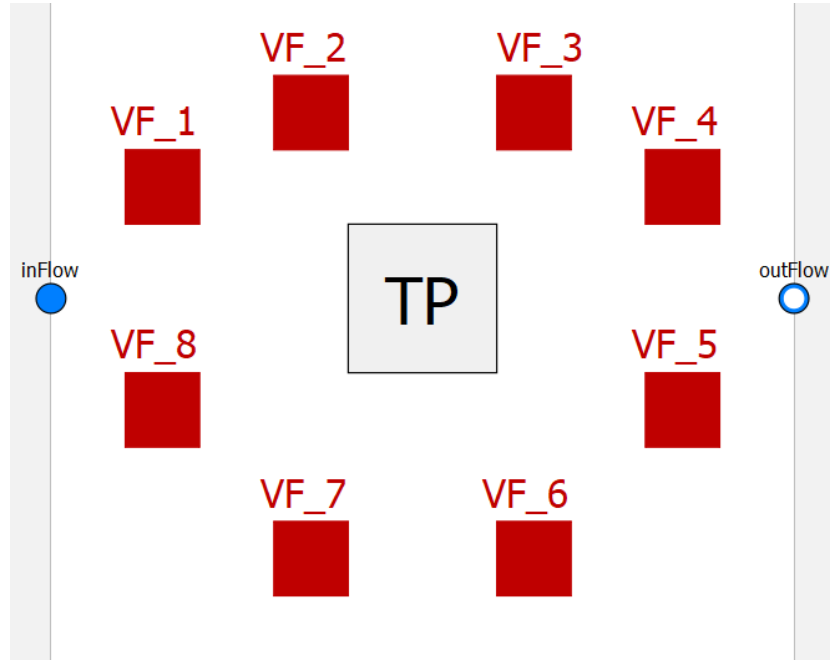


Figure 4.6: RadiaTube characterized by 8 view factor and tritium permeation calculus

The emissivities adopted in the lumped model are the same of those adopted in the CFD simulations and they constitute the *surface sesistance* to thermal radiation.

The other resistance, in the thermal radiation, is the *geometrical resistance* given by the view factors. Intuitively, if two surfaces, at different temperatures, are very close to each other, they will *greatly interact*. If the same two surfaces are pushed away from each other they will interact less and less. The limiting case is when the two surfaces does not see each other, in that case the interaction by thermal radiation will be null. This concept of *View Factor* can be reduced to a single formula (4.3)

$$F_{ij} = \frac{1}{A_i} \cdot \int_{A_i} \int_{A_j} \frac{\cos\theta_i \cdot \cos\theta_j}{\pi \cdot R^2} \cdot dA_i dA_j \quad (4.3)$$

where the labels  $i$  and  $j$ , and the different angles, refer to the areas in Fig.(4.8).

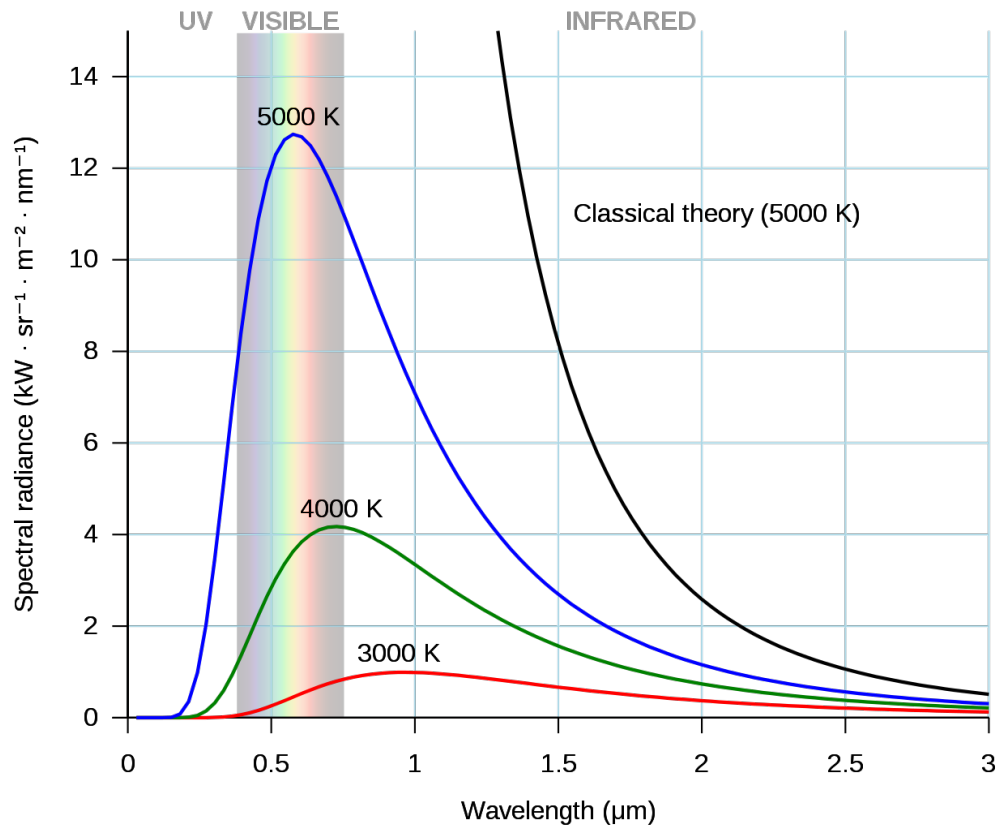


Figure 4.7: Planck's law that shows the spectrum of thermal radiation at different temperatures.

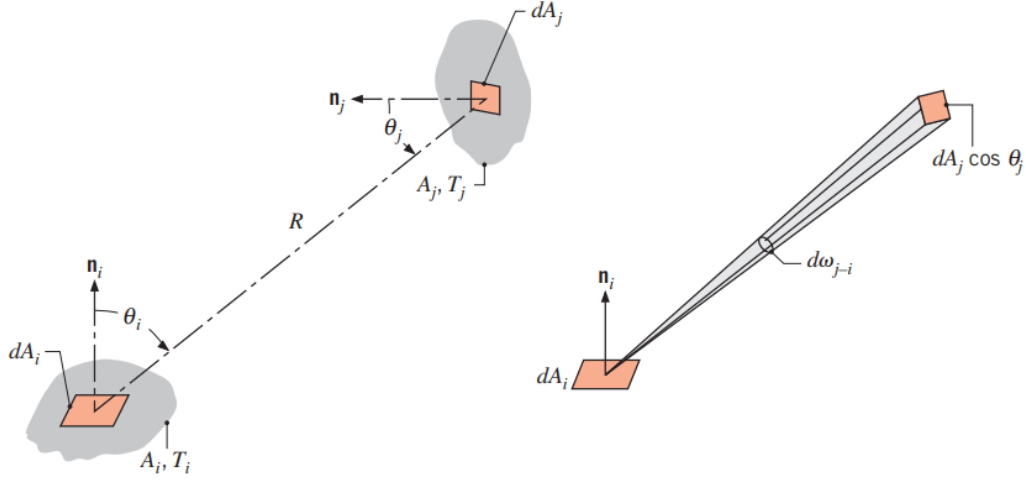


Figure 4.8: View factor associated with radiation exchange between elemental surfaces of area  $dA_i$  and  $dA_j$ . Image from [22].

Luckily the integral in (4.3) has been evaluated for different configurations. For the evaluation of the view factors between tubes (4.4) is used, taken from [24]

$$F_{1 \rightarrow 2} = F_{2 \rightarrow 1} = \frac{1}{\pi} \cdot \left( \sqrt{X^2 - 1} + \sin^{-1} \frac{1}{X} - X \right) \quad (4.4)$$

where  $X = 1 + s/2r$ , with  $s$  and  $r$  given in Fig.4.9. In the PAV mock-up configuration  $s = 20 \text{ mm}$  for the tubes located at: north, south, east, west and  $s = 32.45 \text{ mm}$  for the tubes located at the diagonals (e.g. north-east).

By means of (4.4), being  $s = 20 \text{ mm}$  and  $r = 5 \text{ mm}$ , the view factors between tubes are equal to 0.054 for *frontal* tubes and equal to 0.038 for *diagonal* ones.

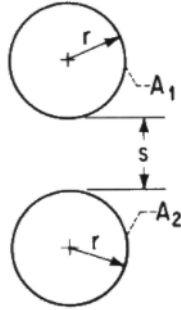


Figure 4.9: Section of two cylinders infinitely long with generic radii  $r$  and pitch  $s$ .

## 4.4 Assembling of RadiaTubes

The final goal of this work is to assemble multiple RadiaTubes to reproduce the PAV mock-up. This assembling will be the starting point for future validation of the model against experimental results, and for the scaling up for future PAV design for fusion reactor.

The assembly is nevertheless quite expensive, two RadiaTube are needed for each passage: one for upward flow and one for downward flow. Eventually, for the PAV mock-up, 32 RadiaTubes are needed. This makes the assembly quite expensive, especially in prospective of future scaling up, development of a proper code, able to consider multiple tubes and automatically connect each thermal radiation connector is required.

### Assumptions

Considering the thermal analysis on a single passage of U-tubes, in particular the field function (4.5) in the first passage

$$\frac{T_{inlet} - T_{average,tube}}{T_{inlet} - T_{ambient}} \quad (4.5)$$

where  $T_{average,tube}$  is the mean temperature of the fluid in the single passage. It is possible to collect the results in Fig.4.10, where it can be notice that the decrease in temperature of each tube is almost the same.

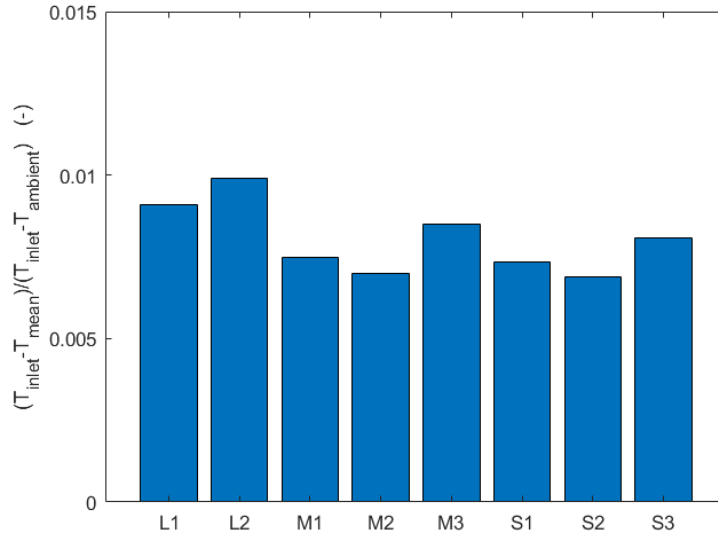


Figure 4.10: Field function (4.5) for each tube of the first passage.

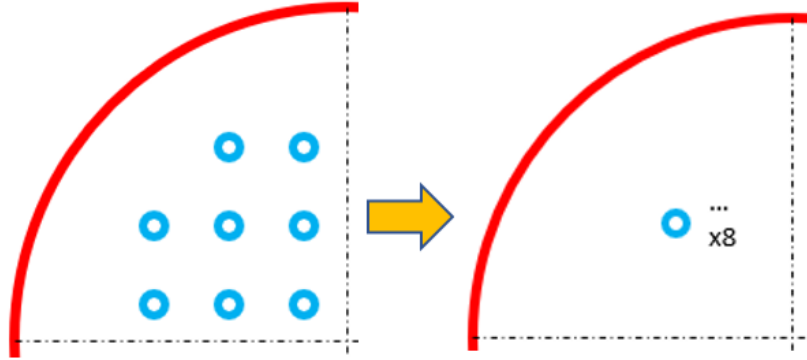


Figure 4.11: Section view of the 8 tubes (1/4 of the whole bank of tubes) lumped in one single, equivalent, tube.

As a consequence it can be assumed that, in case of the PAV mock-up, the tubes of the same passage undergo the same temperature reduction, thus a single tube can be considered in the thermal radiation. Then the lumped model is built according to Fig. 4.12 and Fig. 4.13, where the *RadiaTube* refers to half single passage of U-tubes. The mass corresponds to the mass flow rate of one single tube (i.e. 1/8 the total mass flow rate of the PAV) allowing the right pressure drop evaluation.

On the other hand, in the energy balance equation this simplification must be accounted by multiplying the power, carried on by the inlet flow rate, by a factor 8. Moreover, the view factors between tubes and envelope must be re-evaluated considering a heat transfer area equivalent to 8 tubes.

The view factor are calculated according (4.4), considering  $s = 70 \text{ mm}$  and  $r = 20 \text{ mm}$ , resulting equal to 0.09 between frontal tubes and equal to 0.06 for diagonal ones. The value of the radius is retrieved by considering an equivalent surface area with diameter equal to eight times half diameter of a single tube (half diameter of each tube is always facing inwards). While the pitch  $s$  is calculated considering the tube located at the middle of the tube array.

To ease the modelling, the manifolds have been not modelled, instead a fixed mass flow rate, pre-existing Modelica object, is imposed on each half-passage tube as shown in Fig. 4.13. Then, considering the simplified geometry, proposed in the view section in Fig. 4.11, the mean temperature of each passage is equal to the one obtained in the CFD simulation. In Table 4.2 the results are almost the same (error less than 0.5%), the lumped model considers an inlet temperature on the second passage equal to the inlet temperature of the first one, for that reason the average temperature is the same.

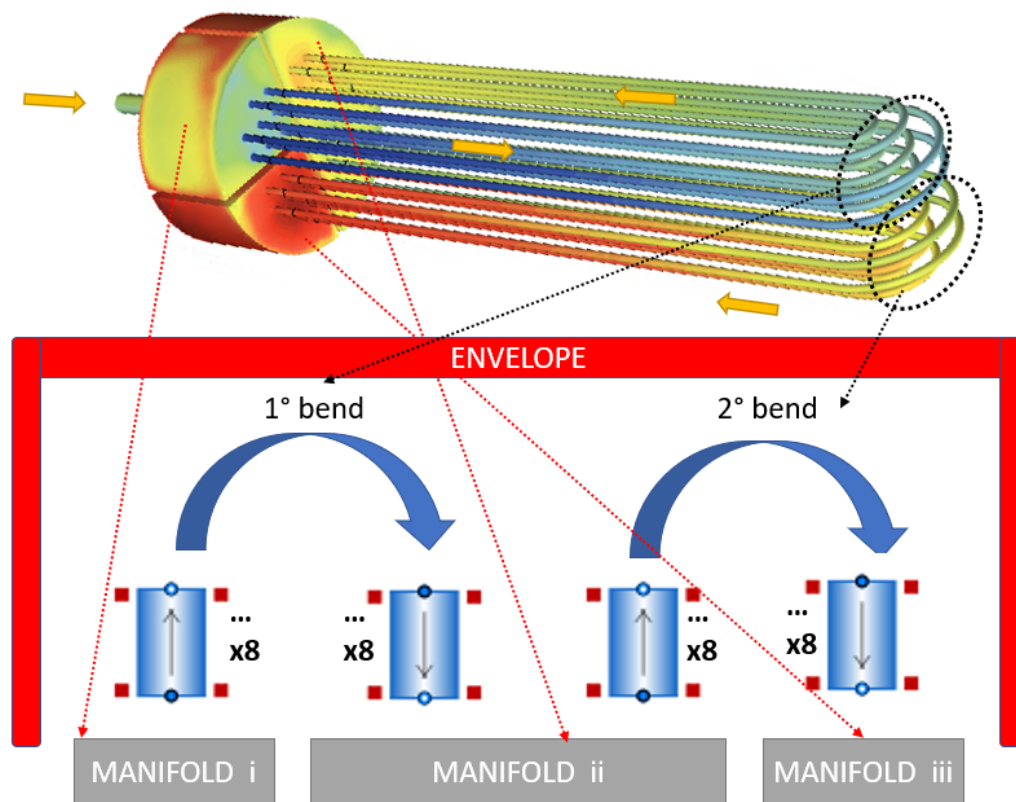


Figure 4.12: Condensation of PAV mock-up tubes. Each passage is modelled with two RadiaTube



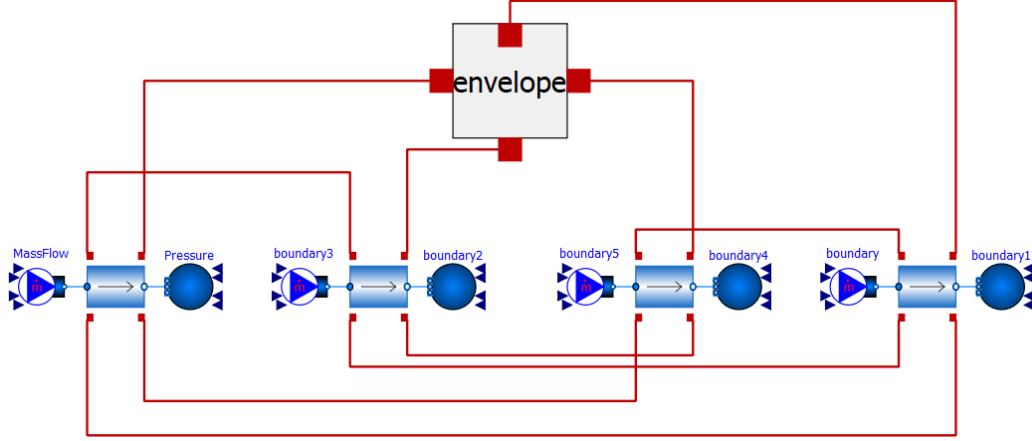


Figure 4.13: Suggested lumped model for PAV mock-up

Table 4.2: Comparison of mean temperature, pressure drop and Tritium extraction efficiency of each U-tubes passage obtained with CFD and lumped RadiaTube model at  $0.75 \text{ kg/s}$ .

Parameter	CFD	Lumped model
Temperature 1 <sup>st</sup> passage	719.5 <i>K</i>	718.8 <i>K</i>
Temperature 2 <sup>nd</sup> passage	717.4 <i>K</i>	718.8 <i>K</i>
$\Delta P$ 1 <sup>st</sup> passage	590 ÷ 610 <i>Pa</i>	590 <i>Pa</i>
$\Delta P$ 2 <sup>nd</sup> passage		590 <i>Pa</i>
Tritium extraction efficiency	22.48 %	22.44 %

# Chapter 5

## Conclusions

The aim of this work was to develop a lumped parameter model of the PAV mock-up capable of calculating the permeation of Tritium and the radiative heat exchange reproducing at the same time the hydraulic characteristic of the PAV.

Thanks to mathematical models of Tritium permeation through niobium membranes, and by means of CFD simulations, it was possible to fully characterize the RadiaTube. The RadiaTube is the basis of the mock-up PAV, it represents the half U-tube model of the mock-up PAV, it is able to calculate the permeation, validated against the results of the mathematical model, correctly reproduces the pressure drops, validated against the CFD model, and is able to simulate the radiation heat exchange that occurs between the tubes and the envelope. This model, together with the CFD thermo-hydraulic model and the tritium permeation model, must be validated against experimental results. An experimental campaign on the mock-up PAV is currently ongoing at ENEA-Brasimone, it will provide the data in order to validate the lumped parameter model, along with the other detailed models. Once the validation has been completed, the lumped model is ready for the scaling up to the design of a PAV for the future DEMO reactor.

## Appendix A

### Engineering design of a Permeator Against Vacuum mock-up with niobium membrane

F. Papa<sup>a</sup>, M. Utili<sup>b</sup>, A. Venturini<sup>b</sup>, G. Caruso<sup>a</sup>, L. Savoldi<sup>c</sup>, R. Bonifetto<sup>c</sup>, D. Valerio<sup>c</sup>, A. Allio<sup>c</sup>, A. Collaku<sup>c</sup>, M. Tarantino<sup>b</sup>

<sup>a</sup>DIAEE Department, Sapienza University of Rome, 00186, Rome – Italy

<sup>b</sup>ENEA, Department of Fusion and Nuclear Safety Technology, 40032, Camugnano (BO) – Italy

<sup>c</sup>Dipartimento Energia “Galileo Ferraris”, Politecnico di Torino, Torino (TO) – Italy

Permeator Against Vacuum (PAV) is one of the technologies proposed for the Tritium Extraction and Removal System (TERS) of the Water-Cooled Lithium Lead Breeding Blanket (WCLL BB). The paper presents the activity aimed at the engineering design of a PAV mock-up with a niobium membrane, in order to later assemble and qualify it. Experience gained in the engineering design of the mock-up, the heating system, the instrumentation, and the vacuum line is illustrated. This experience will be useful for the preliminary design, the manufacturing and the operation of the PAV with niobium membrane for DEMO. Niobium was selected as membrane material of this mock-up because of its high permeability and for its lower cost compared to vanadium, the other candidate material for membranes. Besides, niobium has a lower tendency to oxidation than vanadium. Oxidation would reduce the hydrogen isotopes permeation flux. In this paper, the solution adopted to manufacture the PAV mock-up, a complex component with niobium and P22 parts, is illustrated. The Nb/P22 welding issues are also presented, in particular related to the compatibility of the welded joints with LiPb. In the chosen design, the LiPb flows with two passages in 16 (8+8) niobium “U” shaped pipes installed in a vacuum chamber and welded to a P22 plate. The U-pipes configuration was selected to minimize the welding area, the volume of the component and the membrane thickness while trying to preserve the highest possible extraction efficiency.

Keywords: Tritium extraction, Permeator Against Vacuum, Niobium membrane, Design, Lead lithium.

#### 1. Introduction

The Permeator Against Vacuum (PAV) is one of the selected technologies [1] for the Tritium Extraction and Removal System (TERS) from LiPb in the WCLL BB (Water-Cooled Lithium Lead Breeding Blanket [2]) of DEMO reactor. TERS has two main functions to close the fuel cycle:

- to extract tritium from the flowing LiPb alloy;
- to supply tritium to the Tritium Plant for final processing.

The PAV technology is based on the phenomenon of tritium permeation through a membrane which separates LiPb on one side and vacuum on the other [3]. In this way, a concentration gradient which promotes tritium extraction is established.

In general, tritium transport occurs in two phases: in LiPb and through the membrane.

In the first phase, the tritium dissolved in LiPb spreads into the alloy: tritium migrates in the cloud of Pb atoms, by unbinding from a Li atom and binding to a different Li atom. Along with this diffusion process, an advection contribution has to be considered to describe the tritium behavior, as LiPb is flowing in the PAV.

Tritium transport through the membrane (second phase) occurs in 5 stages [4],[5]: adsorption, absorption, diffusion, recombination and desorption. Starting from the LiPb side, tritium atoms are attracted by the metal membrane (adsorption), which tends to complete its valence orbitals. So, tritium occupies the interstitial sites of the membrane lattice. Then, tritium atoms move from the surface to the bulk of the metal membrane (absorption). Later, tritium diffuses between the interstitial sites due to the concentration gradient (diffusion). When tritium reaches the vacuum-facing side of the membrane, recombination and desorption processes occur, allowing tritium to leave the membrane in a molecular form.

One of the strengths of the PAV is that, once the tritium is extracted from LiPb, there is no need to separate it from a stripping gas, at the contrary of what happens in the Gas-Liquid Contactor extraction technology. This also minimizes the tritium residence time in the system [6].

#### 1. PAV conceptual design

Within EUROfusion project, two configurations and two membrane materials are currently investigated as main alternatives: planar or cylindrical configuration and niobium or vanadium materials.

\*Corresponding author: pierdomenico.lorusso@enea.it

The planar configuration with vanadium membranes is being investigated in CIEMAT laboratories [7]. In this work, niobium was selected as membrane material for the mock-up because of its high permeability [8] and for its lower cost compared to vanadium (at the time of writing the vanadium price is about 3 times higher than that of niobium). Moreover, this choice was also motivated by the lower tendency to oxidation of niobium with respect to vanadium, as it can be seen in Ellingham diagram (i.e. standard free energy of formation of important oxides as a function of the temperature) [9]. Oxidation would reduce the hydrogen isotopes permeation flux [10]. Regarding the configuration, the cylindrical one was chosen in this work to minimize the welding area, the volume/area ratio and the membrane thickness while preserving a high theoretical extraction efficiency.

This configuration minimizes the welding area with respect to the planar configuration because only the ends of the pipes have to be welded, while, using plates, the entire profile has to be welded in order to create a channel. Moreover, using U-pipes and a single collector, it is possible to make a double passage of the LiPb inside the vacuum chamber, making half of the welds.

Using circular pipes instead of rectangular ducts, allows to adopt a lower thickness to withstand the operative loads. A lower thickness enhances the tritium permeation through the membrane.

Therefore, in the selected design, the LiPb flows, in two passage, through 16 niobium “U” shaped pipes installed in a vacuum chamber and welded to an F22 plate (10CrMo9-10, ASTM A182 Grade F22), as shown in Figure 1.



Figure 1: view of PAV mock-up

The actual efficiency of the PAV mock-up will be characterized with TRIEX-II facility, a flowing LiPb facility dedicated to the characterization of TERS technologies, in ENEA Brasimone Research Centre [11]. The conceptual design of this mock-up was made by ENEA and Politecnico di Torino for the WCLL BB [12],

while the engineering design was carried out by ENEA and Sapienza University of Rome to adapt the mock-up to the size of TRIEX-II facility. Additional thermal-hydraulic simulations were carried out by Politecnico di Torino, supporting the engineering design.

The efficiency of the PAV is defined as [13]:

$$\eta = 1 - \frac{C_{out,PAV}}{C_{in,PAV}} \quad (1)$$

where,  $C_{in,PAV}$  is the hydrogen isotopes concentration at the inlet of the PAV mock-up, while  $C_{out,PAV}$  is the hydrogen isotopes concentration at the outlet of the PAV mock-up. In (1),  $C_{in,PAV}$  is an input parameter depending on the tritium production rate in the reactor, while  $C_{out,PAV}$  depends on the PAV design.

This paper targets the engineering design of the PAV mock-up, with particular attention devoted to the solutions to two challenges of the project, and namely:

- The manufacturing process and in particular the best solution to perform the niobium-F22 joining between the pipes and the plate.
- A heating strategy that does not disturb the tritium diffusion through the niobium membrane, allowing at the same time to keep the temperature at the rated value. The use of conventional heating cables was in fact prevented as they would reduce the permeation area, also adsorbing hydrogen.

## 2. PAV mock-up description

The geometrical description of the mock-up, the selected instrumentation and the strategy to join F22 and Nb are reported in this section.

### 2.1 Geometrical description

Geometrically, the PAV mock-up is structured as a tube-and-shell heat exchanger, obtained simplifying the design proposed in [14], see Figure 2.a. The PAV mock-up is composed by a cylindrical vessel with 16 niobium U-tubes, the membranes for hydrogen permeation, welded on a F22 plate. This material has been chosen for his corrosion resistance in LiPb environments. A medium vacuum is pumped in the vessel while the LiPb flows in the niobium pipes. The LiPb is distributed into the niobium pipes by a collector which constitutes the lower part of the PAV. The collector is divided in three parts; each part is connected with one pipe in P22 (10CrMo9-10, ASTM A335 Grade P22), which connects the mock-up with the LiPb loop of the facility. The three pipes are:

- the inlet pipe;
- the discharge pipe;
- the outlet pipe.

The inlet pipe is connected with the part of the collector that allows the LiPb distribution in the first 8 niobium pipes. This part is indicated in red in Figure 2.b.

The discharge pipe is connected with the part of the collector (called mixing collector) where the LiPb coming out from the first 8 niobium pipes mixes. From this section of the collector, indicated in yellow in Figure 2.b, the LiPb is distributed in the remaining 8 niobium pipes. The discharge pipe is needed to allow the gravity draining of the mixing collector. The outlet pipe is connected with the section of the collector, indicated in red in Figure 2.b, where the LiPb coming out from the last 8 niobium pipes mixes before leaving the mock-up. Therefore, LiPb will double pass through the vessel, as shown in Figure 2.c and Figure 2.d. The main dimensions of the mock-up are reported in Table 1, while the operative conditions are listed in Table 2. The cylindrical vessel is divided into two parts so that the upper part can be removed to inspect the Nb pipes or for maintenance. The two parts are joined

together by a flange. The upper part is connected to the gas and vacuum line and hosts two feedthrough connectors (in red in Figure 3) for the power supply of the heating systems of niobium pipes (IR lamps, in yellow in Figure 3), which are attached inside the vessel. In this way, when the upper part of the vessel is lifted, the heating systems will also be lifted. Moreover, the upper part of the vessel is equipped with a quartz porthole to allow the visual inspection of the tube bundle also during operation. Quartz has been chosen for its impermeability to hydrogen isotopes [15]. Instead, the lower part of the vessel has two thermocouple feedthrough connectors (in blue in Figure 3), as 50 thermocouples are needed to monitor LiPb temperature in the 16 Nb tubes. The tube plate is wide enough to work also as upper flange of a connection with the collector.

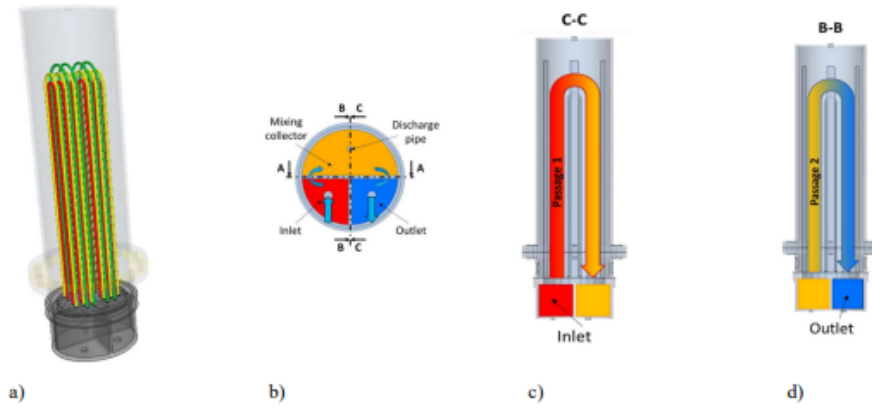


Figure 2: Sketches of the PAV mock-up: (a) simplified sketch of the cylindrical vessel with the 16 niobium U-tubes: Long pipes (L) in green, medium-length pipes (M) in yellow and short pipes (S) in red; (b) horizontal section of the PAV collector showing its 3 parts and the connecting pipes; (c) vertical section of the PAV showing the first passage of LiPb through the vessel; (d) vertical section of the PAV showing the second passage of LiPb through the vessel.

Table 1: main dimensions of the PAV mock-up.

Dimensions	[mm]
Height of the vessel	1106.00
External diameter of the vessel	323.85
Thickness of the vessel	6.35
Length of the Nb pipes (including the portions welded in the plate, 30 mm on each side)	1805.25 (S)
	1899.50 (M)
	1993.74 (L)
External diameter of the Nb pipes	10.00
Internal diameter of the Nb pipes	9.20
Pitch of the Nb pipes	30.00



Height of the LiPb collector	156.00
Thickness of the plate	38.00
External diameter of the P22 pipes (inlet/outlet LiPb)	33.40
Thickness of P22 pipes (inlet/outlet LiPb)	3.38
External diameter of the draining pipe	21.34
Thickness of the draining pipe	2.77

Table 2: PAV mock-up operative conditions.

Parameter	Value	Unit
Operative internal pressure of the vessel	$10^{-1} - 10^5$	[Pa]
Max internal pressure of the vessel	$1.1 \cdot 10^5$	[Pa]
Max internal pressure of the Nb pipes	$4 \cdot 10^5$	[Pa]
Max internal pressure of the LiPb collector	$5 \cdot 10^5$	[Pa]
Max temperature of the collector	530	[°C]
Max temperature of the Nb pipes	500	[°C]
Max temperature of the vessel	100	[°C]
Operative LiPb temperature	350-500	[°C]
Max speed of LiPb in the Nb pipes (at 4.6kg/s)	0.97	[m/s]
Total flow rate of LiPb in the Nb pipes	0.2-4.6	[kg/s]
Vessel filling gas (during long stops)	Helium	[-]

Instead, the lower part of the vessel is directly welded on the tube plate, as shown in Figure 4.

Instead, the lower part of the vessel has two thermocouple feedthrough connectors (in blue in Figure 3), as 50 thermocouples are needed to monitor LiPb temperature in the 16 Nb tubes.

The tube plate is wide enough to work also as upper flange of a connection with the collector. Instead, the lower part of the vessel is directly welded on the tube plate, as shown in Figure 4.

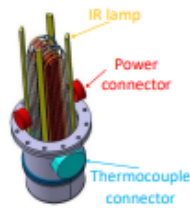


Figure 3: View of PAV connectors and IR lamps

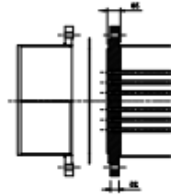


Figure 4: Detail of the connection between F22 plate with the collector

The most important issue to be solved in order to manufacture the PAV mock-up was to perform the joining between the niobium pipes and the F22 plate, as there are three main problems to be solved:

- niobium easily oxidizes at high temperatures;
- the melting points of niobium and F22 are very different, so that performing a welding is really difficult;
- most of the brazing alloys are made of materials that are highly soluble in LiPb, such as nickel.

The solution proposed in this paper to join the niobium pipe with the F22 plate is to use a vacuum brazing based on a nickel-based brazing alloy. The vacuum brazing avoids the oxidation of niobium, while, to prevent nickel from solubilizing in LiPb, the brazing procedures are carried out in such a way that avoids the contact between the filler material and the LiPb. The brazing will be performed on almost the entire depth of the plate in order to create a strong joint between the two materials. The brazing alloy can withstand up to 1100°C, about 600°C higher than the operative condition of the mock-up. Each brazing will be later inspected with not destructive testing (radiography).

However, a testing joint has also been assessed with destructive testing before starting the manufacturing, as the brazing of these materials has never been performed

## 2.2 Joining niobium and F22 steel

earlier. The testing joint will undergo tensile testing to evaluate its resistance.

A thermal analysis of the mock-up, shown in the following section, demonstrated the necessity of additional heating systems to keep constant the temperature of the niobium pipes. For this reason, infrared lamps will be installed in the vessel.

### 2.3 Heating system of niobium pipes

The heating strategy adopted to keep the LiPb at the rated temperature and to avoid disturbing the tritium diffusion through the niobium membrane is described in this section.

The use of heating cables as heating system would not only be difficult for the installation, since the number of pipes is high compared to the dimensions of the component, but also the presence of the cables would create an additional obstacle to the diffusion of tritium through the Nb membrane. For these reasons, a different solution is proposed.

The heating system of the niobium pipes will consist of 4 double-tube infrared lamps mounted inside the vessel. The lamps are made of quartz, a material that prevents hydrogen permeation, so that their presence will not affect the measurement of the permeated flux [15]. The lamps will allow to keep the temperature of the Nb pipes at about 450°C to avoid the solidification of the LiPb inside the pipes. The lamps, 100 cm long and positioned symmetrically with respect to the center, will have a maximum power of 3.5 W/cm, they will be 100 cm long and they will have an angle of action of 60°. A lamp and their positions are shown in Figure 5.

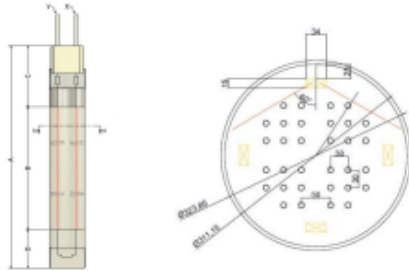


Figure 5: Sketch of an IR lamp and PAV technical drawing, horizontal section of the vessel showing the IR lamps position and their angle of action.

## 3 Detailed analyses in support of the mock-up design

This section presents the most important calculations that were made in support of the mock-up engineering design. In particular the hydraulic, thermal and mechanical analyses and the tritium transport analysis.

### 3.1 Hydraulic analysis: flow distribution in the Nb pipes

First, the LiPb flow distribution among the different pipes must be computed to check the homogeneity of the flow distribution: a severe flow unbalance, causing a deviation from the average speed, would affect the extraction efficiency. 3D CFD analyses of the LiPb flow, with special attention to the manifolds (where the flow is split among the pipes), have been carried out using the commercial software STAR-CCM+[16], solving the problem of 3D conjugate heat transfer in the entire mock-up with a segregated solver.

The LiPb flow in the pipes is in turbulent conditions for the entire range of operational mass flow rate. A two-equation Reynolds-averaged Navier-Stokes (RANS)  $k-\omega$  SST [17] model is adopted in the simulations, with an all- $y^+$  wall treatment. The chosen model SST-Menter  $k-\omega$  works as a standard  $k-\omega$  in the near-wall region, and as a  $k-\epsilon$  model in the fully turbulent region. The mesh developed to describe the mock-up geometry is reported in Figure 6. While in the manifolds the cell base size is 10 mm for the fluid, a significant refinement (to 1 mm) is needed for the bulk fluid near the inlets and outlets of Nb tubes. Four prismatic layers at the wall allow a good solution of the Navier-Stokes equations in the boundary layer. In the Nb tubes, an extruded mesh with element of 45 mm is used. For the solid computational domain, the mesh is made by a mix of polyhedral cells in thick regions, and prismatic cells, in thin regions, with a base size that locally matches the fluid one. The total number of cells resulted to be 4.5MCells.

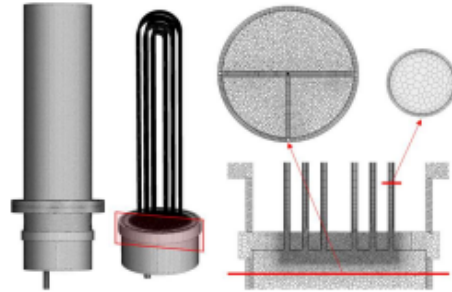


Figure 6: Grid developed for the 3D CFD simulations of the PAV mock-up with its main features: (a) the polyhedral cells in core fluid in the manifold; (b) a finer mesh in the inlet/outlet of the Nb tubes; (c) prism layers at the walls; (d) extruded mesh in the Nb tubes.

Figure 7.a shows that the flow repartition is close to the average value within <5% for different values of the mass flow rates giving an acceptable homogeneity of the speed. Values of maximum speed around 0.5 m/s could be achieved with mass flow rates of 2-2.5 kg/s. Note that the maximum spread between the speed values stays below 0.1 m/s in the worst case (maximum flow rate). The flow repartition shows a slightly lower flow rate in the longest channels, while the shortest channels have on average the largest flow rate, as expected. This is especially true for the second pipe passage, while the first passage is affected by some jet effects from the inlet pipe that affects, in

particular, the central pipes, as shown in Figure 8.

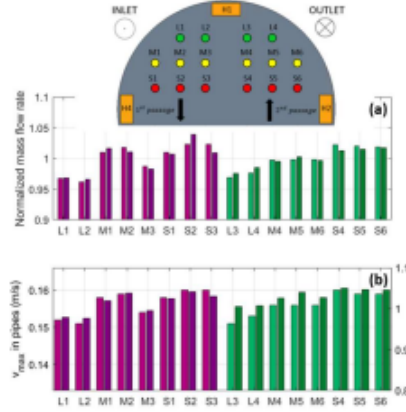


Figure 7: (a) Mass flow rate repartition among the mock-up pipes, normalized to the average value and (b) maximum speed in the pipes (first passage: pipes L1-L2, M1-M3, S1-S3, see inset, and second passage: pipes L3-L4, M4-M6, S4-S6), for the total mass flow rate of 0.75 kg/s (light bars) and 4.5 kg/s (dark bars). In (b), the dark bars refer to the right axis.

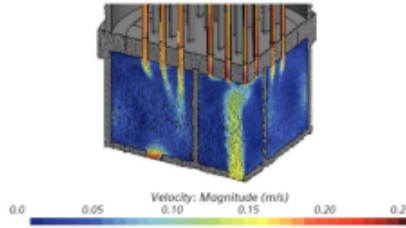


Figure 8: Flow field computed in the manifolds, for a mass flow rate of 0.75 kg/s.

### 3.2 Thermal analysis: thermal losses from niobium pipes

The steady-state thermal-fluid analysis of the entire mock-up has been performed in the most conservative case (higher LiPb temperature) imposing a uniform temperature of 450°C (723 K) on the outer surface of the manifolds, while allowing convective and radiative heat transfer from the vessel to the environment, assumed at 15°C (288 K), with a heat transfer coefficient of 10 W/m<sup>2</sup>K [18] and an emissivity of the surface of 0.4 for the vessel wall and of 0.15 for the niobium pipes. The LiPb is entering the manifold conservatively at a constant temperature of 450°C. In the simulations, the internal radiation transfer from the pipes to the vessel is modeled using a surface-to-surface approach, which automatically evaluates the view factors for all the radiative surfaces.

The resulting temperature map in the mock-up is shown in normalized form in Figure 9. While the manifolds are globally at a temperature close to the fluid nominal inlet temperature (as expected, see Figure 9.a),

the pipes lose power by radiation to the vessel, which is at the temperature very close to the ambient one. Without an additional heating inside the vessel, at low mass flow rates, the pipes are expected to be at a temperature quite lower than the nominal one, and non-uniform along their length due to the thermal bridge of the plate, see Figure 9.b.

The power balance of the vessel is reported in the Sankey diagram in Figure 10, highlighting the fraction of power in input to the mock-up which is released by the vessel to the environment through convective and radiative heat transfer. At all mass flow rates, the conductive load from the plate roughly balances the convective and radiative losses to the environment. Note that convection dominates over the radiative heat transfer because the small temperature difference between the vessel and the surrounding, see Figure 9.a.

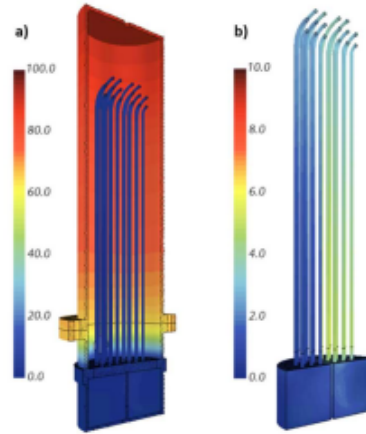


Figure 9: Steady-state normalized temperature difference computed as  $(T_{inlet} - T)/(T_{inlet} - T_{ambient})$  in the mock-up (a), with a zoom on the fluid domain (b), for the minimum mass flow rate (0.2 kg/s).

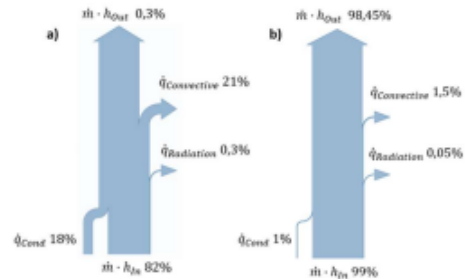


Figure 10: Sankey diagram highlighting the power balance on the mock-up for a mass flow of a) 0.2 kg/s and b) 4.5 kg/s.

### 3.4 Mechanical analysis and tritium transport analysis



The pre-dimensioning of the mock-up is based on the actual constraints due to the allowable pressure drop (0.5 bar at the maximum mass flow rate of 4.6 kg/s, given the pump characteristics and the pressure drops of the rest of the loop components) and to the space allocated for its installation in TRIEX-II. The constraints on the dimensions are a maximum manifold height of 160 mm, an allowed height of the niobium pipes of about 1000 mm (including the U curve) and a maximum external diameter of the vessel of 330 mm. The vessel height results about 1160 mm. The minimum pitch among the pipes is 30 mm to allow proper welding in the plate.

The design process is composed of the following steps:

- 1) The preliminary sizing of the martensitic steel (10CrMo9-10 [19]) vessel and plate thickness using the thick shell theory [20] to withstand the operating ( $10^6$  bar) and design (10 bar) pressures in the vessel;
- 2) The sizing of the niobium pipes (membrane) diameter in order to satisfy the constraints on the pressure drop and maximum dimensions (i.e. assuming the maximum possible membrane length of ~2000 mm), as well as a suitable LiPb speed allowing the best performances in terms of hydrogen permeation [21], computed to be ~0.5 m/s;
- 3) The design of the layout (and definition of the number) of the niobium pipes to be inserted in the plate, satisfying the given constraint on the pitch.

As a result, the minimum vessel and plate thickness is 4.3 mm and 12 mm, respectively, the Nb pipe inner/outer diameter is 9.2/10 mm [22] and the number of U-pipes per passage is 8.

The mechanical stress was assessed by a thermo-mechanical model, using COMSOL 5.1 Multiphysics tool [23]. The deformation of the upper plate in nominal conditions is presented in Figure 11. At the junction between the vessel and the plate, the thick shell theory (suitable for cylindrical wall, thick shell and axial symmetry, far from geometrical discontinuities) loses its validity, and indeed the deformation is quite large (although the stress is acceptably below the ~21 MPa limit, accounting for the safety factor from ASME VIII Div.1). This (local) effect can be compensated by a series of clamps, to assure the structural resistance in all operating conditions. Instead, the bottom plate deformation can be seen in Figure 12, conservatively at a LiPb temperature of 500°C and during normal operating conditions.

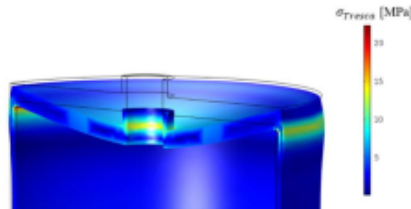


Figure 11: Stress distribution (and deformation) close to the upper plate in normal operating conditions for a PbLi temperature of 330 °C.

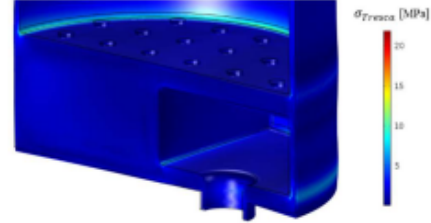


Figure 12: Stress distribution close to the holed plate in normal operating conditions for PbLi temperature of 500 °C.

Finally, the resulting hydrogen extraction efficiency is assessed for the maximum allowed pipe length by means of the surface-limited model (SLM), similar to that described in [21]. The LiPb properties used in the calculations were taken from [24].

Tritium transport can be modelled in two ways: surface-limited regime and diffusion-limited regime. In the diffusion-limited regime [25] the hydrogen isotopes permeation process is limited by the atomic diffusion in the Nb membrane. Instead, the kinetics of Q transport is said to be surface-limited when the surface effects, adsorption and recombination, provide the biggest resistance to permeation [21][26][27][28].

The hydrogen concentration along the LiPb flow direction in the PAV channels is evaluated with a transport model. The pressure gradient between the inner side of the pipes (Nb membrane), where LiPb flows, and the outer side (the vessel) drives the tritium permeation across the pipe wall together with the surface phenomena. The motion of the LiPb, as well as the tritium concentration along the pipe, is modelled by 1D advection equation along the axial coordinate of each pipe

$$\nabla \cdot \vec{J} = -\vec{v} \cdot \nabla C_T$$

where:

- $\vec{J}$  is the tritium mass flux [ $\frac{mol}{m^2 \cdot s}$ ]
- $\vec{v}$  is the speed of LiPb in the pipes [ $\frac{m}{s}$ ]
- $C_T$  is the hydrogen concentration in LiPb [ $\frac{mol}{m^3}$ ]

To correctly identify in which regime the mock-up operates, the dimensionless permeation parameter should be used as a criterion:

$$W = \frac{2K_r t K_s \sqrt{p_{in}}}{D}$$

where:

- $K_r$  is the recombination constant ([ $m^4/s/mol$ ]),
- $t$  is the membrane thickness ([m]),
- $K_s$  is the solubility constant ([ $mol/m^3/Pa^{0.5}$ ]),
- $D$  is the mass diffusion coefficient ([ $m^2/s$ ]) of

the membrane,

- $p_{in}$  is the partial pressure ([Pa]) of the gas impinging on the surface.

This number expresses the ratio among the superficial effects and the diffusion phenomena inside the bulk. Therefore, if  $W \ll 1$  the regime can be considered surface-limited, whereas a  $W \gg 1$  implies that the permeation is completely diffusion-driven. An exhaustive explanation on the permeation parameter is reported in [28]. The values used for the evaluation of  $W$  are reported in Table 3.

This leads to a  $W \sim 4 \cdot 10^{-2}$  for the niobium membrane for  $T = 330^\circ\text{C}$ .

The permeated flux calculated across the LiPb flow direction is instead evaluated on the basis of the tritium concentration gradient in the pipe cross section, as in the following eq.

$$J_T(r_i, z) = h_T (C_{T,b}(z) - C_{T,wall}(z))$$

where

- $h_T$  ([m/s]) is the mass transfer coefficient in LiPb, evaluated according to [29]; for a LiPb speed of 0.5 m/s and a temperature of  $330^\circ\text{C}$  and  $500^\circ\text{C}$ , the  $h_T$  is  $7 \cdot 10^{-5}$  m/s and  $2 \cdot 10^{-4}$  m/s, respectively
- $C_{T,wall}$  is the tritium concentration next to the wall on the LiPb side.

The results of hydrogen extraction efficiency reported in Figure 13 for different LiPb temperatures show that the efficiency is limited by the short length of the mock-up permeator membrane ( $< 4$  m, considering the double passage). The former is representative of a non-oxidized Nb surface, while the latter is the reference for an oxidized membrane surface.

The maximum efficiency of  $\sim 50\%$  is reached for high temperature values, while at  $330^\circ\text{C}$  the efficiency should be between 5 and 20%.

The physical constants of the Nb membrane and the mass transfer coefficient in LiPb at different temperatures have been evaluated using the references quoted in Table 3 and the correlations in [29], in order to obtain the results shown in Figure 13.

Table 3: Physical constants of the Nb membrane for  $W$  at different temperatures at fixed thickness.

$T$ [ $^\circ\text{C}$ ]	$K_T$ [21] [ $\text{m}^3/\text{s}/\text{mol}$ ]	$K_S$ [8] [ $\text{mol}/\text{m}^2/\text{Pa}^{0.5}$ ]	$p_{H_2}$ [Pa]	$D$ [8] [ $\text{m}^2/\text{s}$ ]	$t$ [m]
330	$6.02 \cdot 10^{-11}$	$1.26 \cdot 10^3$	100	$6.51 \cdot 10^{-9}$	$0.4 \cdot 10^{-3}$
500	$6.02 \cdot 10^{-7}$	107.64	100	$1.12 \cdot 10^{-6}$	$0.4 \cdot 10^{-3}$

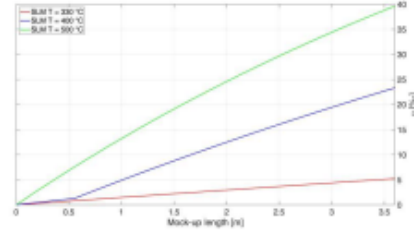


Figure 13: Effect of the variation of the LiPb temperature on the H extraction efficiency computed by the SLM (flow velocity fixed at 0.5 m/s).

#### 4. Mock-up instrumentation

One of the main aims of the PAV mock-up is to quantify the hydrogen permeation flux through a 0.4 mm thick niobium pipe with flowing LiPb inside and under different working conditions. To this end, a helium leak detector (ASM340 series by Pfeiffer Vacuum) will be connected to the vacuum side of the PAV vessel through a 1/4" vacuum-tight Swagelok line. The instrument will perform an integral measurement of the permeated hydrogen, from which it will be possible to evaluate the average permeation flux per unit area. This value will be used as a reference for the results of numerical models. The leak detector is equipped with a rotary vane pump with 15 m<sup>3</sup>/h backing pump capacity and it has a minimum detectable rate as low as  $5 \cdot 10^{-12}$  mbar-l/s.

Heating cables and bands will be used to heat up the collector and the P22 pipes that connect the collector to the facility, to maintain the LiPb that flows in the niobium pipes at  $450^\circ\text{C}$ .

In order to control the niobium pipes temperature, 50 thermocouples will be installed at different heights on the pipes. Each pipe will be equipped with two thermocouples at the inlet and outlet. Additionally, six pipes will have one more thermocouple at the top of the U-bend and two more at half height. These six pipes were chosen in order to have a good mapping of the temperature in the various positions, taking advantage of the cylindrical symmetry.

#### Conclusions

The main objective of this work was to perform the engineering design of a PAV mock-up with niobium membrane with the aim to successively install it in TRIEX-II facility and to characterize its performances.

A cylindrical shape with U-tubes was selected to minimize the overall size of the components, the welding area and the membrane thickness with respect to the planar configuration. Niobium was selected as membrane material for its high hydrogen permeability, its lower tendency to oxidation and its lower cost with respect to vanadium.

The design took into account thresholds for the overall dimensions and pressure losses and was optimized to limit the spread of LiPb speed among the pipes. 0.5 m/s was evaluated the optimal LiPb speed for hydrogen isotopes

permeation. At 500°C, the obtained mock-up shows a theoretical maximum extraction efficiency of about 40%.

Thermal simulations highlighted the need for a heating system to maintain the LiPb temperature almost uniform in the niobium pipes. Quartz-made infrared lamps were chosen as heating system of the Nb pipes for an advantage in installation with respect to heating cables/bands and for the very low permeability of quartz to hydrogen isotopes, thus minimizing the negative influence on the experiments.

A helium leak detector was selected to measure the permeated flux on the vacuum side of the mock-up. The integral measurement of permeated flux will allow to evaluate the permeation per unit area and will be used as reference for the numerical simulations.

The choice of the procedure to join Niobium and F22 ferritic/martensitic steel considered the very different melting points of these materials, the nickel solubility in LiPb and the tendency to oxidation of niobium at high temperature. An innovative vacuum brazing with a nickel-based alloy was developed to overcome these issues. The joint will penetrate almost the entire thickness of the plate and will have high temperature resistance.

### Acknowledgments

This work has been carried out within the framework of the EUROfusion Consortium and has received funding from the Euratom research and training programme 2014-2018 and 2019-2020 under grant agreement No 633053. The views and opinions expressed herein do not necessarily reflect those of the European Commission.

### References

- [1] F. Cismondi et al., Progress of the conceptual design of the European DEMO breeding blanket, tritium extraction and coolant purification systems, *Fusion Engineering and Design* 157 (2020), 111640.
- [2] A. Del Nevo et al., WCLL BB design and Integration studies 2019 activities, February 2020, BB-3.2.1-T006-D001, EFDA\_D\_2P5NE5.
- [3] H. Moriyama et al., Tritium recovery from liquid metals, *Fusion Engineering and Design* 28 (1995), 226-239.
- [4] V. D'Auria et al., Tritium extraction from lithium-lead in the EU DEMO blanket using Permeator Against Vacuum, *Fusion Science and Technologies* 71 (2017), 537-543.
- [5] A. M. Polcaro et al., The Kinetics of Hydrogen Absorption in Molten Pb/Li Alloy, *Journal of Nuclear Materials* 119 (1983), 291-295.
- [6] D. Demange et al., Tritium extraction technologies and DEMO requirements, *Fusion Engineering and Design* 109-111, Part A (2016), 912-916.
- [7] B. Garcinuño et al., Design and fabrication of a Permeator Against Vacuum prototype for small scale testing at Lead-Lithium facility, *Fusion Engineering and Design* 124 (2017), 871-875.
- [8] S. A. Steward, Review of hydrogen isotope permeability through materials, Technical report UCRL-53441, Lawrence Livermore National Laboratory, [www.osti.gov/scitech/servlets/purl/5277693](http://www.osti.gov/scitech/servlets/purl/5277693), 1983.
- [9] L.S. Darken, *Physical Chemistry of Metals*. ISBN 13: 9780070153554. Mc Graw Hill, 1953.
- [10] R.A. Strehlow and H.C. Savage, The Permeation of Hydrogen Isotopes through Structural Metals at Low Pressures and through Metals with Oxide Film Barriers, *Nuclear Technology* 22 (1974), 127-137.
- [11] L. Candido et al., An integrated hydrogen isotopes transport model for the TRIEX-II facility, *Fusion Engineering and Design* 155 (2020), 111585.
- [12] R. Bonifetto et al., Conceptual design of a mock-up for the EU DEMO Tritium Extraction System based on Permeator Against Vacuum technology", presented at the 12th International Conference on Tritium Science and Technology April 22-26, 2019.
- [13] M. Utili et al., Investigation on efficiency of gas liquid contactor used as tritium extraction unit for HCLL-TBM Pb-16Li loop, *Fusion Engineering and Design* 109-111, Part A (2016), 1-6.
- [14] V. D'Auria et al., Design of a Permeator-Against-Vacuum mock-up for the tritium extraction from PbLi at low speed, *Fusion Engineering and Design* 121 (2017) 198-203.
- [15] J. E. Shelby, Molecular diffusion and solubility of hydrogen isotopes in vitreous silica, *Journal of Applied Physics* 48 (1977), 3387-3394.
- [16] Star-CCM+ User's Manual, CD ADAPCO, New York, 2019.
- [17] F. R. Menter, Two-Equation Eddy-Viscosity Turbulence Models for Engineering Applications, *AIAA J.* 1994, 32, 1598-1605.
- [18] TL Bergman et al., *Fundamentals of heat and mass transfer*, 2011
- [19] Gruppo Lucefin [Online]. Available: [www.lucefin.com/wp-content/files\\_mf/10crmo910.pdf](http://www.lucefin.com/wp-content/files_mf/10crmo910.pdf), accessed on 07 Sept. 2020.
- [20] S. Timoshenko and J. N. Goodier, *Theory of elasticity*, McGRAW-HILL, 1951.
- [21] M. A. Pick and K. Sonnenberg, "A model for atomic hydrogen-metal interactions-application to recycling, recombination and permeation," *J. Nucl. Mater.*, vol. 131, pp. 208-220, 1985.



- [22] Goodfellow: Supplier of materials for research and development [Online]. Available: <https://www.goodfellow.com/it/>, accessed on 07 Sept. 2020.
- [23] COMSOL 5.1 Multiphysics.
- [24] D. Martelli, A. Venturini, and M. Utili, "Literature review of lead-lithium thermophysical properties," *Fusion Engineering and Design*, vol. 138, no. September 2018, pp. 183–195, 2019.
- [25] P. W. Humrickhouse and B. J. Merrill, "Vacuum Permeator Analysis for Extraction of Tritium from DCLL Blankets," *Fusion Sci. Technol.*, 68, 295 (2015).
- [26] I. Ali-Khan, K. J. Dietz, F. G. Waelbroeck, and P. Wienhold, "The rate of hydrogen release out of clean metallic surfaces," *J. Nucl. Mater.*, vol. 76–77, no. C, pp. 337–343, 1978.
- [27] P. L. Andrew and A. A. Haasz, "Models for hydrogen permeation in metals," *J. Appl. Phys.*, vol. 72, no. 7, pp. 2749–2757, 1992.
- [28] E. A. Denisov, M. V. Kompaniets, T. N. Kompaniets, and V. I. Spitsyn, "Surface-limited permeation regime in the study of hydrogen interactions with metals," *Meas. J. Int. Meas. Confed.*, vol. 117, no. August 2017, pp. 258–265, 2018.
- [29] P. Harriott and R. M. Hamilton, "Solid-liquid mass transfer in turbulent pipe flow," *Chem. Eng. Sci.*, vol. 20, no. 12, pp. 1073–1078, 1965.

## Appendix B

### Modelica code

```

package The_RadiaTube
  package Media
    package PbLi
      extends Modelica.Media.Incompressible.TableBased(mediumName = "PbLi",
        T_min = 508.15, T_max = 800, TinK = true, T0 = 603.15, npol = 1, npolViscosity =
        3, tableDensity = [TempData, DensityData], tableHeatCapacity = [TempData,
        HeatCapacityData], tableConductivity = [TempData, ConductivityData],
        tableViscosity = [TempData, ViscosityData], tableVaporPressure = [TempData,
        VaporData], Temperature(min = 508.15, max = 800, nominal = 603.15, start =
        603.15, displayUnit = "K"));

      redeclare function extends density_derT_p "Return density derivative wrt
      temperature at constant pressure"
        algorithm
          // density = 10520.35-1.19051*T
          ddTp := -1.19051;
        end density_derT_p;

      redeclare function extends density_derp_T "Return density derivative wrt
      pressure at const temperature"
        algorithm
          // incompressible medium: density doesn't depend on pressure
          ddpT := 0.0;
        end density_derp_T;

      redeclare function extends density_derh_p "Return density derivative wrt
      specific enthalpy at constant pressure"
        algorithm
          // density = -4.1876E-04*h + const
          ddhp := -4.1876e-04;
        end density_derh_p;

      redeclare function extends density_derp_h "Return density derivative wrt
      pressure at const specific enthalpy"
        algorithm
          // incompressible medium: density doesn't depend on pressure
          ddph := 0.0;
        end density_derp_h;
    protected
      constant Real[13, 1] TempData = [508; 525; 550; 575; 600; 625; 650; 675;
      700; 725; 750; 775; 800];
      constant Real[13, 1] ViscosityData = [0.0029423; 0.0026911; 0.0023839;
      0.0021341; 0.0019282; 0.0017564; 0.0016114; 0.0014879; 0.0013816; 0.0012896;
      0.0012092; 0.0011385; 0.0010760];
      constant Real[13, 1] DensityData = [9916; 9895; 9866; 9836; 9806; 9776;
      9747; 9717; 9687; 9657; 9627; 9598; 9568];
      constant Real[13, 1] HeatCapacityData = [0.1903690e3; 0.1902141e3;
      0.1899862e3; 0.1897583e3; 0.1895304e3; 0.1893025e3; 0.1890746e3; 0.1888467e3;
      0.1886188e3; 0.1883909e3; 0.1881630e3; 0.1879351e3; 0.1877072e3];
      constant Real[13, 1] ConductivityData = [0.19123285; 0.19457012;
      0.19947787; 0.20438562; 0.20929337; 0.21420112; 0.21910887; 0.22401662;
      0.22892437; 0.23383212; 0.23873987; 0.24364762; 0.24855537];
      constant Real[13, 1] VaporData = [4, 38775E-12; 1, 77686E-11; 1, 18104E-
      10; 6, 66418E-10; 3, 27662E-09; 1, 4326E-08; 5, 66035E-08; 2, 04755E-07; 6,
      85371E-07; 2, 14168E-06; 6, 29416E-06; 1, 75065E-05; 4, 63303E-05];
    annotation(

```

```

Documentation(info = "<html>

</html>"));
end PbLi;
end Media;

package Types
  type VolumetricHeat = Real(unit = "W/m3");
  type Sieverts_constant = Real(unit = "mol/m3/Pa0.5");
  type Recombination_constant = Real(unit = "m4/s/mol");
  type Permeation_constant = Real(unit = "mol/m/s/Pa0.5");
  type MoleFlux = Real(unit = "mol/m2/s");
end Types;

package Functions
  package Properties
    function rho_W
      input Modelica.Units.SI.Temperature T;
      output Modelica.Units.SI.Density rho;
    algorithm
      rho := 19302.7 - 2.3786e-01 .* (T - 273.15) - 2.2448e-05 .* (T - 273.15)
      .^ 2;
    end rho_W;

    package Niobio
      function Sieverts_const
        input Modelica.Units.SI.Temperature T;
        output Types.Sieverts_constant K_S;
      algorithm
        K_S := 0.127 * exp(5550 / T) "(mol/m3/Pa0.5) Sieverts' constant
        Steward (1975)";
      end Sieverts_const;

      function Diffusivity
        input Modelica.Units.SI.Temperature T;
        output Modelica.Units.SI.DiffusionCoefficient D "(m2/s) diffusivity in
        the solid. Volk&Alefed (1975)";
      algorithm
        D := 5e-8 * exp(-1230 / T);
      end Diffusivity;

      function Recombination_const
        input Modelica.Units.SI.Temperature T;
        output Types.Recombination_constant k_rec "(m4/s/mol)";
      algorithm
        k_rec := 1e-16 + 2e-12 * (T - 500) * Modelica.Constants.N_A * 10e-8;
      end Recombination_const;

      function Permeation_const
        input Modelica.Units.SI.Temperature T;
        output Types.Permeation_constant Phi "(m4/s/mol)";
      algorithm
        Phi := 1.28e-8;
      end Permeation_const;
    end Niobio;

    package PbLi
      function rho_PbLi
        input Modelica.Units.SI.Temperature T;
        output Modelica.Units.SI.Density rho;
      algorithm
        rho := 10.52 * (1 - 113e-6 * T) * 1e3;
      end rho_PbLi;
    end PbLi;
  end Properties;
end Functions;

```

```

function visc_PbLi
  input Modelica.Units.SI.Temperature T;
  output Modelica.Units.SI.DynamicViscosity visc;
algorithm
  visc := 1.87e-4 * exp(11640 / Modelica.Constants.R / T);
end visc_PbLi;

function Sieverts_const
  input Modelica.Units.SI.Temperature T;
  output Types.Sieverts_constant K_S;
algorithm
  K_S := 0.237 * exp(-12844 / Modelica.Constants.R / T) * (mol/m3/Pa0.5)
AIELLO";
end Sieverts_const;

function Diffusivity
  input Modelica.Units.SI.Temperature T;
  output Modelica.Units.SI.DiffusionCoefficient D "(m2/s)";
algorithm
  D := 2.5e-7 * exp(-27000 / Modelica.Constants.R / T);
end Diffusivity;
end PbLi;
end Properties;

function Reynolds "Reynolds Number"
  input Modelica.Units.SI.Density rho "Density";
  input Modelica.Units.SI.Velocity v "Fluid speed";
  input Modelica.Units.SI.Diameter D "Characteristic length";
  input Modelica.Units.SI.DynamicViscosity mu "Dynamic viscosity";
  output Modelica.Units.SI.ReynoldsNumber Re "Reynolds Number";
algorithm
  Re := rho * abs(v) * D / mu;
end Reynolds;

function Prandtl "Prandtl Number"
  input Modelica.Units.SI.DynamicViscosity mu "Dynamic viscosity";
  input Modelica.Units.SI.SpecificHeatCapacity cp "Specific heat capacity";
  input Modelica.Units.SI.ThermalConductivity k "Thermal conductivity";
  output Modelica.Units.SI.PrandtlNumber Pr "Prandtl Number";
algorithm
  Pr := mu * cp / k;
end Prandtl;

function Rayleigh "Rayleigh Number for ideal gases"
  input Modelica.Units.SI.Temperature T_a "Surface temperature";
  input Modelica.Units.SI.Temperature T_b "Ambient temperature";
  input Modelica.Units.SI.Length D "Characteristic length";
  input Modelica.Units.SI.KinematicViscosity ni "Kinematic viscosity at
T_film";
  input Modelica.Units.SI.ThermalDiffusivity alpha "Thermal diffusivity at
T_film";
  output Modelica.Units.SI.RayleighNumber Ra "Rayleigh Number";
protected
  parameter Modelica.Units.SI.Temperature T_film = (T_a + T_b) / 2 "Average
temperature";
  parameter Real beta = 1 / T_film "Volumetric thermal expansion coefficient
(ideal gas)";
  constant Real g = Modelica.Constants.g_n;
algorithm
  Ra := g * beta * (T_a - T_b) * D ^ 3 / (alpha * ni);
end Rayleigh;

function Grashof "Grashof Number"
  input Modelica.Units.SI.Temperature T_a "Surface temperature";

```

```

    input Modelica.Units.SI.Temperature T_b "Ambient temperature";
    input Modelica.Units.SI.Length D "Characteristic length";
    input Modelica.Units.SI.KinematicViscosity ni "Kinematic viscosity at
T_film";
    output Real Gr "Grashof Number";
    protected
    parameter Modelica.Units.SI.Temperature T_film = (T_a + T_b) / 2 "Average
temperature";
    parameter Real beta = 1 / T_film "Volumetric thermal expansion coefficient
(ideal gas)";
    constant Real g = Modelica.Constants.g_n;
    algorithm
    Gr := g * beta * (T_a - T_b) * D ^ 3 / ni ^ 2;
    end Grashof;
end Functions;

model TP
    parameter input Integer N_DX = 40 "(-) # axial elements";
    parameter input Modelica.Units.SI.Length length = 40 "(m) length";
    parameter input Modelica.Units.SI.Diameter diameter_in = 0.0092 "(m) inner
diameter";
    parameter input Modelica.Units.SI.Length thickness = 4e-4 "(m) membrane
thickness";
    parameter input Modelica.Units.SI.Pressure p_0 = 100 "(Pa) partial pressure
of H/D/T at the inlet";
    parameter input Modelica.Units.SI.Temperature T = 603.15 "(K) temperature
mean value for properties";
    input Modelica.Units.SI.Velocity V_permeation = 0.1 "(m/s) fluid mean
velocity";
    // Nb and PbLi properties.
    Types.Sieverts_constant Ks_Nb =
Functions.Properties.Niobio.Sieverts_const(T);
    Modelica.Units.SI.DiffusionCoefficient D_Nb =
Functions.Properties.Niobio.Diffusivity(T);
    Types.Permeation_constant Phi_Nb =
Functions.Properties.Niobio.Permeation_const(T);
    Types.Sieverts_constant Ks_PbLi =
Functions.Properties.PbLi.Sieverts_const(T);
    Modelica.Units.SI.DiffusionCoefficient D_PbLi =
Functions.Properties.PbLi.Diffusivity(T);
    Modelica.Units.SI.Density rho_PbLi = Functions.Properties.PbLi.rho_PbLi(T);
    Modelica.Units.SI.DynamicViscosity visc_PbLi =
Functions.Properties.PbLi.visc_PbLi(T);
    // Dimensionless number
    Modelica.Units.SI.ReynoldsNumber Re = abs(rho_PbLi * V_permeation *
diameter_in / visc_PbLi) "(-) Reynolds";
    Modelica.Units.SI.SchmidtNumber Sc = visc_PbLi / (rho_PbLi * D_PbLi) "(-)
Schmidt number for PbLi";
    Modelica.Units.SI.NusseltNumberOfMassTransfer Sh = 0.0096 * Re ^ 0.913 * Sc
^ 0.346;
    Modelica.Units.SI.Velocity h_t = Sh * D_PbLi / diameter_in "(m/s) mass
transport coeff";
    Modelica.Units.SI.MolalConcentration C0 = Ks_PbLi * sqrt(p_0) "(kg/m3) inlet
Tritium concentration";
    Modelica.Units.SI.MolalConcentration C_DL[N_DX] "(Kg/m3) Tritium
concentration along the pipe";
    Types.MoleFlux J_DL[N_DX] "(mol/m2/s) molar flux";
    Modelica.Units.SI.Efficiency Extraction_Efficiency "(-) extraction
efficiency";
    Modelica.Units.SI.Efficiency eta[N_DX] "(-) extraction efficiency along
axial direction";
    equation
    // Permeation performed in DLR
    for ii in 1:N_DX loop

```



```

    if ii == 1 then
        J_DL[ii] = h_t * C0 * (1 - 1 / (1 + Phi_Nb / h_t / Ks_PbLi / thickness))
    "permeated flux";
        C_DL[ii] = C0 - 4 / diameter_in / V_permeation * length / N_DX *
J_DL[ii] "ii-th Tritium concentration";
        eta[ii] = 1 - C_DL[ii] / C0 "efficiency along axial direction";
    else
        J_DL[ii] = h_t * (C_DL[ii - 1] - C_DL[ii - 1] / (1 + Phi_Nb / h_t /
Ks_PbLi / thickness)) "permeated flux";
        C_DL[ii] = C_DL[ii - 1] - 4 / diameter_in / V_permeation * length / N_DX
* J_DL[ii] "ii-th Tritium concentration";
        eta[ii] = 1 - C_DL[ii] / C0 "efficiency along axial direction";
    end if;
end for;
Extraction_Efficiency = 1 - C_DL[end] / C0;
end TP;

model RadiaTube
    Modelica.Units.SI.PressureDifference DeltaP;
    constant Real pi = Modelica.Constants.pi;
    constant Real g = Modelica.Constants.g_n;
    constant Real sigma = Modelica.Constants.sigma;
    replaceable package Medium = Media.PbLi;
    parameter Integer N(min = 3) = 3 "Number of nodes";
    parameter input Modelica.Units.SI.Length Lt = 1.9/2 "(m) Length" annotation(
        Dialog(group = "Geometry"));
    parameter input Modelica.Units.SI.Length thickness = 4e-4 "Membrane
thickness" annotation(
        Dialog(group = "Geometry"));
    parameter Modelica.Units.SI.Diameter Dt = 0.0092 "Pipe inner diameter"
annotation(
        Dialog(group = "Geometry"));
    // Radiation properties
    parameter input Real ems1 = 0.15 "ems";
    parameter input Real F11 = 0.06 "View Factor diagonal";
    parameter input Real A1 = 0.358/2/Nv "Area scambio termico tubicino";
    final parameter Real RR1 = 1 / ((1 - ems1) / (ems1 * A1 / Nv) + 1 / (A1 *
F11/ Nv) / 2);
    parameter input Real F12 = 0.09 "View Factor frontal";
    parameter input Integer flag2 = 1 "1=active; 0=non active";
    final parameter Real RR2 = 1 / ((1 - ems1) / (ems1 * A1 / Nv) + 1 / (A1 *
F12/ Nv) / 2);
    parameter input Real F13 = 0.09 "View Factor frontal";
    parameter input Integer flag3 = 1 "1=active; 0=non active";
    final parameter Real RR3 = 1 / ((1 - ems1) / (ems1 * A1 / Nv) + 1 / (A1 *
F13/ Nv) / 2);
    parameter input Real F14 = 0.76 "View Factor w/ Envelope";
    parameter input Integer flag4 = 1 "1=active; 0=non active";
    final parameter Real RR4 = 1 / ((1 - ems1) / (ems1 * A1 / Nv) + 1 / (A1 *
F14/ Nv) / 2);
    // Initialization
    parameter Modelica.Units.SI.MassFlowRate m_start = 0.5 "Start mass flow
rate" annotation(
        Evaluate = true,
        Dialog(tab = "Initialization"));
    parameter Modelica.Units.SI.AbsolutePressure p_start = 1e5 "Start pressure"
annotation(
        Evaluate = true,
        Dialog(tab = "Initialization"));
    parameter Modelica.Units.SI.Temperature Tf_start(each displayUnit = "K") =
723.15 "Start fluid temperature" annotation(
        Evaluate = true,
        Dialog(tab = "Initialization"));
    // Variables

```

```

Medium.MassFlowRate m(start = m_start) "Mass flow rate";
Medium.Temperature Tf[N] (each start = Tf_start) "Fluid temperature at
nodes";
Medium.Temperature Tfv[Nv] (each start = Tf_start) "Fluid temperature at
volumes";
Medium.SpecificEnthalpy h[N] (each start = h_start) "Fluid specific enthalpy
at nodes";
Medium.Density rho[Nv] (each start = rho_start) "Density";
Medium.ThermalConductivity k[Nv] (each start = k_start) "Thermal
conductivity";
Medium.SpecificHeatCapacity cp[Nv] (each start = cp_start) "Specific heat";
Medium.DynamicViscosity mu[Nv] (each start = mu_start) "Dynamic viscosity";
Modelica.Units.SI.Velocity v[Nv] (each start = m_start / rho_start / A)
"Fluid speed";
Modelica.Units.SI.CoefficientOfFriction ff[Nv] "Friction factor";
Modelica.Units.SI.Power Qf1[Nv] "Rad heat transfer";
Modelica.Units.SI.Power Qf2[Nv] "Rad heat transfer";
Modelica.Units.SI.Power Qf3[Nv] "Rad heat transfer";
Modelica.Units.SI.Power Qf4[Nv] "Rad heat transfer";
Modelica.Units.SI.Power dedt[Nv] "J/s";
Modelica.Units.SI.MassFlowRate dMdt[Nv];
Modelica.Units.SI.PrandtlNumber Pr[Nv] "Prandtl number";
Modelica.Units.SI.ReynoldsNumber Re[Nv] "Reynolds number";
// Interfaces
Modelica.Fluid.Interfaces.FluidPort_a inFlow(redeclare package Medium =
Medium) annotation(
  Placement(transformation(extent = {{-110, -10}, {-90, 10}})));
Modelica.Fluid.Interfaces.FluidPort_b outFlow(redeclare package Medium =
Medium) annotation(
  Placement(transformation(extent = {{90, -10}, {110, 10}})));
Permeation_Validation.TP TP(T=723.15, V_permeation = v[1], diameter_in = Dt,
length = Lt, thickness = thickness) annotation(
  Placement(visible = true, transformation(origin = {0, 0}, extent = {{-20,
-20}, {20, 20}}, rotation = 0)));
Modelica.Thermal.HeatTransfer.Interfaces.HeatPort_a VF_1[Nv] annotation(
  Placement(visible = true, transformation(origin = {-70, 30}, extent = {{-
20, -20}, {20, 20}}, rotation = 0), iconTransformation(origin = {-90, 90},
extent = {{-10, -10}, {10, 10}}, rotation = 0)));
Modelica.Thermal.HeatTransfer.Interfaces.HeatPort_a VF_2[Nv] annotation(
  Placement(visible = true, transformation(origin = {-30, 50}, extent = {{-
20, -20}, {20, 20}}, rotation = 0), iconTransformation(origin = {-90, -90},
extent = {{-10, -10}, {10, 10}}, rotation = 0)));
Modelica.Thermal.HeatTransfer.Interfaces.HeatPort_a VF_3[Nv] annotation(
  Placement(visible = true, transformation(origin = {30, 50}, extent = {{20,
-20}, {-20, 20}}, rotation = 0), iconTransformation(origin = {90, -90}, extent =
{{-10, -10}, {10, 10}}, rotation = 0)));
Modelica.Thermal.HeatTransfer.Interfaces.HeatPort_a VF_4[Nv] annotation(
  Placement(visible = true, transformation(origin = {70, 30}, extent = {{-
20, -20}, {20, 20}}, rotation = 0), iconTransformation(origin = {90, 90}, extent
= {{-10, -10}, {10, 10}}, rotation = 0)));

protected
parameter Integer Nv = N - 1 "(-) # of CV in the tube";
parameter Modelica.Units.SI.Length dx[Nv] = fill(Lt / Nv, Nv) "Length of the
CVs";
parameter Modelica.Units.SI.Area A = pi / 4 * Dt ^ 2 "(m2) cross section";
parameter Modelica.Units.SI.Area Ah[Nv] = pi * Dt / 2 .* dx "(m2) heat
transfer Area";
parameter Medium.ThermodynamicState startState = Medium.setState_pT(1e5,
Tf_start);
parameter Modelica.Units.SI.Density rho_start = Medium.density(startState);
parameter Modelica.Units.SI.ThermalConductivity k_start =
Medium.thermalConductivity(startState);

```

```

parameter Modelica.Units.SI.SpecificHeatCapacity cp_start =
Medium.specificHeatCapacityCp(startState);
parameter Modelica.Units.SI.DynamicViscosity mu_start =
Medium.dynamicViscosity(startState);
parameter Modelica.Units.SI.SpecificEnthalpy h_start =
Medium.specificEnthalpy(startState);
Medium.ThermodynamicState stateNodes[N];
Medium.ThermodynamicState stateVolumes[Nv];
Medium.DerDensityByEnthalpy drdT[Nv];
Medium.AbsolutePressure Dp_f[Nv];
initial equation
der(Tf[2:N]) = zeros(N - 1);
equation
DeltaP = inFlow.p - outFlow.p;
m = inFlow.m_flow;
h[1] = inStream(inFlow.h_outflow);
sum(m * h[N]) = inFlow.m_flow * outFlow.h_outflow;
for ii in 1:N loop
stateNodes[ii] = Medium.setState_pT(1e5, Tf[ii]);
h[ii] = Medium.specificEnthalpy(stateNodes[ii]);
end for;
for ii in 1:Nv loop
Tfv[ii] = (Tf[ii] + Tf[ii + 1]) / 2;
stateVolumes[ii] = Medium.setState_pT(1e5, Tfv[ii]);
rho[ii] = Medium.density(stateVolumes[ii]);
k[ii] = Medium.thermalConductivity(stateVolumes[ii]);
cp[ii] = Medium.specificHeatCapacityCp(stateVolumes[ii]);
mu[ii] = Medium.dynamicViscosity(stateVolumes[ii]);
drdT[ii] = Medium.density_derT_p(stateVolumes[ii]);
v[ii] = m / (A * rho[ii]);
end for;
// Dimensionless numbers
for ii in 1:Nv loop
Re[ii] = Functions.Reynolds(rho[ii], v[ii], Dt, mu[ii]);
Pr[ii] = Functions.Prandtl(mu[ii], cp[ii], k[ii]);
end for;
// Energy balance
for ii in 1:Nv loop
Qf1[ii] = +sigma / RR1 * (VF_1[ii].T ^ 4 - Tfv[ii] ^ 4);
Qf2[ii] = +sigma / RR2 * (VF_2[ii].T ^ 4 - Tfv[ii] ^ 4) * flag2;
Qf3[ii] = +sigma / RR3 * (VF_3[ii].T ^ 4 - Tfv[ii] ^ 4) * flag3;
Qf4[ii] = +sigma / RR4 * (VF_4[ii].T ^ 4 - Tfv[ii] ^ 4) * flag4;
VF_1[ii].Q_flow = Qf1[ii];
VF_2[ii].Q_flow = Qf2[ii];
VF_3[ii].Q_flow = Qf3[ii];
VF_4[ii].Q_flow = Qf4[ii];
dedt[ii] = A * dx[ii] * (rho[ii] * cp[ii] * der(Tf[ii + 1]) + h[ii + 1] *
drdT[ii] * der(Tf[ii + 1]));
dedt[ii] + m * (h[ii + 1] - h[ii]) = Qf1[ii] + Qf2[ii] + Qf3[ii] +
Qf4[ii];
end for;
// Mass balance
sum(dMdt) = inFlow.m_flow + outFlow.m_flow;
for ii in 1:Nv loop
dMdt[ii] = A * dx[ii] * drdT[ii] * der(Tf[ii + 1]);
end for;
// Momentum balance
0 = inFlow.p - outFlow.p - sum(Dp_f);
for ii in 1:Nv loop
Dp_f[ii] = 0.5 * ff[ii] * (dx[ii] / Dt) * rho[ii] * v[ii] ^ 2;
ff[ii] = 0.2413 * Re[ii] ^ (-0.235);
end for;
// Reverse flow (NOT USED!)
sum(h[N] - h[1]) = inStream(outFlow.h_outflow) - inFlow.h_outflow;

```

```

    annotation(
      Icon(coordinateSystem(preserveAspectRatio = false), graphics =
        {Rectangle(lineColor = {28, 108, 200}, fillColor = {255, 255, 255}, fillPattern
          = FillPattern.HorizontalCylinder, extent = {{-100, 60}, {100, -60}}},
          Line(points = {{-60, 0}, {60, 0}}, thickness = 0.5), Line(points = {{60, 0},
            {40, 14}}, thickness = 0.5), Line(points = {{60, 0}, {40, -14}}, thickness =
            0.5)),
        Diagram(coordinateSystem(preserveAspectRatio = false)));
    end RadiaTube;

model RadiaTube_simple
  Modelica.Units.SI.PressureDifference DeltaP;
  // Constants
  constant Real pi = Modelica.Constants.pi;
  constant Real g = Modelica.Constants.g_n;
  constant Real sigma = Modelica.Constants.sigma;
  // Medium
  replaceable package Medium = Media.PbLi;
  // Mesh
  parameter Integer N(min = 3) = 3 "Number of nodes";
  // Geometry
  parameter input Modelica.Units.SI.Length Lt = 10 "Length" annotation(
    Dialog(group = "Geometry"));
  parameter input Modelica.Units.SI.Length thickness = 4e-4 "Membrane
thickness" annotation(
    Dialog(group = "Geometry"));
  parameter Modelica.Units.SI.Diameter Dt = 0.01 "Pipe inner diameter"
annotation(
  Dialog(group = "Geometry"));
  // Initialization
  parameter Modelica.Units.SI.MassFlowRate m_start = 0.5 "Start mass flow
rate" annotation(
    Evaluate = true,
    Dialog(tab = "Initialization"));
  parameter Modelica.Units.SI.AbsolutePressure p_start = 1e5 "Start pressure"
annotation(
    Evaluate = true,
    Dialog(tab = "Initialization"));
  parameter Modelica.Units.SI.Temperature Tf_start(each displayUnit = "K") =
603.15 "Start fluid temperature" annotation(
    Evaluate = true,
    Dialog(tab = "Initialization"));
  // Variables
  Medium.MassFlowRate m(start = m_start) "Mass flow rate";
  Medium.Temperature Tf[N] (each start = Tf_start) "Fluid temperature at
nodes";
  Medium.Temperature Tfv[Nv] (each start = Tf_start) "Fluid temperature at
volumes";
  Medium.SpecificEnthalpy h[N] (each start = h_start) "Fluid specific enthalpy
at nodes";
  Medium.Density rho[Nv] (each start = rho_start) "Density";
  Medium.ThermalConductivity k[Nv] (each start = k_start) "Thermal
conductivity";
  Medium.SpecificHeatCapacity cp[Nv] (each start = cp_start) "Specific heat";
  Medium.DynamicViscosity mu[Nv] (each start = mu_start) "Dynamic viscosity";
  Modelica.Units.SI.Velocity v[Nv] (each start = m_start / rho_start / A)
"Fluid speed";
  Modelica.Units.SI.CoefficientOfFriction ff[Nv] "Friction factor";
  Modelica.Units.SI.Power Qf1[Nv] "Rad heat transfer";
  Modelica.Units.SI.Power dedt[Nv] "J/s";
  Modelica.Units.SI.MassFlowRate dMdt[Nv];
  Modelica.Units.SI.PrandtlNumber Pr[Nv] "Prandtl number";
  Modelica.Units.SI.ReynoldsNumber Re[Nv] "Reynolds number";
  // Interfaces

```



```

    Modelica.Fluid.Interfaces.FluidPort_a inFlow(redeclare package Medium =
Medium) annotation(
    Placement(transformation(extent = {{-110, -10}, {-90, 10}})));
    Modelica.Fluid.Interfaces.FluidPort_b outFlow(redeclare package Medium =
Medium) annotation(
    Placement(transformation(extent = {{90, -10}, {110, 10}})));
    Permeation_Validation.TP TP(T (displayUnit = "degC") = 603.15, V_permeation
= v[1], diameter_in = Dt, length = Lt, thickness = thickness) annotation(
    Placement(visible = true, transformation(origin = {0, 0}, extent = {{-20,
-20}, {20, 20}}, rotation = 0)));

    protected
    parameter Integer Nv = N - 1 "(-) # of CV in the tube";
    parameter Modelica.Units.SI.Length dx[Nv] = fill(Lt / Nv, Nv) "Length of the
CVs";
    parameter Modelica.Units.SI.Area A = pi / 4 * Dt ^ 2 "(m2) cross section";
    parameter Modelica.Units.SI.Area Ah[Nv] = pi * Dt / 2 .* dx "(m2) heat
transfer Area";
    parameter Medium.ThermodynamicState startState = Medium.setState_pT(1e5,
Tf_start);
    parameter Modelica.Units.SI.Density rho_start = Medium.density(startState);
    parameter Modelica.Units.SI.ThermalConductivity k_start =
Medium.thermalConductivity(startState);
    parameter Modelica.Units.SI.SpecificHeatCapacity cp_start =
Medium.specificHeatCapacityCp(startState);
    parameter Modelica.Units.SI.DynamicViscosity mu_start =
Medium.dynamicViscosity(startState);
    parameter Modelica.Units.SI.SpecificEnthalpy h_start =
Medium.specificEnthalpy(startState);
    Medium.ThermodynamicState stateNodes[N];
    Medium.ThermodynamicState stateVolumes[Nv];
    Medium.DerDensityByEnthalpy drdT[Nv];
    Medium.AbsolutePressure Dp_f[Nv];
    initial equation
    der(Tf[2:N]) = zeros(N - 1);
    equation
    DeltaP = inFlow.p - outFlow.p;
    // Boundary conditions
    m = inFlow.m_flow;
    h[1] = inStream(inFlow.h_outflow);
    sum(m .* h[N]) = inFlow.m_flow * outFlow.h_outflow;
    // Fluid properties
    for ii in 1:N loop
    // "each node"
    stateNodes[ii] = Medium.setState_pT(1e5, Tf[ii]);
    h[ii] = Medium.specificEnthalpy(stateNodes[ii]);
    end for;
    // Average properties
    for ii in 1:Nv loop
    // "each cv"
    Tfv[ii] = (Tf[ii] + Tf[ii + 1]) / 2;
    stateVolumes[ii] = Medium.setState_pT(1e5, Tfv[ii]);
    rho[ii] = Medium.density(stateVolumes[ii]);
    k[ii] = Medium.thermalConductivity(stateVolumes[ii]);
    cp[ii] = Medium.specificHeatCapacityCp(stateVolumes[ii]);
    mu[ii] = Medium.dynamicViscosity(stateVolumes[ii]);
    drdT[ii] = Medium.density_derT_p(stateVolumes[ii]);
    v[ii] = m / (A * rho[ii]);
    end for;
    // Dimensionless numbers
    for ii in 1:Nv loop
    Re[ii] = Functions.Reynolds(rho[ii], v[ii], Dt, mu[ii]);
    Pr[ii] = Functions.Prandtl(mu[ii], cp[ii], k[ii]);
    end for;

```

```

// Energy balance
for ii in 1:Nv loop
  Qf1[ii] = 0;
  dedt[ii] = A * dx[ii] * (rho[ii] * cp[ii] * der(Tf[ii + 1]) + h[ii + 1] *
drdT[ii] * der(Tf[ii + 1]));
  dedt[ii] + m * (h[ii + 1] - h[ii]) = Qf1[ii];
end for;
// Mass balance
sum(dMdt) = inFlow.m_flow + outFlow.m_flow;
for ii in 1:Nv loop
  dMdt[ii] = A * dx[ii] * drdT[ii] * der(Tf[ii + 1]);
end for;
// Momentum balance
0 = inFlow.p - outFlow.p - sum(Dp_f);
for ii in 1:Nv loop
  Dp_f[ii] = 0.5 * ff[ii] * (dx[ii] / Dt) * rho[ii] * v[ii] ^ 2;
  ff[ii] = 0.2413 * Re[ii] ^ (-0.235);
end for;
// Reverse flow
sum(h[N] - h[1]) = inStream(outFlow.h_outflow) - inFlow.h_outflow;
annotation(
  Icon(coordinateSystem(preserveAspectRatio = false), graphics =
{Rectangle(lineColor = {28, 108, 200}, fillColor = {255, 255, 255}, fillPattern
= FillPattern.HorizontalCylinder, extent = {{-100, 60}, {100, -60}}),
Line(points = {{-60, 0}, {60, 0}}, thickness = 0.5), Line(points = {{60, 0},
{40, 14}}, thickness = 0.5), Line(points = {{60, 0}, {40, -14}}, thickness =
0.5)}),
Diagram(coordinateSystem(preserveAspectRatio = false)));
end RadiaTube_simple;

model Envelope
  parameter Modelica.Units.SI.Temperature T_amb=15+273.15 "Temperature
ambient";
  parameter Modelica.Units.SI.Area A_env= 1.125 "External Area of the vessel";
  // Constants
  constant Real pi = Modelica.Constants.pi;
  constant Real sigma = Modelica.Constants.sigma;
  // Mesh
  parameter Integer N(min = 3) = 3 "Number of nodes";
  // Geometry
  parameter input Modelica.Units.SI.Length Lt = 1 "(m) Length" annotation(
    Dialog(group = "Geometry"));
  // Radiation properties

  parameter input Real ems1 = 0.4 "emissività superficiale";
  parameter input Real F11 = 0.24/2 "View Factor w/ tube";
  parameter input Real A1 = A_env / Nv "Area tubicino";
  final parameter Real RR1 = 1 / ((1 - ems1) / (ems1 * A1/ Nv) + 1 / (A1/ Nv
* F11) / 2);
  parameter input Real F12 = 0.24/2 "View Factor w/ tube";
  parameter input Integer flag2 = 1 "1=active; 0=non active";
  final parameter Real RR2 = 1 / ((1 - ems1) / (ems1 * A1/ Nv) + 1 / (A1/ Nv *
F12) / 2);
  parameter input Real F13 = 0.24/2 "View Factor w/ tube";
  parameter input Integer flag3 = 1 "1=active; 0=non active";
  final parameter Real RR3 = 1 / ((1 - ems1) / (ems1 * A1/ Nv) + 1 / (A1/ Nv *
F13) / 2);
  parameter input Real F14 = 0.24/2 "View Factor w/ tube";
  parameter input Integer flag4 = 1 "1=active; 0=non active";
  final parameter Real RR4 = 1 / ((1 - ems1) / (ems1 * A1/ Nv) + 1 / (A1/ Nv *
F14) / 2);
  // Initialization
  parameter Modelica.Units.SI.Temperature Tf_start(each displayUnit = "K") =
T_amb "Start fluid temperature" annotation(

```

```

    Evaluate = true,
    Dialog(tab = "Initialization"));
// Variables
Modelica.Units.SI.Temperature Tfv[Nv] (each start = Tf_start) "Fluid
temperature at volumes";
Modelica.Units.SI.Power Qf1[Nv] "Rad heat transfer";
Modelica.Units.SI.Power Qf2[Nv] "Rad heat transfer";
Modelica.Units.SI.Power Qf3[Nv] "Rad heat transfer";
Modelica.Units.SI.Power Qf4[Nv] "Rad heat transfer";
Modelica.Units.SI.Power Q_amb[Nv] "heat transfer w/ ambient";
// Interfaces
Modelica.Thermal.HeatTransfer.Interfaces.HeatPort_a VF_1[Nv] annotation(
    Placement(visible = true, transformation(origin = {-115, -1}, extent = {{-
29, -29}, {29, 29}}, rotation = 0), iconTransformation(origin = {-120, 2.22045e-
16}, extent = {{-20, -20}, {20, 20}}, rotation = 0)));
Modelica.Thermal.HeatTransfer.Interfaces.HeatPort_a VF_2[Nv] annotation(
    Placement(visible = true, transformation(origin = {1, -115}, extent = {{-
29, -29}, {29, 29}}, rotation = 0), iconTransformation(origin = {-2.22045e-16, -
120}, extent = {{-20, -20}, {20, 20}}, rotation = 0)));
Modelica.Thermal.HeatTransfer.Interfaces.HeatPort_a VF_3[Nv] annotation(
    Placement(visible = true, transformation(origin = {115, -1}, extent = {{-
29, -29}, {29, 29}}, rotation = 0), iconTransformation(origin = {120, 2.22045e-
16}, extent = {{-20, -20}, {20, 20}}, rotation = 0)));
Modelica.Thermal.HeatTransfer.Interfaces.HeatPort_a VF_4[Nv] annotation(
    Placement(visible = true, transformation(origin = {-1, 85}, extent = {{-
29, -29}, {29, 29}}, rotation = 0), iconTransformation(origin = {0, 80}, extent
= {{-20, -20}, {20, 20}}, rotation = 0)));
protected
    parameter Integer Nv = N - 1 "(-) # of CV in the tube";
    parameter Modelica.Units.SI.Length dx[Nv] = fill(Lt / Nv, Nv) "Length of the
CVs";
// Constant properties
    parameter Modelica.Units.SI.Density rho = 7800 "Density";
    parameter Modelica.Units.SI.SpecificHeatCapacity cp = 560 "Specific heat";
    initial equation
//der(Tfv[2:N]) = zeros(N - 1);
    equation
// Energy balance
    for ii in 1:Nv loop
        Qf1[ii] = +sigma / RR1 * (VF_1[ii].T ^ 4 - Tfv[ii] ^ 4);
        Qf2[ii] = +sigma / RR2 * (VF_2[ii].T ^ 4 - Tfv[ii] ^ 4) * flag2;
        Qf3[ii] = +sigma / RR3 * (VF_3[ii].T ^ 4 - Tfv[ii] ^ 4) * flag3;
        Qf4[ii] = +sigma / RR4 * (VF_4[ii].T ^ 4 - Tfv[ii] ^ 4) * flag4;
        Q_amb[ii] = A_env/Nv*10*(T_amb-Tfv[ii]);
        VF_1[ii].Q_flow = Qf1[ii];
        VF_2[ii].Q_flow = Qf2[ii];
        VF_3[ii].Q_flow = Qf3[ii];
        VF_4[ii].Q_flow = Qf4[ii];
        Qf1[ii] + Qf2[ii] + Qf3[ii] + Qf4[ii] + Q_amb[ii] = A1 * dx[ii] * (rho * cp
* der(Tfv[ii]));
    end for;
end Envelope;

package Tests_Simple

    model Permeation
        Permeation_Validation.RadiaTube_simple Radiatube(DeltaZ = 0, Dt = 0.0092,
Lt = 40, thickness = 4e-4) annotation(
            Placement(visible = true, transformation(origin = {48, -48}, extent =
{{-10, -10}, {10, 10}}, rotation = 0)));
        Modelica.Fluid.Sources.MassFlowSource_T MassFlow_BC(redeclare package
Medium = Permeation_Validation.Media.PbLi, T = 603.15, nPorts = 1, use_T_in =
true, use_m_flow_in = true) annotation(

```

```

        Placement(visible = true, transformation(origin = {23, -49}, extent =
        {{-7, -7}, {7, 7}}, rotation = 0));
        Modelica.Fluid.Sources.Boundary_pT Pressure_BC(redeclare package Medium =
        Permeation_Validation.Media.PbLi, T = 603.15, nPorts = 1, p = 1e5, use_p_in =
        true) annotation(
        Placement(visible = true, transformation(origin = {73, -49}, extent =
        {{5, -5}, {-5, 5}}, rotation = 0));
        Modelica.Blocks.Sources.RealExpression Mass_Flow_Inlet(y = 0.1358)
        annotation(
        Placement(visible = true, transformation(origin = {26, -26}, extent =
        {{10, -10}, {-10, 10}}, rotation = 0));
        Modelica.Blocks.Sources.RealExpression Pressure_Outlet(y = 1e5)
        annotation(
        Placement(visible = true, transformation(origin = {70, -26}, extent =
        {{-10, -10}, {10, 10}}, rotation = 0));
        Modelica.Blocks.Sources.RealExpression Temperature_Inlet(y = 603.15)
        annotation(
        Placement(visible = true, transformation(origin = {26, -68}, extent =
        {{10, -10}, {-10, 10}}, rotation = 0));
        equation
        connect(MassFlow_BC.ports[1], Radiatube.inFlow) annotation(
        Line(points = {{30, -49}, {38, -49}, {38, -48}}, color = {0, 127,
        255}));
        connect(Radiatube.outFlow, Pressure_BC.ports[1]) annotation(
        Line(points = {{58, -48}, {68, -48}}, color = {0, 127, 255}));
        connect(MassFlow_BC.m_flow_in, Mass_Flow_Inlet.y) annotation(
        Line(points = {{16, -44}, {15, -44}, {15, -26}}, color = {0, 0, 127}));
        connect(Pressure_BC.p_in, Pressure_Outlet.y) annotation(
        Line(points = {{80, -44}, {82, -44}, {82, -26}}, color = {0, 0, 127}));
        connect(MassFlow_BC.T_in, Temperature_Inlet.y) annotation(
        Line(points = {{14, -46}, {14, -57}, {16, -57}, {16, -68}}, color = {0,
        0, 127}));
        end Permeation;

    model Hydraulic
        Permeation_Validation.Radiatube_simple Radiatube(DeltaZ = 0, Dt = 0.0092,
        Lt = 1.8995, thickness = 4e-4) annotation(
        Placement(visible = true, transformation(origin = {48, -48}, extent =
        {{-10, -10}, {10, 10}}, rotation = 0));
        Modelica.Fluid.Sources.MassFlowSource_T MassFlow_BC(redeclare package
        Medium = Permeation_Validation.Media.PbLi, T = 723.15, m_flow = 0.0925, nPorts =
        1, use_T_in = true, use_m_flow_in = false) annotation(
        Placement(visible = true, transformation(origin = {23, -49}, extent =
        {{-7, -7}, {7, 7}}, rotation = 0));
        Modelica.Fluid.Sources.Boundary_pT Pressure_BC(redeclare package Medium =
        Permeation_Validation.Media.PbLi, T = 723.15, nPorts = 1, p = 1e5, use_p_in =
        true) annotation(
        Placement(visible = true, transformation(origin = {73, -49}, extent =
        {{5, -5}, {-5, 5}}, rotation = 0));
        Modelica.Blocks.Sources.RealExpression Mass_Flow_Inlet(y = 0.09)
        annotation(
        Placement(visible = true, transformation(origin = {26, -26}, extent =
        {{10, -10}, {-10, 10}}, rotation = 0));
        Modelica.Blocks.Sources.RealExpression Pressure_Outlet(y = 1e5)
        annotation(
        Placement(visible = true, transformation(origin = {70, -26}, extent =
        {{-10, -10}, {10, 10}}, rotation = 0));
        Modelica.Blocks.Sources.RealExpression Temperature_Inlet(y = 723.15)
        annotation(
        Placement(visible = true, transformation(origin = {26, -68}, extent =
        {{10, -10}, {-10, 10}}, rotation = 0));
        equation
        connect(MassFlow_BC.ports[1], Radiatube.inFlow) annotation(

```



```

    Line(points = {{30, -49}, {38, -49}, {38, -48}}, color = {0, 127,
255}));
    connect(Pressure_BC.p_in, Pressure_Outlet.y) annotation(
    Line(points = {{80, -44}, {82, -44}, {82, -26}}, color = {0, 0, 127}));
    connect(MassFlow_BC.T_in, Temperature_Inlet.y) annotation(
    Line(points = {{14, -46}, {14, -57}, {16, -57}, {16, -68}}, color = {0,
0, 127}));
    connect(Radiatube.outFlow, Pressure_BC.ports[1]) annotation(
    Line(points = {{58, -48}, {68, -48}}, color = {0, 127, 255}));
    end Hydraulic;
    end Tests_Simple;

    package Thermal_Validation
    model FourTubes
        Modelica.Units.SI.Temperature T_medial;
        Modelica.Units.SI.Temperature T_medial2;
        Modelica.Units.SI.Temperature T_medial3;
        parameter Modelica.Units.SI.MassFlowRate mf = 0.75 "mass flow rate in each
tube";
        Permeation_Validation.RadiaTube rt(flag2 = 1, flag3 = 1, flag4 = 1)
    annotation(
        Placement(visible = true, transformation(origin = {-71, 0}, extent = {{-
5, -6}, {5, 6}}, rotation = 0)));
        Modelica.Fluid.Sources.MassFlowSource_T MassFlow(redeclare package Medium
= Permeation_Validation.Media.PbLi, T = 723.15, m_flow = mf, nPorts = 1)
    annotation(
        Placement(visible = true, transformation(origin = {-84, 0}, extent = {{-
4, -4}, {4, 4}}, rotation = 0)));
        Modelica.Fluid.Sources.Boundary_pT Pressure(redeclare package Medium =
Permeation_Validation.Media.PbLi, T = 723.15, nPorts = 1, p = 1e5) annotation(
        Placement(visible = true, transformation(origin = {-58, -2.22045e-16},
extent = {{4, -4}, {-4, 4}}, rotation = 0)));
        Modelica.Fluid.Sources.Boundary_pT boundary2(redeclare package Medium =
Permeation_Validation.Media.PbLi, T = 723.15, nPorts = 1, p = 1e5) annotation(
        Placement(visible = true, transformation(origin = {-12, 0}, extent =
{{4, -4}, {-4, 4}}, rotation = 0)));
        Permeation_Validation.RadiaTube radiaTube1(flag2 = 1, flag3 = 1, flag4 =
1) annotation(
        Placement(visible = true, transformation(origin = {-25, 0}, extent = {{-
5, -6}, {5, 6}}, rotation = 0)));
        Modelica.Fluid.Sources.MassFlowSource_T boundary3(redeclare package Medium
= Permeation_Validation.Media.PbLi, T = 723.15, m_flow = mf, nPorts = 1,
use_T_in = false) annotation(
        Placement(visible = true, transformation(origin = {-38, 0}, extent = {{-
4, -4}, {4, 4}}, rotation = 0)));
        Permeation_Validation.RadiaTube radiaTube(flag2 = 1, flag3 = 1, flag4 = 1)
    annotation(
        Placement(visible = true, transformation(origin = {71, 0}, extent = {{-
5, -6}, {5, 6}}, rotation = 0)));
        Permeation_Validation.RadiaTube radiaTube2(flag2 = 1, flag3 = 1, flag4 =
1) annotation(
        Placement(visible = true, transformation(origin = {25, 0}, extent = {{-
5, -6}, {5, 6}}, rotation = 0)));
        Modelica.Fluid.Sources.MassFlowSource_T boundary(redeclare package Medium
= Permeation_Validation.Media.PbLi, T = 723.15, m_flow = mf, nPorts = 1,
use_T_in = false) annotation(
        Placement(visible = true, transformation(origin = {58, 0}, extent = {{-
4, -4}, {4, 4}}, rotation = 0)));
        Modelica.Fluid.Sources.Boundary_pT boundary1(redeclare package Medium =
Permeation_Validation.Media.PbLi, T = 723.15, nPorts = 1, p = 1e5) annotation(
        Placement(visible = true, transformation(origin = {84, 0}, extent = {{4,
-4}, {-4, 4}}, rotation = 0)));
        Modelica.Fluid.Sources.Boundary_pT boundary4(redeclare package Medium =
Permeation_Validation.Media.PbLi, T = 723.15, nPorts = 1, p = 1e5) annotation(

```

```

    Placement(visible = true, transformation(origin = {38, 0}, extent = {{4,
-4}, {-4, 4}}, rotation = 0));
    Modelica.Fluid.Sources.MassFlowSource_T boundary5(redeclare package Medium
= Permeation_Validation.Media.PbLi, T = 723.15, m_flow = mf, nPorts = 1)
    annotation(
      Placement(visible = true, transformation(origin = {12, 0}, extent = {{-
4, -4}, {4, 4}}, rotation = 0));
      Permeation_Validation.Envelope envelope(Tfv(each start = 723.15), flag2 =
1, flag3 = 1, flag4 = 1) annotation(
        Placement(visible = true, transformation(origin = {-2, 36}, extent = {{-
10, -10}, {10, 10}}, rotation = 0));
        /*Modelica.Blocks.Sources.RealExpression realExpression(y = rt.Tfv[end])
        annotation(
          Placement(visible = true, transformation(origin = {-54, 24},
extent = {{-10, -10}, {10, 10}}, rotation = 0));
          Modelica.Blocks.Sources.RealExpression realExpression1(y =
radiaTube2.Tfv[end]) annotation(
            Placement(visible = true, transformation(origin = {44, 24}, extent
= {{-10, -10}, {10, 10}}, rotation = 0));
            */
      equation
        connect(MassFlow.ports[1], rt.inFlow) annotation(
          Line(points = {{-80, 0}, {-76, 0}}, color = {0, 127, 255}));
        connect(rt.outFlow, Pressure.ports[1]) annotation(
          Line(points = {{-66, 0}, {-62, 0}}, color = {0, 127, 255}));
        connect(radiaTube.VF_4, envelope.VF_4) annotation(
          Line(points = {{76, 6}, {76, 50}, {-2, 50}, {-2, 44}}, color = {191, 0,
0}, thickness = 0.5));
        connect(envelope.VF_3, radiaTube2.VF_4) annotation(
          Line(points = {{10, 36}, {30, 36}, {30, 6}}, color = {191, 0, 0},
thickness = 0.5));
        connect(envelope.VF_1, rt.VF_4) annotation(
          Line(points = {{-14, 36}, {-66, 36}, {-66, 6}}, color = {191, 0, 0},
thickness = 0.5));
        connect(envelope.VF_2, radiaTube1.VF_4) annotation(
          Line(points = {{-2, 24}, {-20, 24}, {-20, 6}}, color = {191, 0, 0},
thickness = 0.5));
        connect(rt.VF_3, radiaTube2.VF_2) annotation(
          Line(points = {{-66, -6}, {-66, -20}, {20, -20}, {20, -6}}, color =
{191, 0, 0}, thickness = 0.5));
        connect(rt.VF_2, radiaTube.VF_3) annotation(
          Line(points = {{-76, -6}, {-76, -26}, {76, -26}, {76, -6}}, color =
{191, 0, 0}, thickness = 0.5));
        connect(radiaTube1.VF_3, radiaTube2.VF_3) annotation(
          Line(points = {{-20, -6}, {-20, -12}, {29, -12}, {29, -5}}, color =
{191, 0, 0}, thickness = 0.5));
        connect(radiaTube1.VF_2, radiaTube.VF_2) annotation(
          Line(points = {{-30, -6}, {-30, -14}, {66, -14}, {66, -6}}, color =
{191, 0, 0}, thickness = 0.5));
        connect(boundary3.ports[1], radiaTube1.inFlow) annotation(
          Line(points = {{-34, 0}, {-30, 0}}, color = {0, 127, 255}));
        connect(radiaTube1.outFlow, boundary2.ports[1]) annotation(
          Line(points = {{-20, 0}, {-16, 0}}, color = {0, 127, 255}));
        connect(boundary5.ports[1], radiaTube2.inFlow) annotation(
          Line(points = {{16, 0}, {20, 0}}, color = {0, 127, 255}));
        connect(radiaTube2.outFlow, boundary4.ports[1]) annotation(
          Line(points = {{30, 0}, {34, 0}}, color = {0, 127, 255}));
        connect(boundary.ports[1], radiaTube.inFlow) annotation(
          Line(points = {{62, 0}, {66, 0}}, color = {0, 127, 255}));
        connect(radiaTube.outFlow, boundary1.ports[1]) annotation(
          Line(points = {{76, 0}, {80, 0}}, color = {0, 127, 255}));
        T_media1 = (envelope.Tfv[2] + envelope.Tfv[1]) * .5;
        T_media1 = (sum(rt.Tfv) + sum(radiaTube1.Tfv)) / 4;
        T_media2 = (sum(radiaTube2.Tfv) + sum(radiaTube.Tfv)) / 4;

```

```

    connect(radiaTube2.VF_1, rt.VF_1) annotation(
      Line(points = {{20, 6}, {20, 12}, {-76, 12}, {-76, 6}}, color = {191, 0,
0}, thickness = 0.5));
    connect(radiaTube1.VF_1, radiaTube.VF_1) annotation(
      Line(points = {{-30, 6}, {-30, 14}, {66, 14}, {66, 6}}, color = {191, 0,
0}, thickness = 0.5));
    end FourTubes;
  end Thermal_Validation;
  annotation(
    uses(Modelica(version = "4.0.0")));
end The_RadiaTube;

```

# Bibliography

- [1] <https://www.wolframalpha.com/input?i=hydrogen-3>
- [2] Wikipedia, "Fusion Power" [https://en.wikipedia.org/wiki/Fusion\\_power#/media/File:Deuterium-tritium\\_fusion.svg](https://en.wikipedia.org/wiki/Fusion_power#/media/File:Deuterium-tritium_fusion.svg)
- [3] <https://scipython.com/blog/nuclear-fusion-cross-sections/>
- [4] <http://www.fusione.enea.it/WHAT/fusion7.html.it>
- [5] J. Raeder et al., Kontrollierte Kernfusion: Grundlagen Ihrer Nutzung Zur Energieversorgung, (Teubner Studienbuecher, 1981)
- [6] D. Demange, R. Antunes, O. Borisevich, L. Frances, D. Rapisarda, A. Santucci, M. Utili, "Tritium extraction technologies and DEMO requirements", Fusion Engineering and Design, Volumes 109–111, Part A, 2016, Pages 912-916, ISSN 0920-3796, <https://doi.org/10.1016/j.fusengdes.2016.01.053>.
- [7] M. Utili, A. Aiello, L. Laffi, A. Malavasi, I. Ricapito, Investigation on efficiency of gas liquid contactor used as tritium extraction unit for HCLL-TBM Pb-16Li loop, Fusion Engineering and Design, Volumes 109–111, Part A, 2016, Pages 1-6, ISSN 0920-3796, <https://doi.org/10.1016/j.fusengdes.2016.03.067>.
- [8] P. Harriott and R. M. Hamilton, "Solid-liquid mass transfer in turbulent pipe flow," Chem. Eng. Sci., vol. 20, no. 12, pp. 1073–1078, 1965.
- [9] Reiter, F. "Solubility and Diffusivity of Hydrogen Isotopes in Liquid PbLi." Fusion Engineering and Design 14.3-4 (1991): 207-11. Web.
- [10] Aiello, A, Ciampichetti, A, and Benamati, G. "Determination of Hydrogen Solubility in Lead Lithium Using Sole Device." Fusion Engineering and Design 81.1 (2006): 639-44. Web.

- [11] Paul W. Humrickhouse & Brad J. Merrill (2015) Vacuum Permeator Analysis for Extraction of Tritium from DCLL Blankets, *Fusion Science and Technology*, 68:2, 295-302, DOI: 10.13182/FST14-941
- [12] P. W. Humrickhouse, "*Permeation of multiple isotopes in the transition between surface and diffusion-limited regimes*," 2014.
- [13] I. Ali-Khan, K. J. Dietz, F. G. Waelbroeck, and P. Wienhold, "*The rate of hydrogen release out of clean metallic surfaces*," *J. Nucl. Mater.*, vol. 76-77, no. C, pp. 337-343, 1978.
- [14] P. W. Humrickhouse, "*Permeation of multiple isotopes in the transition between surface and diffusion-limited regimes*," 2014.
- [15] D'Auria, V, Dulla, S, Ravetto, P, Savoldi, L, Utili, M, and Zanino, R. "Tritium Extraction from Lithium-Lead in the EU DEMO Blanket Using Permeator Against Vacuum." *Fusion Science and Technology* 71.4 (2017): 537-43. Web.
- [16] Garcinuño, Belit, Rapisarda, David, Fernández, Iván, Moreno, Carlos, Palermo, Iole, and Ibarra, Ángel. "Design of a Permeator against Vacuum for Tritium Extraction from Eutectic Lithium-lead in a DCLL DEMO." *Fusion Engineering and Design* 117 (2017): 226-31. Web.
- [17] Bonifetto, R, Utili, M, Valerio, D, and Zanino, R. "Conceptual Design of a PAV-based Tritium Extractor for the WCLL Breeding Blanket of the EU DEMO: Effects of Surface-limited vs. Diffusion-limited Modeling." *Fusion Engineering and Design* 167 (2021): 112363. Web.
- [18] Froio, A., "Introduction to the Modelica language", Politecnico di Torino, 2020.
- [19] Xu Cheng, Nam-il Tak, "*Investigation on turbulent heat transfer to lead-bismuth eutectic flows in circular tubes for nuclear applications*", *Nuclear Engineering and Design*, Volume 236, Issue 4, 2006, Pages 385-393, ISSN 0029-5493, <https://doi.org/10.1016/j.nucengdes.2005.09.006>.
- [20] Star-CCM+ User's Manual, CD ADAPCO, New York, 2019.
- [21] Menter, F.R. 1994. "*Two-equation eddy-viscosity turbulence modeling for engineering applications*", *AIAA Journal*, 32(8), pp. 1598-1605.
- [22] T.L. Bergman, et al., *Fundamentals of Heat and Mass Transfer*, 2011.

- [23] F. Papa, M. Utili, A. Venturini, G. Caruso, L. Savoldi, R. Bonifetto, D. Valerio, A. Allio, A. Collaku, M. Tarantino, " *Engineering design of a Permeator Against Vacuum mock-up with niobium membrane*", Fusion Engineering and Design, Volume 166, 2021, 112313, ISSN 0920-3796, <https://doi.org/10.1016/j.fusengdes.2021.112313>.
- [24] <http://www.thermalradiation.net/sectionc/C-68.html>
- [25] Thermal Properties of Metals, ASM Ready Reference, Editor: Fran Cverna, Materials Park, Ohio, 44073-0002, December 2002, page 61.
- [26] ASME, Sec II, Part D - Properties, Table TCD, page 663, Material Group J, 18Cr-8Ni, Edition June 2001.
- [27] ASME, Sec II, Part D - Properties, Table TCD, page 663, Material Group J, 18Cr-8Ni, Edition June 2001.
- [28] Paradis, PF., Ishikawa, T. & Yoda, S. Non-contact measurements of thermophysical properties of niobium at high temperature. Journal of Materials Science 36, 5125–5130 (2001). <https://doi.org/10.1023/A:1012477308332>
- [29] D. Martelli, A. Venturini, M. Utili, Literature review of lead-lithium thermophysical properties, Fusion Engineering and Design, Volume 138, 2019, Pages 183-195, ISSN 0920-3796, <https://doi.org/10.1016/j.fusengdes.2018.11.028>.
- [30] Utili, M, Venturini, A. "WCLL LiPb DDD - final version 2020." EURO-fusion (BB5.1.1-T003-D002), 04-jan-2021.
- [31] L. Savoldi, A. Collaku, L. Candido, " *Conceptual Design of TES with operation condition and operative range, thermo-fluid-dynamic evaluation, and comparison with PAV and GLC*", EFDA\_ D\_ 2P632L, 2021, <https://idm.euro-fusion.org/?uid=2P632L&version=v1.0>